QUALITATIVE MODELLING OF THE NATURAL VENTILATION POTENTIAL IN URBAN CONTEXT

THÈSE N^{O} 3482 (2006)

PRÉSENTÉE LE 7 AVRIL 2006

À LA FACULTÉ ENVIRONNEMENT NATUREL, ARCHITECTURAL ET CONSTRUIT
Laboratoire d'énergie solaire et physique du bâtiment
SECTION D'ARCHITECTURE

ÉCOLE POLYTECHNIQUE FÉDÉRALE DE LAUSANNE

POUR L'OBTENTION DU GRADE DE DOCTEUR ÈS SCIENCES

PAR

Mario GERMANO

Ingénieur physicien diplômé EPF
et de nationalité italienne

acceptée sur proposition du jury:

Prof. C. Morel, président du jury
Prof. C.-A. Roulet, directeur de thèse
Dr A. Clappier, rapporteur
Prof. G. Guarracino, rapporteur
Prof. M. Santamouris, rapporteur

ÉCOLE POLYTECHNIQUE
FÉDÉRALE DE LAUSANNE
Lausanne, EPFL
2006

Version abrégée

Les deux objectifs de la ventilation naturelle dans les bâtiments sont l'amélioration de la qualité de l'air intérieur et du confort thermique. La méthodologie proposée ci-après donne une évaluation du potentiel de ventilation naturelle pour la qualité de l'air intérieur, tout en prenant en considération l'autre objectif. Plus précisément, les besoins inhérents au confort imposent une stratégie spécifique pour chaque situation météorologique. Partant de cette stratégie, la méthode déduit si un lieu donné se prête bien ou non à la ventilation naturelle.

Après une brève introduction historique (Chapitre 1), la position du problème (Chapitre 2) et un passage en revue de l'état de l'art (Chapitre 3), le Chapitre 4 présente un méthodologie originale pour l'évaluation du potentiel de ventilation naturelle qui s'appuie sur ses moteurs (*le vent* et *l'effet de cheminée*) et sur ses contraintes (*les nuisances sonores* et *la pollution atmosphérique*), et qui met en application l'aide multicritère à la décision. La méthode utilise les résultats d'un modèle de simulation atmosphérique *Lokal-Modell* (LM, décrit au paragraphe 3.4). Le logiciel associé, développé dans le cadre du projet européen URBVENT, et validé avec des cas réels, est présenté également.

Le Chapitre 5 présente les résultats d'un modèle atmosphérique à mésoéchelle (*Finite Volume Model*, FVM), dans lequel est incorporé un *module urbain* (décrit au paragraphe section 3.6) et qui permet de calculer les effets du tissu urbain sur les variables météorologiques. Ce modèle a été adapté dans le cadre du présent travail afin d'utiliser les résultats du modèle ci-dessus (*Lokal-Modell*, LM) comme conditions de bord. (Pour ce faire, les travaux précédents avaient recours à des données *NCEP/NCAR Reanalysis data*, avec une résolution spatiale originale 40 fois plus basse que LM en latitude, 25

fois plus basse en longitude et 6 fois plus basse temporellement.)

Après une vérification des résultats du modèle urbain, menée à bien au moyen de mesures *in situ* faites dans la région de Bâle (Suisse) pendant une période estivale, le Chapitre 6 présente l'utilisation de ces résultats dans la méthode URBVENT du Chapitre 4. Le potentiel de ventilation naturelle qui en découle fait l'objet d'une vérification utilisant une étude d'exposition à la pollution atmosphérique (EXPOLIS) au paragraphe 6.4.

Le lecteur est rendu attentif ici au fait qu'il a été décidé de déterminer le potentiel de ventilation naturelle du site lui-même de la façon la plus indépendante du bâtiment. Ainsi, une analyse des résultats permet d'indiquer quel type de ventilation se prête le mieux à un site et quel type de bâtiment devrait y être construit (ou comment y rénover un existant). En d'autres termes, le modèle permet de dire si les conditions extérieures favorables à la ventilation naturelle coexistent. L'intention ici n'est pas de dire comment exploiter au mieux ces conditions. Ceci est laissé au soin du lecteur ou du concepteur qui trouvera d'ailleurs une littérature passablement abondante sur ce sujet spécifique.

Mots-clés

Potentiel de ventilation naturelle, environnement urbain, vent, portance, effet de cheminée, bruit, pollution, conception préliminaire, modélisation qualitative, aide multicritère à la décision

Abstract

The two objectives of natural ventilation in buildings are the improvement of indoor air quality and thermal comfort. The methodology proposed hereafter provides an assessment of the natural ventilation potential for indoor air quality, while taking into consideration the other objective. More precisely, requirements on comfort impose the appropriate ventilation strategies to be applied for each given meteorological situation. On the basis of these strategies, the methodology evaluates the appropriateness of a given location to natural ventilation.

After a historical introduction (Chapter 1), the statement of the problem (Chapter 2) and a review of the state of the art (Chapter 3), Chapter 4 presents a novel methodology to assess the natural ventilation potential starting from its driving forces (*wind-induced* and *buoyancy-induced pressures*) and from its constraints (*noise pollution* and *atmospheric pollution*), which applies multicriteria analysis. The method uses the results of the atmospheric simulation model *Lokal-Modell* (LM, described in section 3.4). The related software tool, developed within the European project URBVENT, and tested against real cases, is presented as well.

Chapter 5 gives a view of the results of an atmospheric mesoscale model, referred to as *Finite Volume Model* (FVM), that includes an *urban module* (described in section 3.6) allowing to compute the effects of the urban tissue on meteorological parameters. This model has been adapted as part of this work to use the outputs of the above-mentioned *Lokal-Modell* (LM) as boundary conditions. (To this end, previous works utilized NCEP/NCAR Reanalysis data, with an original spatial resolution 40 times lower than LM in latitude, 25 times lower in longitude and 6 times lower in time.)

After a verification of the urban model results against on site measurements carried out in the Basel region (Switzerland) over a summertime period, Chapter 6 presents the utilization of these results within the URBVENT method of Chapter 4. The ensuing potential for natural ventilation is the object of a verification resorting to an air pollution exposure study (EXPOLIS) in section 6.4.

Attention is drawn to the fact that it has been decided to assess the natural ventilation potential of the site itself, in the most building-independent way. In so doing, an analysis of the results can tell what type of ventilation a given site is suited for and what kind of building should be built there (or how to refurbish an existing one). Put another way, the model examines whether external conditions required for applying natural ventilation coexist. How to properly design a building taking advantage of theses conditions is not addressed here. This is left to the reader or to the designer. Incidentally, the bibliography dealing with this very topic is quite abundant.

Key Words

Natural ventilation potential, urban environment, wind, buoyancy, stack effect, noise, pollution, preliminary design, qualitative modelling, multicriteria analysis

Remerciements

Je tiens à remercier le professeur Claude-Alain Roulet, mon directeur de thèse, pour ses conseils avisés et pour avoir partagé ses connaissances impressionnantes, ainsi que le professeur Jean-Louis Scartezzini pour m'avoir accueilli (moi et quelques amis importuns) dans son laboratoire et pour la lecture du manuscrit. Je remercie le Secrétariat d'État à l'éducation et à la recherche (anciennement Office fédéral de l'éducation et de la science) pour son soutien financier lors du projet URBVENT.

J'aimerais exprimer ma gratitude également aux personnes suivantes :

- Dr Alain Clappier et Clive Muller du Laboratoire de pollution atmosphérique et du sol (LPAS), ainsi qu'Alberto Martilli du Centre de recherches énergétiques, environnementales et technlogiques de Madrid, Espagne (CIEMAT), pour m'avoir permis d'accéder à FVM et pour leurs nombreuses explications.
- Dr Flourentzos Flourentzou pour m'avoir encadré en début de thèse et pour l'intelligence de ses idées.
- Tous les membres de l'équipe URBVENT et plus particulièrement Dr Cristian Ghiaus pour les nombreux et fructueux échanges, Nicolas Heijmans pour ses remarques et encouragements, Dr Chrissa Georgakis et les professeurs Mat Santamouris et Francis Allard.
- Emanuele Zala et Francis Schubiger de MétéoSuisse pour les données LM et pour leurs explications.
- Le Service des systèmes d'information et de géomatique de l'État de Genève pour la distribution de données du Système d'information du territoire genevois.
- Gérard Greuter pour son initiation aux systèmes d'information géographique (et au snowboard).
- Dr Andreas Christen et l'Université de Bâle pour l'accès aux données BUBBLE et pour les explications du premier sur les courants urbains.
- Les professeurs Nino Kuenzli, Matti Jantunen et Otto Hänninen pour l'accès aux données EXPOLIS et leurs explications.

- Dr Darren Robinson pour son initiation à *ESP–r*, pour sa contribution sur les modèles thermiques et pour son soutien dans la recherche de fonds.
- Dr Simon Bossoney pour son amitié, pour sa précieuse compagnie, son support moral et sa vision perspicace du monde.
- Marylène Montavon pour son indispensable présence (et ses inévitables petites absences).
- Pascal Meylan pour avoir partagé péniblement mon bureau et pour son initiation à la batterie et au death metal.
- Le docteur Jérôme Sobel, mon ORL et président d'Exit–Suisse romande, pour ne pas m'avoir euthanasié.
- Tous mes collègues pour l'ambiance très amicale qu'ils apportent au LESO.
- Josée pour son amour inconditionnel.

Merci enfin à mes amis et à ma famille.

To Madeleine

Contents

Introduction

Sales of air-conditioning units are growing rapidly in Europe since several decades. A recent study (EECCAC, 2002) showed that in the EU the annual *additional* building floor area conditioned by central air conditioners went from approximately 20 million square metres in 1980 to approximately 100 million in 2000.

In a country like Greece, air-conditioned buildings will consume more energy than naturally ventilated buildings, ranging between 4 % to over 54 %, depending on the type of building (Santamouris & Asimakopoulos, 1996).

Moreover, the heat rejection coming from the operation of air-conditioning units enhances the production of the 'heat island effect', which in turn demands more from air-conditioning. (It may come as something of a surprise that "5–10 % of the current [2001] urban electricity demand [in American cities] is spent to cool buildings just to compensate for the increased 0.5–3.0 °C in urban temperatures." (Akbari *et al.*, 2001))

Peak electricity loads already oblige utilities to build additional power plants in order to satisfy the demand, thus increasing the average cost of electricity. (Santamouris, 2005)

Natural ventilation is an alternative to air-conditioning. Applied in mild climate, it can provide effective cooling during day and night, while night ventilation is a very effective strategy in hot continental climates. Passive cooling presents several advantages as regards the environment, as it doesn't lead to an increased use of fossil fuels

and to the ensuing greenhouse gases emissions.

Apart from purely energy-related concerns, natural ventilation has other benefits concerning the occupants' health. Symptoms like lethargy, headache, blocked or runny nose, dry or sore eyes—often referred to as 'sick building syndrome'—are regularly observed in air-conditioned buildings, not to mention that comfort criteria have proven to be less restrictive in a naturally ventilated environment (see for instance the results of the HOPE project (Johner *et al.*, 2005) or De Dear & Brager (1999)).

Yet despite the benefits of natural ventilation, designers and architects still keep on turning to mechanical ventilation or air-conditioning, lest their building should be subject to risks inherent in natural ventilation and in its associated external conditions. They usually prefer to rely on a constant airflow rate and on setpoint indoor temperatures. Furthermore, they may also think that technology leaves more freedom to architectural design.

The primary reason for this using of 'non-passive' techniques, is the current lack of design tools related to natural ventilation. One of the goals of the software tool presented in Chapter 4 is to make up for this gap.

Chapter 1

A Short Historical Introduction

Introducing the first historical applications of natural ventilation and passive cooling is of particular interest because—in addition to showing how these techniques appeared—this allows to explain the whole range of phenomena taking place while applying them.

Relatively evolved systems, such as curved-roof systems, were integrated in buildings as early as 3000 B.C.; others, like wind towers[1], cooling cisterns or ice makers may not have appeared before 900 A.D. Many of such cooling systems are still in use nowadays. (Bahadori, 1978)

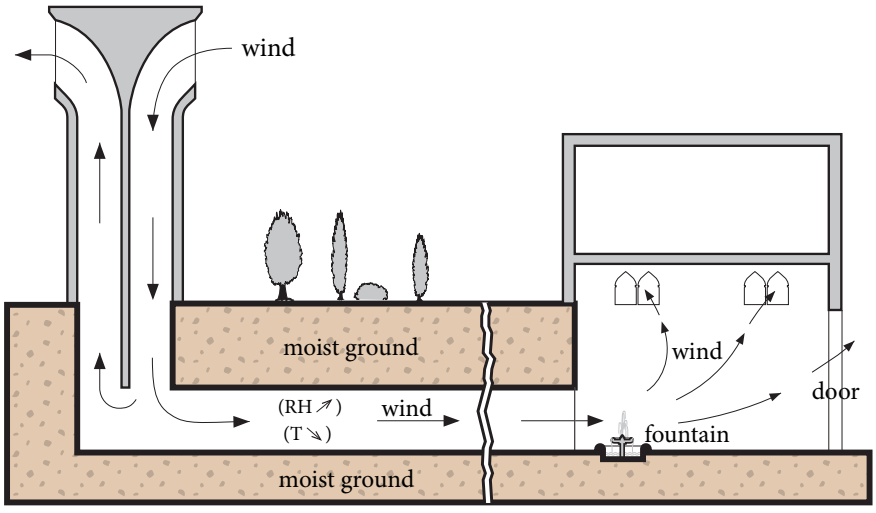

Figure 1.1: Wind tower. Sketch by Bernard Paule, after Bahadori (1978).

[1] *Badgir* in Persian.

The wind tower shown in Figure 1.1 is used in conjunction with a damp tunnel whose humidity is ensured by watered trees, shrubs and grass.

During daytime, air entering the tower is firstly *sensibly* cooled: the walls of the upper part of the tower, earlier cooled down during the night, lower the penetrating air temperature (without changing the air water-vapor content). Being denser than the hot air, the cool air sinks down through the tower, creating a downdraught. If wind blows, this circulation is increased. The coolness of the rest of the tower and of the ground continues this cooling.

Then, this unsaturated air is *evaporatively* cooled: heat evaporates the water in the tunnel, increasing thus its water-vapor content. The tunnel length is about fifty metres. Pool and fountain in the basement of the building further cool the air.

Both these sensible and evaporative contribution are particularly efficient.

During nighttime, in the absence of wind, the thermal inertia induced draught is reversed. Otherwise, wind pushes down cool night air it the rooms.

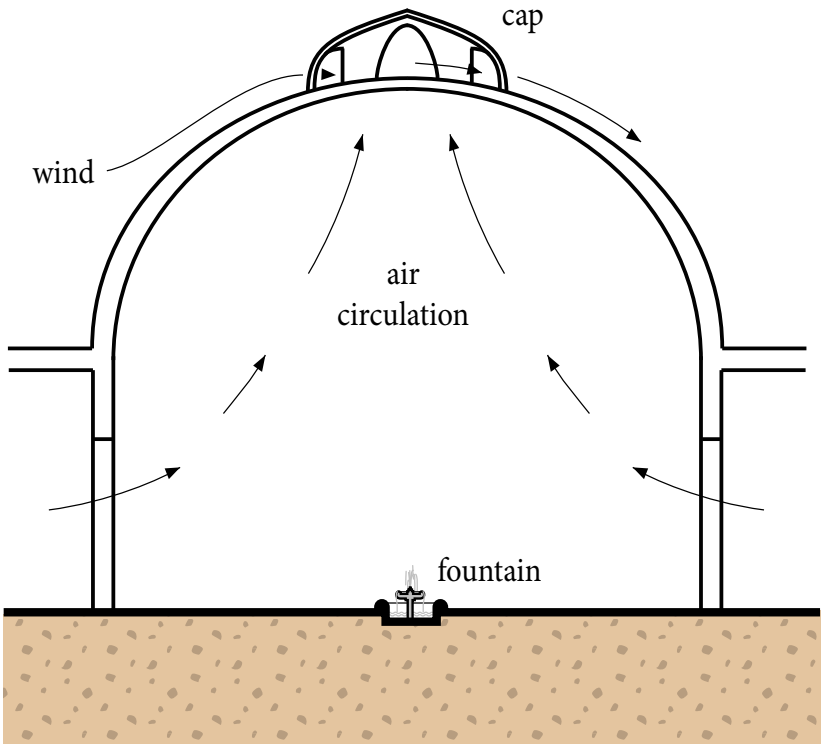

Figure 1.2: Curved roof (Bahadori, 1978)

Another example is the curved roof system (Figure 1.2). Here, the wind is accelerated on the rooftop creating a pressure drop and hence a suction. Hot air situated beneath the dome is evacuated. Moreover, a curved roof has a larger convection heat-transfer area and transfers heat more efficiently than a flat roof.

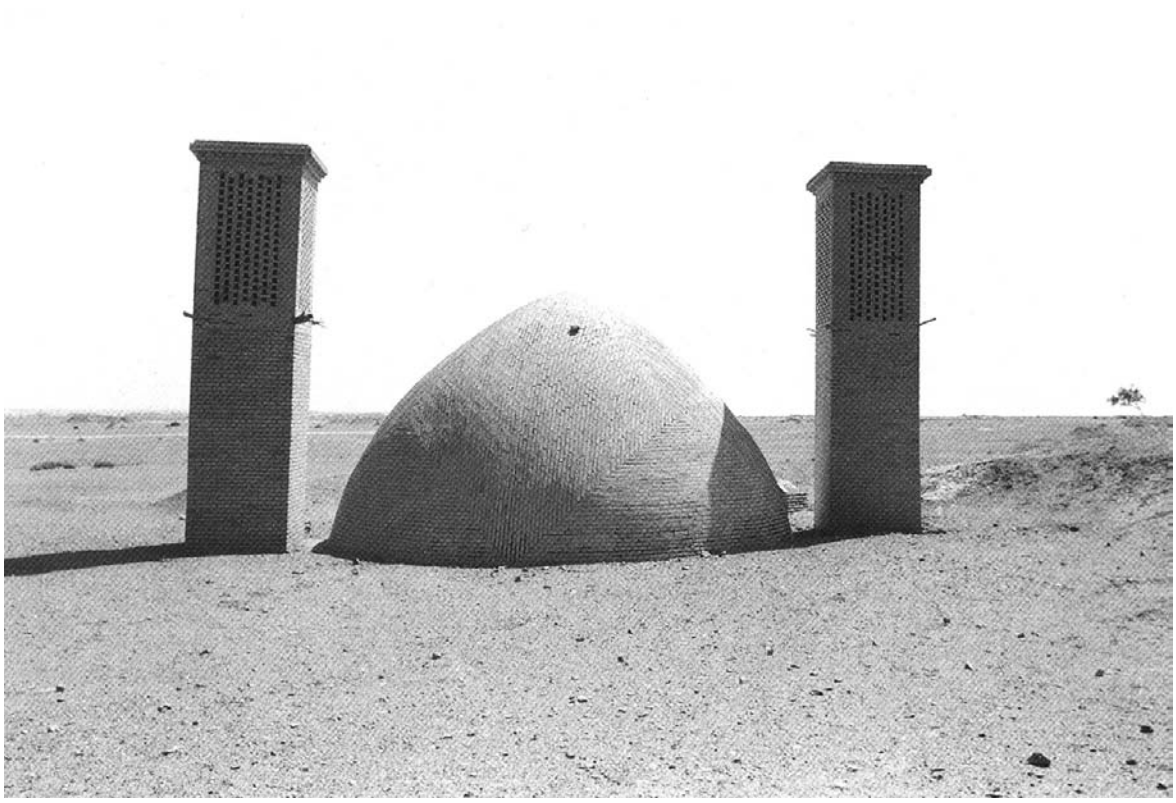

Figure 1.3: Brick cistern with wind towers in Yazd (Khansari & Yavari, 1986)

Wind towers and curved roofs can been combined to cool down the water or even ice in a cistern (Figure 1.3) (Khansari & Yavari, 1986).

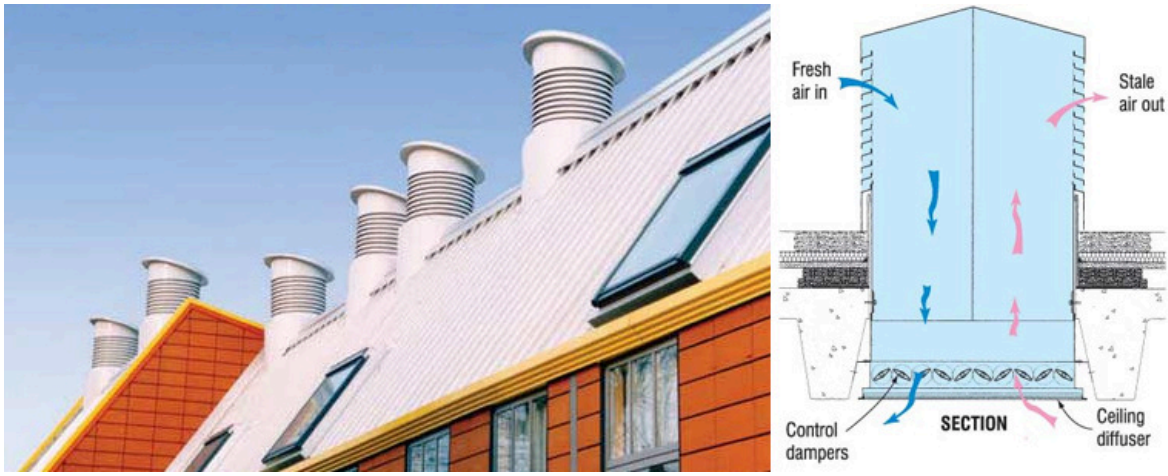

Figure 1.4: Modern version of windcatchers. Addy and Stanhope School, Deptford London. Source: `http://www.monodraught.com/`

Chapter 2

Problem Statement

2.1 The Air-conditioning Issue

The first motivation for conducting the present work came from the realization that air-conditioning systems are increasingly used. Some figures have been given in the introduction about the past trends (EECCAC, 2002).

Predictions have also been made (Adnot, 2005), according to which the air-conditioned surface will rise from 500 million square metres today (2005) to 2 500 million in 2020 in the (former) fifteen-member European Union.

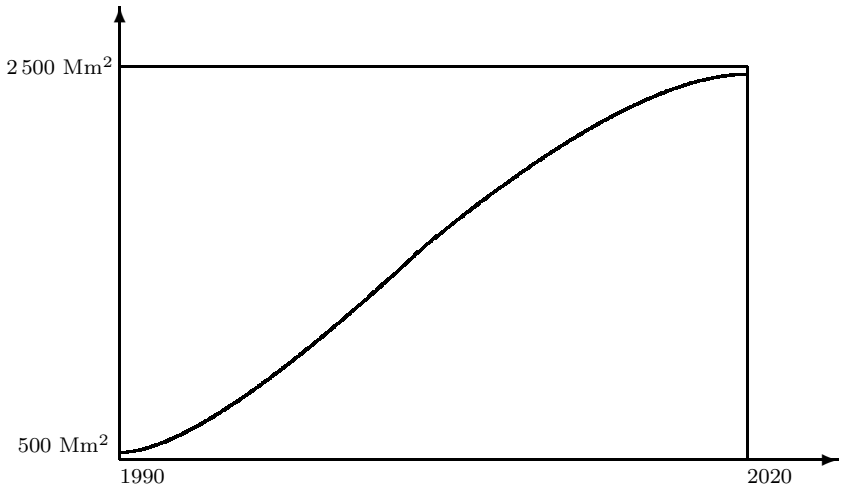

Figure 2.1: Predicted cooled surface in the fifteen-member European Union (Adnot, 2005)

Per inhabitant, this surface will double (from 3 m^2 to 6 m^2) in the same time,

whereas the consumption of electricity devoted to air-conditioning will increase from 50 TWh to 100 TWh.

These predictions are made assuming no change in behaviour, which is questionable. For instance, after the heatwave of summer 2003, for which France only reported a death toll[1] of 14 800 (Hémon & Jougla, 2003), the sales of air-conditioners increased by 40 % in that country.

On the other hand, a new regulation may induce a change: a minimum energy standard (EPBD) is envisaged in Europe for 2006 (Wouters, 2004): unlike the United States, Japan and China, the European Union imposes no legal obligation for the efficiency of air-conditioning systems, except in Portugal and in the United Kingdom.

2.2 An Adapted Tool

2.2.1 A Comprehensive Tool

The other motivation came from the lack of tools adapted for the assessment of natural ventilation in a building taking into account *all* of the factors involved, particularly those external to the building:

- meteorology
- influence of the city
- influence of the near surroundings
- noise pollution
- atmospheric pollution

In order to include in the model this entire set of factors, and for several other reasons, it was decided to resort to 'qualitative modelling' (also referred to as 'soft-computing').

There exists no airflow model taking into account simultaneously fluid dynamics, noise and pollution. The reason for this is that their effects cannot be accounted for in the same equations. (Mathematicians would say that they are 'incommensurable'.)

[1] Exceeding deceases in comparison to the previous years.

2.2.2 A Design Tool

Moreover, the intention was to provide a method that could be used at the early stage of urban and building design, that is when the most influential decisions have to be come to. Since the details of the building needed for airflow estimation cannot be known until the project is well advanced, the method had to be able to cope with the less information possible—and this is where qualitative modelling comes into play.

The architectural solutions planned during this phase have a major influence on the application of natural ventilation. Most of the time, a new building resembles more or less to existing solutions. For a building designer it is interesting to obtain a quick comparison of the potential of known 'example' buildings for using natural ventilation. Then, the designer may adapt the example that suits better the demands, but in the initial stage of design, the information needed for decision making is vague and inaccurate.

Therefore, the external conditions of the building, particularly meteorology, happened to be the prevailingly influential factors for assessing the natural ventilation potential in the present work. This is why the potential to assess will be mainly the potential of a *site* rather than the potential of a *building*. In other words, the model should be able to state whether a given location is appropriate for using natural ventilation.

2.2.3 A 'Simple' Tool

As another reason for using qualitative modelling, several studies (Fürbringer, 1994) showed that the uncertainty of the results coming out of an airflow model increases with its complexity. For instance the uncertainty of the mean air age can be higher in a 'detailed' model like CoMIS[2] than in 'simple' models.

Table 2.1: Uncertainty of the mean air age in 'detailed' and 'simple' models, taking into account of the experimental precision of the input data. The complexity of the models decreases from left to right. The first situation is buoyancy-dominated, whereas the third is wind-dominated. (Fürbringer, 1994)

wind speed	CoMIS	BREVENT	LBL	AIDA	TURBUL
0.3 m/s	51 %	34 %	26 %	16 %	15 %
1.0 m/s	38 %	22 %	29 %	24 %	19 %
3.0 m/s	32 %	24 %	37 %	24 %	24 %

[2]Conjunction of Multizone Infiltration Specialists

These uncertainties issue from the uncertainties of the input data (called *external* source of errors) propagated by the model. They don't reflect the accuracy of the results from the physical point of view, which is assessed by a validation process.

In addition, Fürbringer *et al.* (1996) performed a user test on the airflow model CoMIS: "Two cases were submitted to several different users and results were compared. One case was simple and clearly defined, with all essential input data provided. For this case, all users but one (who made a modelling error) provided the same results. The other case, however, was more realistic, since data were provided as usually provided in practice. [...] Very large differences in the results were found in this instance. Most discrepancies can be explained by modelling errors which are partly due to some unclear instructions in the draft User Guide, since corrected, and others from differences in input data."

This established fact led us toward the development of the less user-dependant tool possible, bearing in mind that this dependance goes hand in hand with the complexity of the model.

2.2.4 An Urban Tool

To our knowledge, no airflow simulation program takes into account the influence of surrounding buildings and of the city in its calculations. While solar radiation simulation programs do factor in shading by neighbouring constructions, the situation is somewhat more complicated when it comes to atmospheric flows. The airflow at façade level is the result of the mesoscale airflow and of the influence of the direct neighbours. The former is influenced by the geostrophic wind and by the city fabric as a whole. Each scale is nested in the larger and requires a different model. Each model provides the boundary conditions to the model it encompasses (see Figure 2.2). In fact, all of these models are governed by the Navier-Stokes equations[3] and by the principles of mass conservation, energy conservation and momentum conservation. The difference lies in the hypotheses made on pressures, densities and turbulence, which are inherent in the scale and in the grid cell size.

[3]Incidentally, in 2000, The Clay Mathematics Institute designated a one-million prize fund for founding the analytical solution of the Navier-Stokes equations. The Institute has recognized the following problem as one of the seven major mathematical problems for the twenty-first century: To prove that the solution of the Navier-Stokes equations remains regular for any time (*i.e.* the speed never becomes infinite) or, on the contrary, to give an example of apparition of a singularity (Temam, 2005).

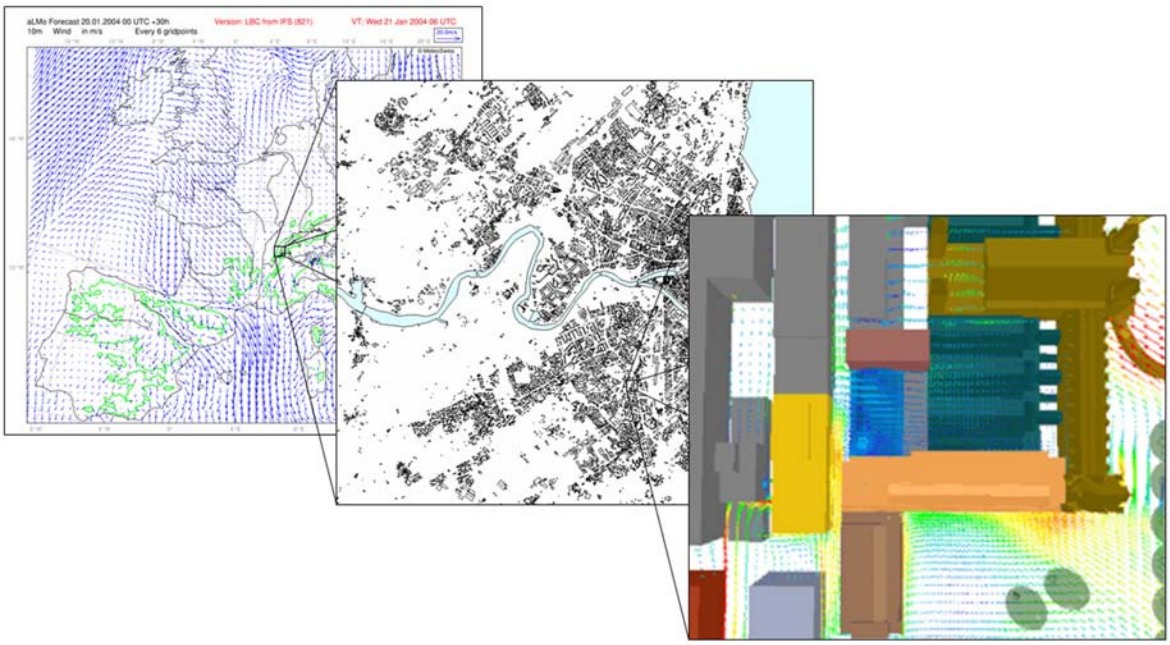

Figure 2.2: Nested scales

Usually airflow models for buildings will use an 'upstream reference wind speed' which is derived by means of power-law type equations such as

$$v/v_r = cH^a \tag{2.2.1}$$

where v is the mean wind speed at height H above the ground, v_r is the mean wind speed measured at a weather station, a and c are factors which depend on the terrain.

Not only is this kind of equation hardly ever fulfilled, but it is only valid in open terrain.

In the urban environment, several authors tend to use an exponential wind speed profile within the urban canopy[4] and a logarithmic one above. Nicholson (1975) for instance uses equations 2.2.2 and 2.2.3 for describing this profile:

$$u(z) = U_0 \exp(\frac{z\ z_0}{h_b\ D^*}) \tag{2.2.2}$$

$$u(z) = u^* \ln(\frac{z + z_d + z_0}{z_0}) \tag{2.2.3}$$

[4]The urban canopy is by definition the space delimited by the ground and the buildings' rooftops.

where U_0 = constant reference speed
h_b = mean building height
D^* = effective diameter of air space between obstacles
u^* = frictional velocity
k = Karman's constant

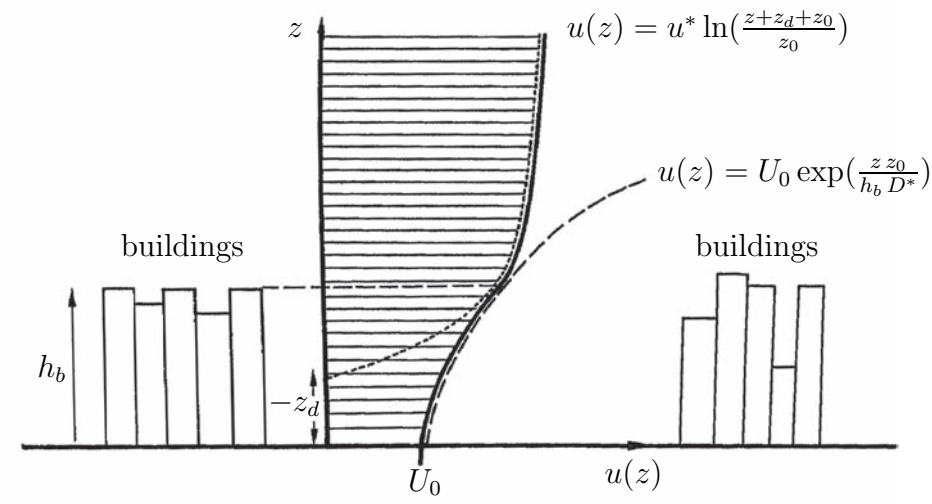

Figure 2.3: Logarithmic and exponential wind profiles in the surface layer above and below building height (Nicholson, 1975)

z_0 and z_d are respectively the *aerodynamic roughness length* and *the zero-plane displacement*. Assessing these two parameters is not a trivial task. Grimmond and Oke (1999) have conducted a sensitivity analysis on seven formulae proposed by different authors to estimate z_d and nine to estimate z_0, covering a wide range of probable urban roughness densities. Figure 2.4 shows the ratio of measured to modelled values of z_d/z_H (first two rows) and z_0/z_H (remaining rows) according to the morphometric method used. The perfect agreement between measured and modelled data, represented by the horizontal dashed line, is hardly ever reached (note that the ordinate is in logarithmic scale).

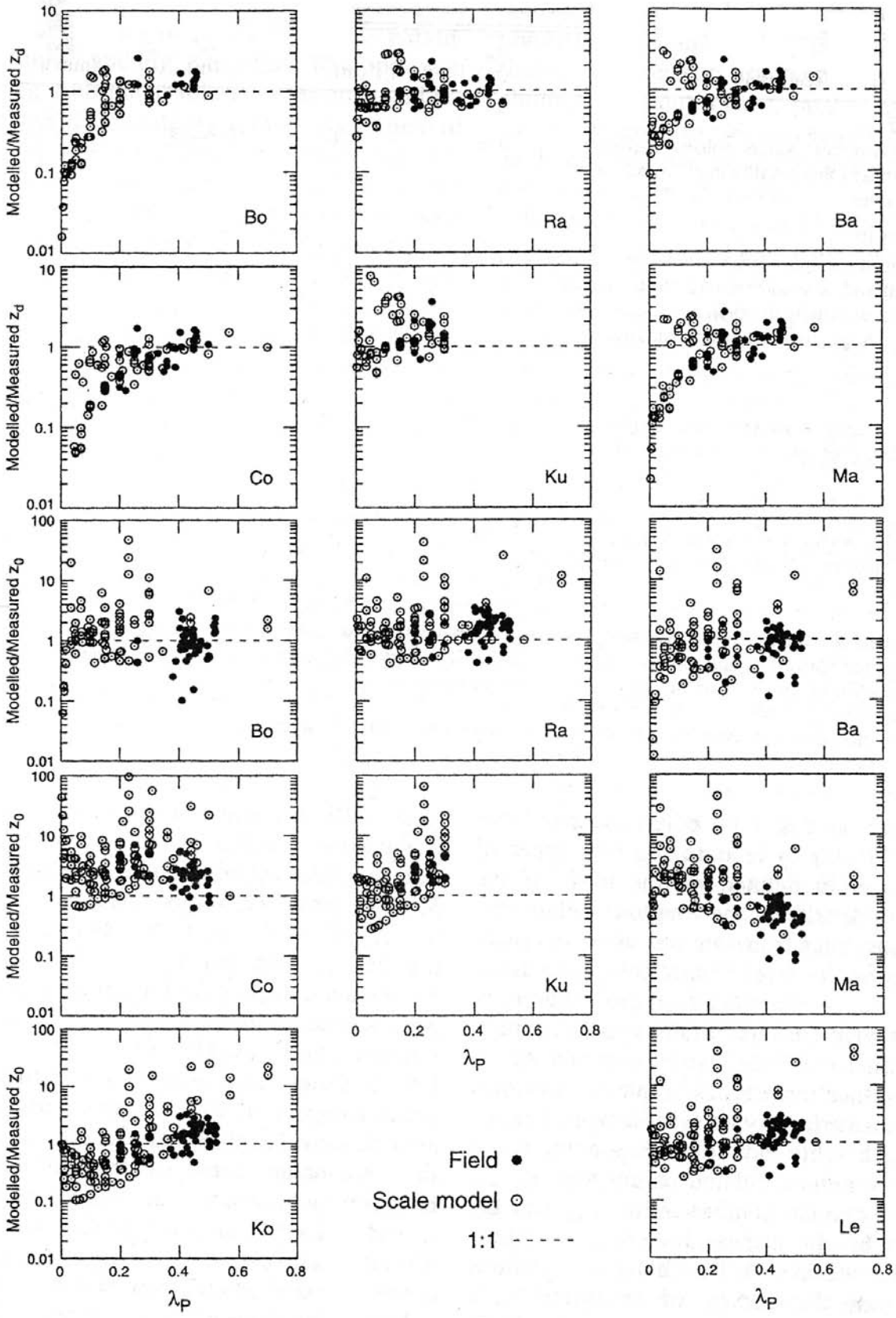

Figure 2.4: ratio of measured to modelled values of z_d/z_H (first two rows) and z_0/z_H (remaining rows) according to the morphometric method used. Perfect agreement between measured and modelled data is unity (horizontal dashed line). The ordinate is in logarithmic scale.(Grimmond & Oke, 1999)

Such discrepancies may show that logarithmic-type laws are not valid in urban context, at least at microscale.

2.2.5 The Pressure Coefficients Issue

Pressure coefficients are used to calculate pressure on façades from the wind speed and direction. They correspond to the ratio between the pressure energy at the solid-fluid interface and the kinetic energy of the flow. The pressure coefficient for a position x and for an angle θ is defined as:

$$C_p(x,\theta) = \frac{p(x) - p_{\text{ref}}}{\frac{1}{2}\ \rho\ v^2} \tag{2.2.4}$$

where $p(x)$ = pressure at position x
p_{ref} = reference pressure
ρ = air density
v = wind speed

The reference pressure must be identical for a given series of coefficients.

Pressure coefficients depend upon the flow structure around the building. As this flow is turbulent, they are not constant, and their average and standard deviation come into play.

Pressure coefficients are thus a function of the building's geometry and of the type of wind, which in turn depends upon the building's environment, *i.e.* upon topography and surroundings.

Pressure coefficients are determined either experimentally in a wind tunnel or numerically using computational fluid dynamics. *In situ* measurements wouldn't be independent on wind conditions during the measurements period.

Eventually, pressure coefficients are used to calculate the wind-induced pressure (2.2.5) and thereby the pressure-induced flow through apertures.

$$\Delta p = \frac{1}{2}\ C_p\ \rho\ v^2 \tag{2.2.5}$$

The fact is that pressure coefficients are at the core of the problematique of airflow exchanges within buildings. The following problems make the pressure coefficients assessment difficult:

- The pressure difference given by equation (2.2.5) is the pressure difference on a closed surface (without openings). If there is an opening through which air may flow, the pressure strongly drops, and the pressure coefficient has no meaning anymore. As mentioned, these coefficients are strongly influenced by the wind direction and the surroundings of the addressed building. They can take any value, depending on the shape, dimension, and location of surrounding buildings. In addition, their value may depend on details that are not modelled in the scale model placed in the wind tunnel or in the computer model.
- Pressure coefficients (initially devised for aircraft studies) are basically used by civil engineers for security purposes in the case of strong winds and are sometimes added security coefficients. Such coefficients are hardly adapted to airflow exchanges. They are to be used in worse-case strong-wind scenarios.
- Most of the pressure coefficients tabulated are provided for isolated buildings.
- Pressure coefficients are evaluated for turbulent wind but for a stable direction, which is rarely the case for medium and low wind speeds.

These difficulties imply the resort of another approach in which pressure coefficients are disregarded.

Chapter 3

State of the Art

This section gives only an overview of the existing models of heat flows and natural ventilation in buildings and focuses on what will be used further on in the current work.

3.1 Modelling Heat Flows in Buildings

Dynamic thermal simulation programs are slowly becoming mainstream tools that are utilized by engineers to design-out, with the collaboration of architects, the need for heating, ventilating and air-conditioning (HVAC) systems, or to optimize these when required. Moreover, with the forthcoming introduction of the European Commission directive on energy performance buildings (European Commission, 2002), many countries are prescribing the use of simulation programs as their national calculation methodology to demonstrate compliance with the Directive's requirements; as is the case in the UK for example.

The first generation of dynamic thermal simulation programs were developed during the 1970s and early 1980s (Clarke, 1977; Gough, 1982). These were essentially command-line interfaces to routines to calculate the dynamic thermal energy exchanges within a building and between this and the outside environment. Subsequent work concentrated on improving the usability of these routines and extending the scope of the core capabilities, for example to incorporate coupled plant (Tang, 1984) and mass flow (Hensen, 1991) modelling. With improved functionality and amidst growing demand for their use by the more pioneering design consultants, attention shifted to proving the validity of their core thermal energy exchange models (Bland, 1992; Judkoff & Neymark, 1995; Lomas *et al.*, 1997). By the mid 1990s, with results from these validation

studies taken on board and with improved usability, attention then focuses upon the addition of further modelling functionality. This included the addition of 3D conduction modelling (Nakhi, 1995), links with ray tracing programs for improved lighting modelling (Janak, 1997), electrical power flow modelling (Kelly, 1998) and embedded computational fluid dynamics (Beausoleil-Morrison, 2000). The results are programs such as *ESP–r* (Clarke, 2001) with a transient finite difference heat flow solver at the core, supporting simultaneous solutions of plant, fluid, electrical power and CFD equation sets.

There has been a recent realization however, that these programs, whilst undoubtedly sophisticated, have some fundamental weaknesses. In particular relating to the (lack of) treatment of human behaviour regarding interactions with passive and active controls and the relationship with the urban context in which the majority of buildings are constructed (Robinson *et al.*, 2003). Work is only now beginning on the former, with the development of stochastic models of human behaviour (Nicol, 2001; Robinson *et al.*, 2003; Roulet *et al.*, 1991), though some good progress has been made regarding the latter.

Many models of various complexities are found in the literature and on the market. These go from the very heavy and comprehensive finite element or finite difference models to simple, quasi-steady state zonal models, now based on international standards (CEN, 1999; CEN, 2004). Simplified dynamic models also exist, allowing to predict temperatures in buildings and on the surface of the building envelope (Roulet *et al.*, 1996; Van der Maas & Maldonaldo, 1997).

3.2 Modelling Natural Ventilation in Buildings

Four types of numerical models exist to solve the problem of airflows in buildings:

1. Computational fluid dynamics (CFD) models. These models are based on the resolution of the fluid dynamics equations. The method divides space into small finite elements in which the Navier-Stokes equation is solved using some simplifying hypotheses.

2. Zonal models. These models divide space in larger zones corresponding to locations where particular phenomena take place. Each zone is processed with an adequate model and the mass transfer between two zones is considered.

3. Nodal models. Mass transfers between building locations, referred to as nodes, are modelled. These models are based on airflow characteristics of openings. Airflows in apertures are a direct function of the pressure difference between both their sides.

4. Empirical models. In these models, buildings are described by means of global parameters, such as the global volume, the total permeability. They are able to reproduce the average ventilation of dwellings of similar conception.

Each of these types of models has its own weaknesses and strengths. CFD models are suited for giving detailed results but are very sensitive to boundary conditions, like the building geometry, and require a high power of computing calculation. They are particularly adapted for instance to describe the discomfort provoked by a vent in a confined area. However, CFD techniques are more and more applied to an entire building or even to a complete built up area.

Figure 3.1: Ground-level wind distribution around Stata Center at the Massachusetts Institute of Technology (yellow: high wind speed, green: moderate wind speed and blue: low wind speed). (Chen, 2004)

Having said that, such applications are not usable in general situations because they require very accurate boundary conditions. This accuracy is hardly ever available, especially since boundary conditions are ever-changing (weather conditions, windows opening, pressure coefficients). Moreover, the problem gets complicated as chaos comes into play.

Nodal models are very commonly used. They allow to calculate airflows between rooms and between a room and the outside if the temperatures of the building zones and of the outside are known or imposed. If not, this kind of model can be coupled with a thermal simulation program calculating temperatures as a function, among other, of airflows. The nodal model, in its turn, calculates airflows as a function, among others, of temperatures.

The CoMIS (Conjunction of Multizone Infiltration Specialists) multizone model is widespread amongst the building physics community (Feustel *et al.*, 1990). It is continuously developed and has been the object of thorough validation processes. A version of this model is a TRNSYS type, allowing automatic coupling with thermal building models.

AIDA and TURBUL, are special cases of nodal models: single-zone zonal models.

3.2.1 Basics of Natural Ventilation in Buildings

3.2.1.1 Wind-driven Natural Ventilation

One of the driving forces of natural ventilation for a building exposed to wind is the wind pressure, given by:

$$\boxed{\Delta p_{\text{wind}} = \frac{1}{2} C_{\text{p}} \rho v^2} \tag{3.2.1}$$

where C_{p} is a pressure coefficient depending upon the wind direction and upon the considered surface of the building envelope, ρ is the air density expressed in kilograms per cubic metre (kg/m^3) and v is the wind speed expressed in metres per second (m/s). Pressure coefficients are determined either experimentally, in wind tunnels, or numerically, using computational fluid dynamics.

3.2.1.2 Buoyancy-driven Natural Ventilation

Stack Pressure

The other driving force of natural ventilation is *stack pressure*, or pressure due to buoyancy. It is induced by density differences between the indoor and outdoor air. When the inside air temperature is greater than that outside, that is when $T_{\text{i}} > T_{\text{e}}$, the air enters through the lower openings and goes out through the upper ones (upward

flow). A downward flow takes place when $T_\mathrm{i} < T_\mathrm{e}$. The height at which transition between inflow and outflow occurs is the *neutral plane* where pressures inside and outside are equal. This height is usually measured and depends upon the overall flow characteristics of the openings.

Let us consider a building with a lower opening at height $h = h_1$, a neutral plane at height h_0 and an upper opening at height h_2 above ground.

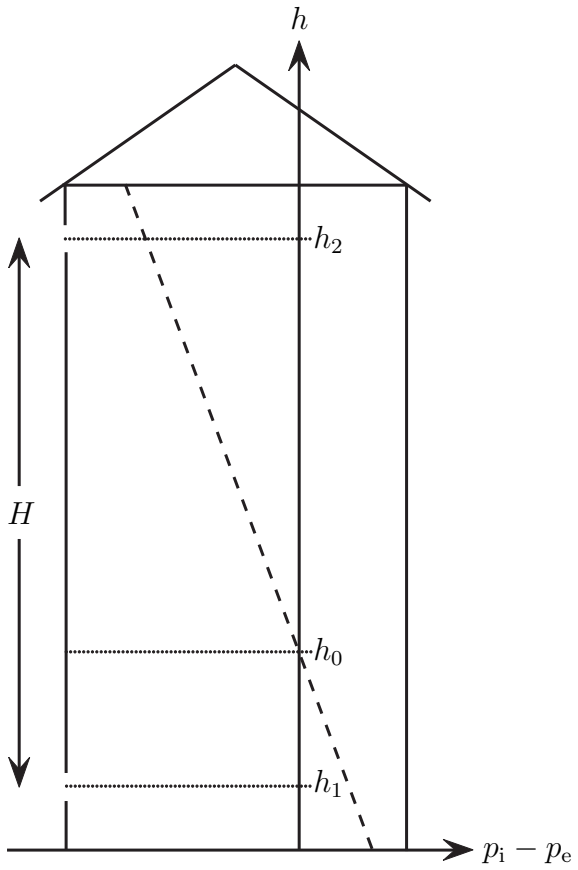

Figure 3.2: Building with a lower opening at height h_1, a neutral plane at height h_0 and an upper opening at height h_2 above ground. The dashed line shows the linear variation of the pressure difference with height when $T_\mathrm{i} < T_\mathrm{e}$, according to equation (3.2.7).

Bernoulli equation applied to the inside air reads:

$$p_\mathrm{i}(h = h_0) + \rho_\mathrm{i} g h_0 + \frac{1}{2}\rho_\mathrm{i} v^2(h = h_0) = p_\mathrm{i}(h = h_1) + \rho_\mathrm{i} g h_1 + \frac{1}{2}\rho_\mathrm{i} v^2(h = h_1) \qquad (3.2.2)$$

where p_i is the internal pressure, ρ_i is the internal air density, g is the acceleration of gravity and v is the air speed.

By neglecting the air speed (an analysis of the orders of magnitude would support this hypothesis), this becomes

$$p_{\mathrm{i}}(h = h_0) + \rho_{\mathrm{i}} g h_0 = p_{\mathrm{i}}(h = h_1) + \rho_{\mathrm{i}} g h_1 \tag{3.2.3}$$

Similarly, for the outside air, one has:

$$p_{\mathrm{e}}(h = h_0) + \rho_{\mathrm{e}} g h_0 = p_{\mathrm{e}}(h = h_1) + \rho_{\mathrm{e}} g h_1 \tag{3.2.4}$$

The pressure difference at the lower aperture between indoors and outdoor is then

$$\Delta p(h = h_1) \overset{\text{def.}}{=} p_{\mathrm{i}}(h = h_1) - p_{\mathrm{e}}(h = h_1) \tag{3.2.5}$$

$$= p_{\mathrm{i}}(h = h_0) - p_{\mathrm{e}}(h = h_0) + (\rho_{\mathrm{e}} - \rho_{\mathrm{i}}) g (h_1 - h_0) \tag{3.2.6}$$

Since, by definition, the pressure difference is equal to zero at the neutral plane level h_0, one has:

$$\Delta p(h = h_1) = (\rho_{\mathrm{e}} - \rho_{\mathrm{i}}) g (h_1 - h_0) \tag{3.2.7}$$

With the same procedure applied to the upper opening, it comes out:

$$\Delta p(h = h_2) = (\rho_{\mathrm{e}} - \rho_{\mathrm{i}}) g (h_2 - h_0) \tag{3.2.8}$$

Equations (3.2.7) and (3.2.8) show that if $\rho_{\mathrm{e}} > \rho_{\mathrm{i}}$ (which means that $T_{\mathrm{e}} < T_{\mathrm{i}}$), an inward flow takes place through the lower aperture ($p_{\mathrm{i}}(h = h_1) < p_{\mathrm{e}}(h = h_1)$), whereas an outward flow occurs through the upper one ($p_{\mathrm{i}}(h = h_2) > p_{\mathrm{e}}(h = h_2)$). An updraught is thus generated. Conversely, if $\rho_{\mathrm{e}} < \rho_{\mathrm{i}}$ a reversed draught is observed.

In both cases, the flows at the apertures contribute to the same draught—either upward or downward. Consequently, the total stack-induced flow is driven by the sum of both pressures:

$$\Delta p_{\text{ stack}} = |\Delta p(h = h_1)| + |\Delta p(h = h_2)| \tag{3.2.9}$$

If $\rho_{\mathrm{e}} > \rho_{\mathrm{i}}$, equation (3.2.9) reads

$$\Delta p_{\text{ stack}} = (\rho_{\mathrm{e}} - \rho_{\mathrm{i}}) g (h_2 - h_1) \tag{3.2.10}$$

because $h_1 < h_0 < h_2$.
If $\rho_{\mathrm{e}} \leq \rho_{\mathrm{i}}$, equation (3.2.9) reads

$$\Delta p_{\text{ stack}} = (\rho_{\mathrm{i}} - \rho_{\mathrm{e}}) g (h_2 - h_1) \tag{3.2.11}$$

The ideal gas equation of state gives:

$$\rho_{\mathrm{e}} - \rho_{\mathrm{i}} = \rho_{\mathrm{i}}(\frac{\rho_{\mathrm{e}}}{\rho_{\mathrm{i}}} - 1) \approx \rho_{\mathrm{i}}(\frac{T_{\mathrm{i}}}{T_{\mathrm{e}}} - 1) = \rho_{\mathrm{i}}(\frac{T_{\mathrm{i}} - T_{\mathrm{e}}}{T_{\mathrm{e}}}) \tag{3.2.12}$$

Therefore, the stack pressure difference between two openings separated by a vertical distance $H = h_2 - h_1$ reads:

$$\boxed{\Delta p_{\text{ stack}} = \rho_{\mathrm{i}}\, g\, H \left| \frac{T_{\mathrm{i}} - T_{\mathrm{e}}}{T_{\mathrm{e}}} \right|} \tag{3.2.13}$$

Mass Airflow Rate

Let us consider a flow entering through the lower aperture ($\rho_{\mathrm{i}} < \rho_{\mathrm{e}}$). The Bernoulli equation for the streamline coming from very far and going through this aperture reads:

$$p_{\mathrm{e}}(h = h_1) + \rho g h_1 + \frac{1}{2}\rho v_\infty^2 = p_{\mathrm{i}}(h = h_1) + \rho g h_1 + \frac{1}{2}\rho v_1^2 \tag{3.2.14}$$

where h_1 is the height of the lower opening and v_1 the air speed within it.

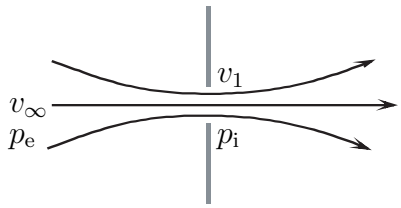

Figure 3.3: Flow entering through an opening.

By assuming that the fluid speed very far from the building is very small ($v_\infty \approx 0$)—we are looking at purely buoyancy-driven natural ventilation—, one has:

$$\Delta p(h = h_1) = \frac{1}{2}\rho v_1^2 \tag{3.2.15}$$

where $\Delta p(h = h_1) = p_{\mathrm{e}}(h = h_1) - p_{\mathrm{i}}(h = h_1)$.
Therefore:

$$v_1 = \sqrt{\frac{2\,|\Delta p(h = h_1)|}{\rho}} \tag{3.2.16}$$

In practice, one is interested in the relationship between the mass airflow rate and the pressure difference on both sides of the opening, more than in (3.2.16). In the expression of the airflow rate, the form of the right-hand term of this equation is preserved, but a

discharge coefficient C_d is included so as to account for the reference pressure change and for the ratio between the speed at the centre of the opening and the discharge speed. The mass airflow rate $\dot{m}_1$ through the the lower aperture of area A_1 is given by:

$$\dot{m}_1 = \rho\, Q = \rho\, C_\mathrm{d}\, A_1 v_1 = \rho\, C_\mathrm{d}\, A_1 \sqrt{\frac{2\,|\Delta p(h = h_1)|}{\rho}} \tag{3.2.17}$$

where Q is the ventilation rate. C_d also accounts for the distortion of the streamlines through the opening and for the turbulence and viscosity effects. Its experimental value is usually 0.6 for definite edges apertures.

Equation (3.2.7) allows to write:

$$\dot{m}_1 = \rho_\mathrm{e}\, C_\mathrm{d}\, A_1 \sqrt{\frac{2(\rho_\mathrm{e} - \rho_\mathrm{i}) g (h_0 - h_1)}{\rho_\mathrm{e}}} \tag{3.2.18}$$

A similar equation can be written for the upper aperture:

$$\dot{m}_2 = \rho_\mathrm{i}\, C_\mathrm{d}\, A_2 \sqrt{\frac{2(\rho_\mathrm{e} - \rho_\mathrm{i}) g (h_2 - h_0)}{\rho_\mathrm{i}}} \tag{3.2.19}$$

Only the height h_0 of the neutral plane is unknown, but it can be appraised by considering that all the air entering the lower opening must exit via the upper one. In other words, by equalizing both flows ($\dot{m}_1 = \dot{m}_2$) expressed by (3.2.18) and (3.2.19), one gets:

$$h_0 = h_2 - \frac{H}{1+X} \qquad \left(= h_1 + X\frac{H}{1+X} \right) \tag{3.2.20}$$

where $H = h_2 - h_1$ and $X = (\rho_\mathrm{i}/\rho_\mathrm{e})(A_2/A_1)^2$.

Using this value of h_0, the mass airflow rate reads (for the exhaust opening):

$$\dot{m} = \dot{m}_2 = \rho_\mathrm{i}\, C_\mathrm{d}\, A_2 \sqrt{\frac{2(\rho_\mathrm{e} - \rho_\mathrm{i}) g \frac{H}{1+X}}{\rho_\mathrm{i}}} \tag{3.2.21}$$

which, using (3.2.12), can further be written as:

$$\dot{m} = \rho_\mathrm{i}\, C_\mathrm{d}\, A_2 \sqrt{\frac{2gH(T_\mathrm{i} - T_\mathrm{e})}{T_\mathrm{e}(1+X)}} \approx \rho_\mathrm{i}\, C_\mathrm{d}\, A_2 \sqrt{\frac{2gH(T_\mathrm{i} - T_\mathrm{e})}{T_\mathrm{i}(1+X)}} \tag{3.2.22}$$

If both openings are of same area, $A(= A_1 = A_2)$, and of same discharge coefficient, C_d, then $X \approx T_\mathrm{e}/T_\mathrm{i}$, and the above mass airflow rate is given by:

$$\boxed{\dot{m} = \rho_\mathrm{i}\, A\, C_\mathrm{d} \sqrt{2\, g\, H\, \left|\frac{T_\mathrm{i} - T_\mathrm{e}}{T_\mathrm{i} + T_\mathrm{e}}\right|}} \tag{3.2.23}$$

where the absolute value has been added to account for the reversed flow ($\rho_\mathrm{e} < \rho_\mathrm{i}$).

3.3 Numerical Weather Prediction Models

Basically developed during the second half of the twentieth century, numerical weather prediction has progressively supplanted methods based upon rules of movement and of evolution of atmospherical structures (fronts and the like). The equations used are those of fluid dynamics in conjunction with simplifications justified by the analysis of orders of magnitude encountered in the atmosphere and according to the scales to be described. The resort to numerical computing is essential to cope with non-linear equations systems with no analytical general solutions.

As soon as 1904, Norwegian geophysicist Vilhelm Bjerknes thought of weather prediction as a deterministic problem with initial values. Between 1916 and 1922, British mathematician, physicist and psychologist Lewis Fry Richardson carried out a six-hour forecast—which turned out to be unrealistic, but subsequently explained—and realized that 64 000 human computers would be necessary to overtake the actual weather evolution. (He imagined a 'forecast factory' made up of a myriad of human calculators synchronized by a conductor.)

After some evolution of the equation system and of the solving methods, his vision came true in 1950 with the first numerical weather prediction by Jule Charney, Ragnar Fjørtoft and John von Neumann (Charney *et al.*, 1950). This model provided quite promising forecasts of the geopotential height near 500 hPa, and could be used as an aid to provide explicit predictions of other variables as surface pressure and temperature distributions.

The first models to be used in an operational way relied on a relation between the pressure field and the wind field, which reduced the number of degrees of freedom. The resulting simplified equations have been referred to as the *filtered equations* and were

used in May 1955 on a three-level model for operational prediction by the US Weather Bureau (Charney, 1954).

The introduction of faster computers led to the use of more and more complex numerical models of the atmosphere. Richardson's more general equations, the *primitive equations*, describing the evolution of a fluid in hydrostatical equilibrium reappeared (Hinkelmann, 1959).

Carrying out relatively long-term predictions required enlarged domains: hemispherical and planetary models came into being. Still, it was worthwhile to have recourse to *Limited Area Models* for providing small-scale short-term forecasts—whose values at the boundary had to be specified from larger-scale models. This resulted in the so-called *nested models* upon which most of the weather services' operational systems are based today.

The water cycle in the atmosphere and the corresponding energy exchanges started to be included in the 1960s (Smagorinsky, 1962). A complete description of the turbulent transfer mechanisms between the ground and the atmosphere, for momentum, sensible heat and water vapour, required the assessment of the turbulent fluxes near the surface. This brought in additional variables such as the ground temperature, the ground dampness, the roughness length or the proportion of vegetation.

Unlike the primitive equations, more elaborate methods allowed, during the 1970s, to explicitly account for convective movements (Kuo, 1965). Taking into account the energy dissipation resulting from the high-altitude breaking of relief waves allowed—relatively recently (Palmer *et al.*, 1986)—to improve the prediction of the jet-streams over mountain areas.

The processing of the physical part has taken more and more importance in comparison to the dynamical one, intensifying the role of parametrization. At the same time, a considerable work has been undertaken in order to accurately determine a given state of the atmosphere by means of available meteorological observations. Several methods of interpolation, in particular taking advantage of statistical properties of variables, were developed.

In the last years, researchers have gone beyond the purely *deterministic prediction* because of the impossibility to provide forecasts beyond a given limit (four to five days for the synoptic scale): the so-called *ensemble prediction* (Buizza *et al.*, 1993), consisting in selecting a judicious set of initial situations, was—and is still—used at the

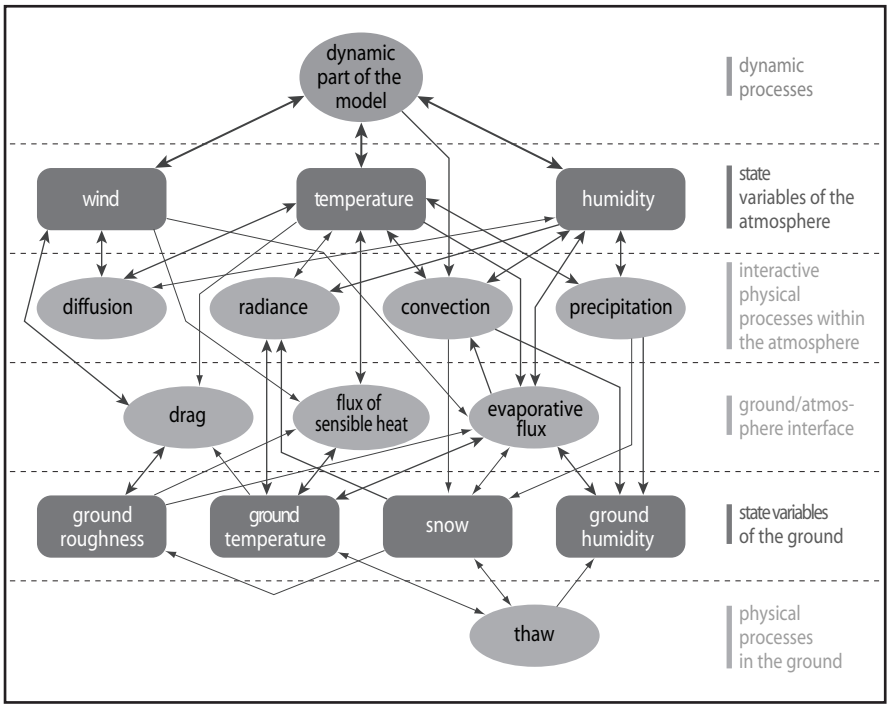

Figure 3.4: Conceptual diagram of physical processes to be included in the numerical weather prediction models and of interactions linking them. (CEPMMT document). (Coiffier, 2000)

European Centre for Medium-Range Weather Forecasts (CEPMMT), based in Reading (UK) and, in a different way, at the National Center for Environmental Prediction (NCEP) in the United States.

It goes without saying that the history of weather forecast is closely linked to the evolution of computers. Without going through the history of simulator, we just mention the use last year (2004) by *Environment Canada* of that date's most powerful computing machine, the Earth Simulator vector super-computer in Yokohama (Japan). The goal was to produce a 1 km horizontal resolution simulation—at that time only possible on that computer—over a large domain, which covers the tropical and extra-tropical re-development of hurricane Earl.

The results of the large scale atmospheric simulation used in this thesis come from the *Lokal-Modell* [1]. This consists of a nonhydrostatic limited-area atmospheric prediction model, whose basic version was developed at the *Deutscher Wetterdienst* (DWD). At present, the following weather services participate within COSMO (Consortium for

[1] see `http://www.cosmo-model.org/`

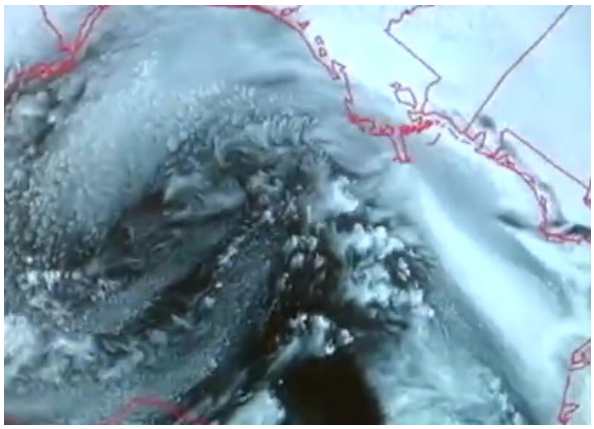

Figure 3.5: Simulation results on the Earth Simulator in Yokohama (Japan) of hurricane Earl. (Naut, 2005)

Small-Scale Modelling):

DWD	Deutscher Wetterdienst, Offenbach, Germany
MeteoSwiss	MeteoSchweiz, Zürich, Switzerland
UGM	Ufficio Generale per la Meteorologia, Rome, Italy
HNMS	Hellenic National Meteorological Service, Athens, Greece
ARPA–SMR	Servizio Meteorologico Regionale di ARPA, Bologna, Italy
AWGeophys	Amt für Wehrgeophysik, Traben–Trarbach, Germany
IMGW	Institute of Meteorology and Water Management, Warsaw, Poland

This model's features are made explicit in section 3.4.

Likewise, the principles of the mesoscale atmospheric model and of its *urban module* are explained in sections 3.5 and 3.6 .

3.4 The *Lokal-Modell*

The weather data used in the URBVENT method (see Chapter 4) come from the atmospheric simulation model referred to as the *Lokal-Modell* (LM). Hereafter are some of this model's basics.

3.4.1 Basic Model Design and Features

The nonhydrostatic fully compressible *Lokal-Modell* (LM) has been developed to meet high-resolution regional forecast requirements of weather services to provide a flexible tool for various scientific applications on a broad range of spatial scales. It captures small-scale severe weather events, at scales where nonhydrostatic effects begin to play an essential role.

The present operational application of LM uses a 7-kilometre grid spacing. The key issue is an accurate numerical prediction of near-surface weather conditions, focusing on clouds, fog, frontal precipitation, and orographically and thermally forced local wind systems.

3.4.2 The Governing Equations

The basic set of equations of the LM model comprises prognostic Eulerian equations for momentum, heat, total mass, mass of water substance and the equation of state.

In order to obtain a suitable mathematical description of atmospheric flow, the atmosphere is considered as a continuum constituted by dry air, water vapour, liquid water and water in solid state forming an ideal mixture.

The system is subject to the external impact due to gravity and Coriolis forces. Internal processes take place as well. The basic conservation laws for momentum, mass and heat are represented by the following budget equations:

$$\rho \frac{\mathrm{d}\vec{v}}{\mathrm{d}t} = -\vec{\nabla} p + \rho\, \vec{g} - 2\, \vec{\Omega} \times (\rho\, \vec{v}) - \vec{\nabla} \cdot \underline{t} \tag{3.4.1}$$

$$\frac{\mathrm{d}\rho}{\mathrm{d}t} = -\rho \vec{\nabla} \cdot \vec{v} \tag{3.4.2}$$

$$\rho \frac{\mathrm{d}q^x}{\mathrm{d}t} = -\vec{\nabla} \cdot \vec{J}^x + I^x \tag{3.4.3}$$

$$\rho \frac{\mathrm{d}e}{\mathrm{d}t} = -p\, \vec{\nabla} \cdot \vec{v} - \vec{\nabla} \cdot (\vec{J}_e + \vec{R}) + \varepsilon\,. \tag{3.4.4}$$

This set of equations has been written in advection form using the Lagrangian time derivative for a more compact representation of the basic conservation laws. Because total mass is conserved, the rate of change of any mass specific quantity ψ can be formulated by:

$$\rho \frac{\mathrm{d}\psi}{\mathrm{d}t} = \frac{\partial(\rho\,\psi)}{\partial t} + \vec{\nabla} \cdot (\rho\,\vec{v}\,\psi) \tag{3.4.5}$$

using the budget operator $\partial(\rho\,\ldots)/\partial t + \vec{\nabla} \cdot (\rho\,\vec{v}\,\ldots)$. With (3.4.5) the prognostic equations can easily be transformed to flux (or budget) form, if required.

The source/sinks terms I^x refer to the processes whereby water undergoes phase changes, and to processes by which water is generated and lost in chemical reactions with the components of dry air.
The following symbols and definitions are used:

t	time
p	pressure
T	temperature
ρ^x	partial density of mixture constituent x
$\rho = \sum_x \rho^x$	total density of the air mixture
$q^x = \rho^x/\rho$	mass fraction (specific content) of constituent x
$v = \rho^{-1}$	specific volume
e	specific internal energy
$h = e + p\,v$	specific enthalpy
$\vec{v}$	barycentric velocity (relative to the rotating Earth)
I^x	sources/sinks of constituent x
$\vec{J^x}$	diffusion flux of constituent x
$\vec{J}_e$	diffusion flux of internal energy (heat flux)
$\vec{R}$	flux density of solar and thermal radiation
$\underline{t}$	stress tensor due to viscosity
$\varepsilon = -\underline{t} \cdot\cdot \vec{\nabla}\vec{v}$	kinetic energy dissipation due to viscosity
$\vec{\Omega}$	constant angular velocity of Earth rotation
$\vec{g}$	apparent acceleration of gravity
$\mathrm{d}/\mathrm{d}t = \partial/\partial t + \vec{v} \cdot \vec{\nabla}$	total (Lagrangian) time derivative operator
$\partial/\partial t$	local (Eulerian) time derivative operator
$\vec{\nabla}$	gradient (Nabla) operator

The index x represents a specific constituent of the mixture:

$$x = \begin{cases} d & \text{for dry air,} \\ v & \text{for water vapour,} \\ l & \text{for liquid water and} \\ f & \text{for ice.} \end{cases} \tag{3.4.6}$$

The equation of state for a moist atmosphere reads

$$v \equiv \rho^{-1} = (R_d\, q^d + R_v\, q^v)\frac{T}{p} + v_l\, q^l + v_f\, q^f \approx (R_d\, q^d + R_v\, q^v)\frac{T}{p} \tag{3.4.7}$$

where R_d and R_v are, respectively, the gas constants for dry air and water vapour; v_l is the partial specific volume of water, v_f is the partial specific volume of ice.

As far as the temperature is concerned, it has to be determined from the internal energy e or, alternatively, from the enthalpy h if the budget equation (3.4.8) for h is used instead of (3.4.4).

$$\rho\frac{\mathrm{d}h}{\mathrm{d}t} = \frac{\mathrm{d}p}{\mathrm{d}t} - \vec{\nabla}\cdot(\vec{J}_e + \vec{R}) + \varepsilon \tag{3.4.8}$$

The so-called *heat equation* (3.4.9) is obtained from (3.4.8) by expansion of the enthalpy $h(T, p, q^x) = \sum_x h_x q^x$ (with $h_x = h_x^0 + c_{p_x}(T - T_0)$):

$$\rho\, c_p\, \frac{\mathrm{d}T}{\mathrm{d}t} = \frac{\mathrm{d}p}{\mathrm{d}t} + l_V I^l + l_S I^f - \vec{\nabla}\cdot(\vec{J}_s + \vec{R}) - \sum_x c_{p_x}\vec{J^x}\cdot\vec{\nabla}T + \varepsilon \tag{3.4.9}$$

T_0 is the absolute zero ($-273.15°$C), h_x^0 is the specific enthalpy of constituent x at T_0, and c_{p_x} is its specific heat at constant pressure. $\vec{J}_s$ is the reduced (or sensible) heat flux, l_V and l_S are, respectively, the latent heat of vaporization and the latent heat of sublimation.

The *heat equation* (3.4.9) reveals clearly the impact of water phase transitions on the temperature.

The total derivative $\frac{\mathrm{d}p}{\mathrm{d}t}$ in (3.4.9) is determined by deriving the equation of state (3.4.7):

$$\frac{\mathrm{d}p}{\mathrm{d}t} = \frac{p}{\rho}\frac{\mathrm{d}\rho}{\mathrm{d}t} + \rho\, R_d\, T\frac{\mathrm{d}\alpha}{\mathrm{d}t} + \rho\, R_d\,(1+\alpha)\frac{\mathrm{d}T}{\mathrm{d}t} \tag{3.4.10}$$

α abbreviates the moisture term:

$$\alpha = (R_v/R_d - 1)\, q^v - q^l - q^f \,. \tag{3.4.11}$$

Defining the diabatic heat production Q_h as

$$Q_h = l_V I^l + l_S I^f - \vec{\nabla} \cdot (\vec{J}_s + \vec{R}) - \sum_x c_{p_x} \vec{J}^x \cdot \vec{\nabla} T + \varepsilon \,, \tag{3.4.12}$$

the moisture source Q_m as

$$Q_m = \rho\, R_d\, T\, \frac{\mathrm{d}\alpha}{\mathrm{d}t} \,, \tag{3.4.13}$$

and the specific heat c_v of moist air at constant volume as

$$c_v = \sum_x c_{vx}\, q^x \,, \tag{3.4.14}$$

yields:

$$\frac{\mathrm{d}p}{\mathrm{d}t} = -\frac{c_p}{c_v}\, p\, \vec{\nabla} \cdot \vec{v} + (\frac{c_p}{c_v} - 1)\, Q_h + \frac{c_p}{c_v}\, Q_m \tag{3.4.15}$$

Eventually, the following set of equations can be applied:

$$\boxed{\begin{aligned} \rho \frac{\mathrm{d}\vec{v}}{\mathrm{d}t} &= -\vec{\nabla} p + \rho\, \vec{g} - 2\, \vec{\Omega} \times (\rho\, \vec{v}) - \vec{\nabla} \cdot \underline{t} \\ \frac{\mathrm{d}p}{\mathrm{d}t} &= -\frac{c_p}{c_v}\, p\, \vec{\nabla} \cdot \vec{v} + (\frac{c_p}{c_v} - 1)\, Q_h + \frac{c_p}{c_v}\, Q_m \\ \rho\, c_p \frac{\mathrm{d}T}{\mathrm{d}t} &= \frac{\mathrm{d}p}{\mathrm{d}t} + Q_h \\ \rho \frac{\mathrm{d}q^x}{\mathrm{d}t} &= -\vec{\nabla} \cdot \vec{J}^x + I^x \\ \rho &= \frac{p}{R_d(1+\alpha)\, T} \end{aligned}} \tag{3.4.16}$$

(3.4.16) forms a *closed* set of equations, likely to predict variables of state $\vec{v}$, T, p, ρ and the mass concentrations q^v, q^l and g^f, provided that the other variables are known.

One can note that exact mass conservation is not guaranteed, as the continuity equation (3.4.2) is not explicitly used. A set of closed equations bringing in (3.4.2) exists, but is almost never used for practical reasons.

This set (3.4.16) of basic equations is defined in terms of differential operators and is thus, in a formal mathematical sense, only valid in the limit when the time interval and the spatial increments approach zero.

However, for a physically meaningful interpretation, such increments should be extended enough to contain a sufficiently large number of molecules to apply statistical thermodynamics. In the atmosphere, this compromise limits the direct application of equations (3.4.16) to space scales on the order of about 1 centimetre and to time scales of about one second.

Yet the domains considered cover scales ranging from 100 m up to 100 km horizontally and up to 10 km vertically. Obviously, this makes the explicit simulation of airflows with grid spacings on the order of one centimetre impossible. Thereby, the LM model averages this set of equations over specified space and time scales, which can be identified with the grid spacings and the time steps of the numerical model.

In practice, any variable ψ is decomposed according to

$$\psi = \overline{\psi} + \psi' \tag{3.4.17}$$

where

$$\overline{\psi} = \frac{1}{\Delta V \Delta t} \int \int \psi \, \mathrm{d}t \, \mathrm{d}V \tag{3.4.18}$$

represents the average of ψ over the finite time interval Δt and the volume element ΔV formed by the grid spacings Δx, Δy and Δz.

The following decomposition is used as well:

$$\psi = \widehat{\psi} + \psi'' \tag{3.4.19}$$

with

$$\widehat{\psi} = \overline{\rho \, \psi} / \overline{\rho} \qquad \text{and} \qquad \widehat{\psi''} = 0, \tag{3.4.20}$$

where $\widehat{\psi}$ is the mass-weighted average of ψ and ψ'' is the deviation of ψ from its mass-weighted mean value.

If the grid spacings defining the domain ΔV for averaging are not too large, the fluctuating part of the flow can be identified with purely *turbulent* motions. Actually, this strongly fluctuating part of the flow (associated with ψ') is nonresolvable and has to be parameterized, *i.e.* formulated in terms of the grid scale variables.

Averaging the initial budget equations and the enthalpy budget equation (3.4.8) gives rise inside them to the following correlation products describing *subgrid scale transport processes*:

$\underline{T} = \overline{\rho \vec{v''} \vec{v''}}$ turbulent flux of momentum (*Reynolds stress tensor*);

$\vec{F^x} = \overline{\rho \vec{v''} q^x}$ turbulent flux of constituent x ($\sum_x \vec{F^x} = \vec{0}$);

$\vec{F_h} = \overline{\rho \vec{v''} h}$ turbulent flux of enthalpy;

$B_h = \overline{\vec{v''} \cdot \vec{\nabla} p}$ source term of enthalpy due to buoyant heat and moisture fluxes.

After the basic equations are rewritten in their averaged form, including the heat equation, the thermodynamical part undergoes some simplifications.

Due to numerical problems ensuing from convergence of the meridians and from the resulting pole singularities, the 'natural' rotating spherical coordinate system is abandoned in aid of a rotated one. In a first step, the Z-axis is tilted toward a new pole P_N, as shown in Figure 3.6. Then the axis system is transformed to orthogonal spherical coordinates (λ, φ, r) in which λ is longitude, φ is latitude and r is the distance from the Earth's centre.

Finally, the coordinates system is transformed in order to follow the terrain.

After these transformations, we arrive at expressions in the form of partial derivatives equations for the following variables:

- Both components of the horizontal wind speed;
- The vertical wind speed;
- The perturbation pressure;
- The temperature;
- The water vapour specific content;
- The liquid and solid forms of water specific content;
- The total density of air;
- The turbulent kinetic energy.

These model equations have to be set in a discretized form. Eventually, initial and boundary conditions must be provided to the model. In such a limited area model, only the lower boundary is physical. The boundaries at the top or at the sides of the model domain are usually artificial. In the present version of LM, an externally specified time dependant *forcing*[2] is taken into account in a one-way interactive nesting method.

[2]The *forcing* consists in assigning to the boundary values of the the nested model variables the values of those of the larger model taken at the frontier between both models.

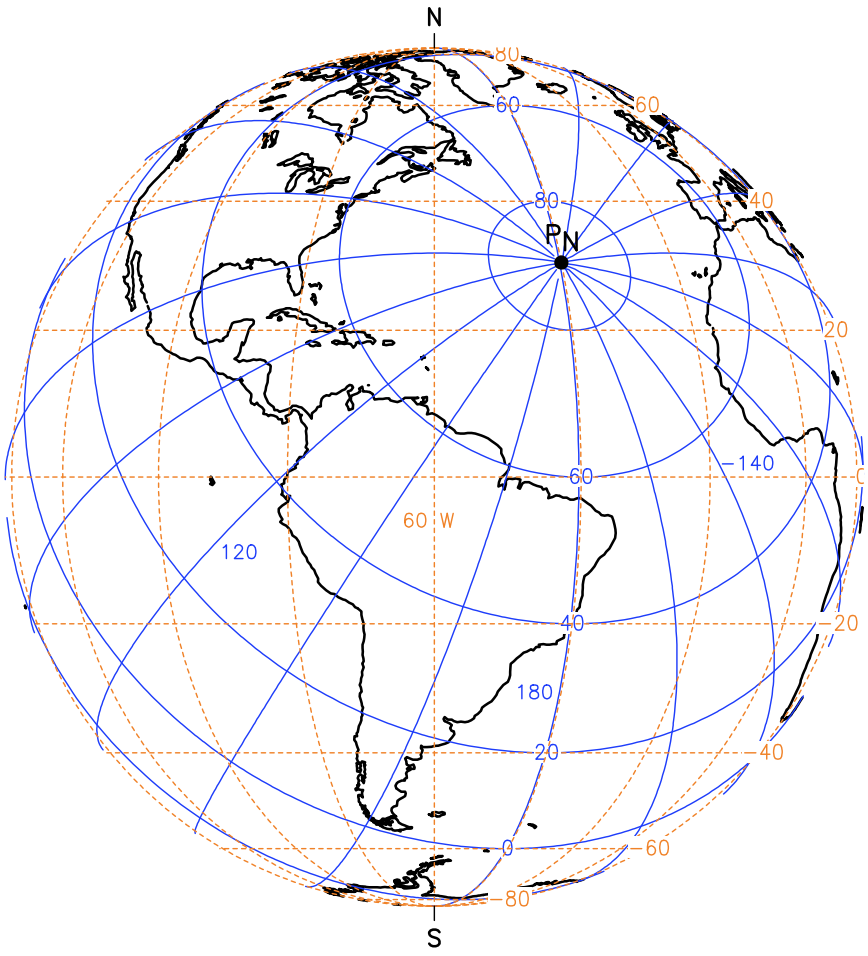

Figure 3.6: Rotated longitude and latitude

3.5 Mesoscale Atmospheric Modelling

One of the weak points of the LM model (*Lokal-Modell*) is that is does not factor in the effects of the urban tissue, particularly the buildings. Furthermore, the horizontal and vertical grid resolution required for urban applications is higher than the one offered by LM.

The mesoscale model selected here, referred to as FVM (*Finite Volume Model*), was partly developed at the *Air and Soil Pollution Laboratory* of the Swiss Federal Institute of Technology in Lausanne (Clappier *et al.*, 1996). Subsequent developments have been carried out by Martilli (2001) and Roulet (2004). The *interpolation preprocessor* has been reprogrammed nearly from scratch as part of the present work, in order to enable FVM to take LM's result as boundary and initial conditions and to make it as independent of the input data as possible (so as to use any weather service's boundary conditions).

Attention is drawn here that FVM's simulation results haven't been included in URBVENT's software tool (see Chapter 4), as LM's were. The reason for this will become clear as soon as the basics of the *urban module* embedded in FVM are presented: it would be impossible (at least within the scope of this PhD work) to tune the urban parameters of each existing city across Europe, as for instance the buildings' height distribution. Not to mention that approximately 45 levels of simulation results (from ground to an altitude of approxiamtely five kilometres) are required around urban areas as boundary conditions for FVM (instead of the sole level used in URBVENT). Needless to say that this makes a great deal of data.

As a result, an analysis of the situation in the region of Basel (Switzerland) is proposed in Chapter 5.4. The main objective is to spot the differences between the results provided by both models, and to see if the new one matches better on site measurements.

Furthermore, FVM's results are used in Chapter 6 over a restricted region (the same region of Basel) and over a restricted time period in order to assess its natural ventilation potential .

3.5.1 The Mesoscale

Two commonly used approaches exist for defining the scales: the dynamical and the scale-analysis approach. The mesoscale ranges from 2 to 2000 kilometres and involves a large set of phenomena going from hurricanes to internal gravity waves, as shown in Table 3.1.

Table 3.1: Orlanski's classification of scales. Scales of motion and related meteorological phenomena with their time and space scales. (After Orlanski (1975))

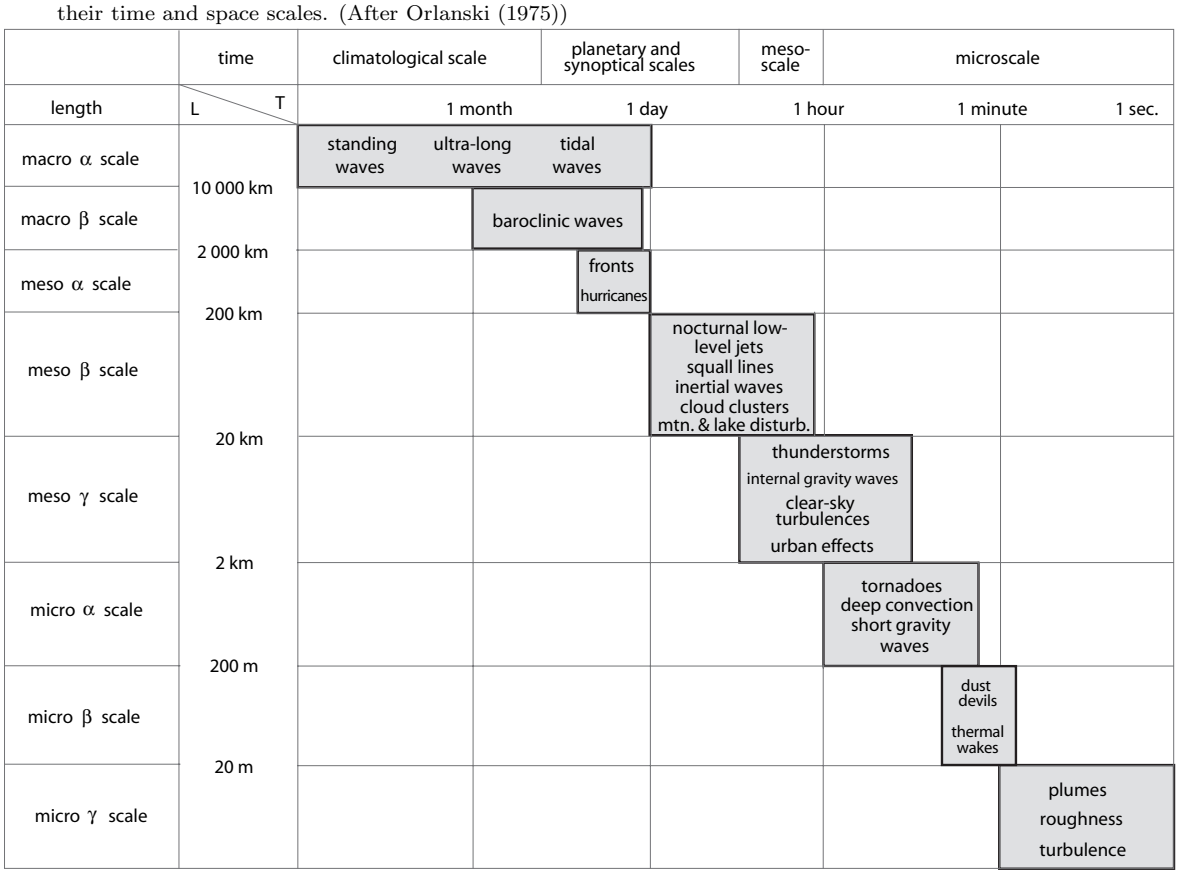

Mesoscale phenomena taking place in the FVM model are influenced both by those occurring in LM and in the urban canopy, namely in the microscale.

3.5.1.1 FVM's Grid

FVM was initially implemented for air quality studies. It uses a finite-volume method for space discretisation. The resulting mesh is terrain-following (deformable), and is thus able to take into account the topography of the domain. The model is typically

applied over areas of 200 by 200 km horizontally, and reaches up to heights of 10 km above the Earth's surface so as to cover the entire troposphere. The volume thus defined is discretised to provide a horizontal resolution with cells of 1 to 5 km and a vertical resolution of typically 10 m close to the ground, where high accuracy is needed, to 1000 m at the top of the domain, near the tropopause.

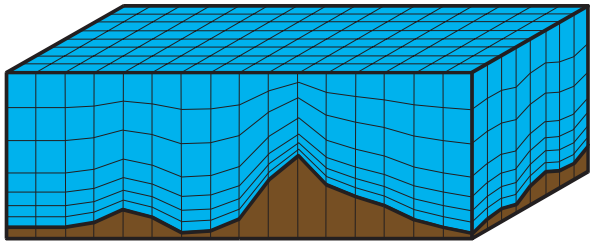

Figure 3.7: Schematic representation of the most commonly used mesh in FVM. After Junier (2004)

3.5.2 The Governing Equations

In the model, the following conservation equations ((3.5.1) to (3.5.5)) are solved in each cell of the domain:

3.5.2.1 Conservation of Mass

The conservation of mass is expressed as follows:

$$\boxed{\frac{\partial \rho}{\partial t} + \vec{\nabla} \cdot (\rho \, \vec{v}) = 0} \tag{3.5.1}$$

where $\vec{v}$ is the wind velocity and ρ the air density. On typical scales of velocity and length for the motions in the mesoscale range, $\partial\rho/\partial t$ is much smaller than $\vec{\nabla} \cdot (\rho \, \vec{v})$, and can therefore be neglected (anelastic approximation).

Here, and in the following, variables are Reynolds averaged. Primed letters (*e.g.* ${v_z}'$) stand for their respective turbulent fluctuations.

Equations (3.5.3) to (3.5.5) hereafter have been written in advection form using the Lagrangian time derivative for a more compact representation of the basic conservation

laws. Because total mass is conserved, the rate of change of any mass-specific quantity ψ can be formulated by

$$\rho \frac{\mathrm{d}\psi}{\mathrm{d}t} = \frac{\partial(\rho\,\psi)}{\partial t} + \vec{\nabla} \cdot (\rho\,\vec{v}\,\psi) \tag{3.5.2}$$

using the budget operator $\partial(\rho \ldots)/\partial t + \vec{\nabla} \cdot (\rho\,\vec{v} \ldots)$.

$\partial(\rho\,\psi)/\partial t$ can always be interpreted as the storage of ψ and $\vec{\nabla} \cdot (\rho\,\vec{v}\,\psi)$ as its mean transport (advection).

3.5.2.2 Conservation of Momentum

The conservation of momentum is expressed as follows:

$$\boxed{\rho \frac{\mathrm{d}\vec{v}}{\mathrm{d}t} = -\vec{\nabla}p + \rho \frac{\theta'}{\theta_0}\,\vec{g} - 2\,\vec{\Omega} \times (\vec{v} - \vec{v^G}) - \frac{\partial \rho\,\overline{\vec{v'} v_z{}'}}{\partial z} + \vec{D_u}} \tag{3.5.3}$$

in which p is the pressure, θ_0 is the potential temperature[3] of the reference hydrostatic state, $\theta' = \theta - \theta_0$ is the fluctuation relative to this state, $\vec{g}$ is the gravity acceleration, $\vec{\Omega}$ is Earth's rotation angular velocity and $\vec{v^G}$ is the geostrophic wind velocity.

The interpretation of the terms of equation (3.5.3) is the following:

$\vec{\nabla}p$	pressure gradient force
$\rho\,(\theta'/\theta_0)\,\vec{g}$	vertical action of gravity (buoyancy)
$2\,\vec{\Omega} \times (\vec{v} - \vec{v^G})$	influence of the Earth's rotation (Coriolis effects)
$\partial(\rho\,\overline{\vec{v'} v_z{}'})/\partial z$	turbulent transport (the fluctuations around mean transport)
$\vec{D_u}$	forces induced by interactions between solid surfaces and airflow (*e.g.* drag forces and frictional forces)

Equation (3.5.3) is in the non-hydrostatic form and the buoyancy term is written using the Boussinesq approximation (see section 3.5.3). This explains the difference with equation (3.4.1).

[3]The potential temperature is the temperature an unsaturated air parcel attains if brought adiabatically from its altitude down to a pressure of $p_0 = 1000$ mb (approximately at sea level).

3.5.2.3 Conservation of Energy

The conservation of energy is expressed as follows:

$$\boxed{\rho \frac{\mathrm{d}\theta}{\mathrm{d}t} = -\frac{\partial \rho \overline{v_z'\theta}}{\partial z} - \frac{1}{C_p}\left(\frac{p_0}{p}\right)^{R/C_p} \frac{\partial R_{\mathrm{LW}}}{\partial z} + D_\theta} \tag{3.5.4}$$

where θ is potential temperature, C_p is the specific heat at constant pressure of the air, R is gas constant, p_0 is the reference pressure (1000 mb) and R_{LW} is the long wave radiation flux. D_θ denotes the impact of the sensible heat fluxes from the 'solid' surfaces (ground or buildings) on the potential temperature budget.

The interpretation of the terms is the following:

$\partial(\rho\overline{v_z'\theta})/\partial z$	turbulent transport of heat (the fluctuations around mean transport)
$(1/C_p)\,(p_0/p)^{R/C_p}\,\partial R_{\mathrm{LW}}/\partial z$	loss through long-wave emissions
D_θ	the impact of sensible heat fluxes from solid surfaces on the potential temperature budget

3.5.2.4 Conservation of Moisture

The conservation of moisture is expressed as follows:

$$\boxed{\rho \frac{\mathrm{d}H}{\mathrm{d}t} = -\frac{\partial \rho \overline{v_z'H'}}{\partial z} + D_h} \tag{3.5.5}$$

where H is absolute humidity of the air. In this equation, condensation and cloud formations are not considered.

The interpretation of the terms is the following:

$\partial(\rho\overline{v_z'H'})/\partial z$	turbulent transport of moisture
D_h	the impact of the latent-heat fluxes from the ground on the humidity budget

The D-terms in equations (3.5.3) to (3.5.5) arise from the consideration of urban elements, and are solved by the urban module presented below.

3.5.2.5 Poisson Equation for Pressure

In the numerical resolution, the mass equation (3.5.1) is combined with the momentum equation (3.5.3) to yield the following Poisson differential equation for pressure:

$$\boxed{\vec{\nabla}^2 p = \vec{\nabla} \cdot \vec{F}} \tag{3.5.6}$$

with $\vec{F}$ defined as ($i = 1, 2, 3$):

$$F_i = -\vec{\nabla} \cdot (\rho \, \vec{v} \, v_i) + \left[\rho \, \frac{\theta'}{\theta_0} \, \vec{g} - 2 \, \vec{\Omega} \times (\vec{v} - \vec{v^G}) - \frac{\partial \rho \, \overline{\vec{v'} v_z'}}{\partial z} + \vec{D_u} \right] \cdot \vec{e_i} \tag{3.5.7}$$

This Poisson equation actually expresses the propagation of acoustic waves through the domain. A study of orders of magnitude shows that this propagation is practically instantaneous.

Equations (3.5.3), (3.5.4), (3.5.5) and (3.5.6) are solved explicitly, except for the pressure which is solved implicitly.

The algorithm used for the transport of scalar variables (temperature, wind, etc.) is based on a third-order Parabolic Piecewise Method (Collella & Woodward, 1984), which has been extended for multidimensional applications (Clappier, 1998).

3.5.2.6 Turbulent Fluxes

The vertical turbulent fluxes above the ground surface are computed with common K-theory (or gradient-transport theory). This theory is a first-order closure approximation for solving the description of turbulent flow. It retains prognostic equations for only the zero-order mean variables such as temperature, wind, and humidity:

$$\overline{u_i' \, \xi'} = -K_i \, \frac{\partial \overline{\xi}}{\partial x_i} \tag{3.5.8}$$

where ξ is the mean part and ξ' the turbulent part of a variable that may be the potential temperature, the air humidity, a velocity component and K_i the diffusion coefficient.

The vertical turbulent-transfer coefficient K_z (*i.e.* for $i = 3$) is parameterized with a $k - l$ closure from Bougeault and Lacarrère (1989). For that purpose, a prognostic

equation is solved to compute the turbulent kinetic energy (TKE), which in turn is used to calculate the vertical diffusion coefficients K_z:

$$K_z = C_k \cdot l_k \cdot \sqrt{E} \tag{3.5.9}$$

where C_k is a numerical constant, l_k is a characteristic length, and E is the turbulent kinetic energy. Turbulent fluxes in the surface layer (the lower part of the boundary layer) are computed with an adaptation of the Monin-Obukhov Similarity Theory (Louis, 1979).

Inputs needed for this parameterisation are the roughness length, surface temperature, and moisture. Roughness lengths can be obtained from GIS data bases. Surface temperature and moisture can be calculated with a soil module (Tremback & Kessler, 1985), which solves two prognostic equations for temperature and for water content of the soil.

3.5.3 Hypotheses

3.5.3.1 Boussinesq Approximation

The Boussinesq approximation is applied in the field of buoyancy-driven flow. It states that density differences are sufficiently small to be neglected, except where they appear in terms multiplied by g, the acceleration due to gravity. The essence of the Boussinesq approximation is that the difference in inertia is negligible but gravity is sufficiently strong to make the specific weight appreciably different between the two fluids.

The approximation's advantage arises because when considering a flow of, say, warm and cold air of densities ρ_1 and ρ_2 one needs only consider a single density ρ: the difference $\rho_1 - \rho_2$ is negligible. Dimensional analysis shows that, under these circumstances, the only sensible way that acceleration due to gravity g should enter into the equations of motion is in the reduced gravity g' where

$$g' = g\,\frac{\rho_1 - \rho_2}{\rho_1} \quad . \tag{3.5.10}$$

Furthermore, neglecting the pressure variation in comparison to the potential temperature variation yields:

$$\frac{\rho_0 - \rho}{\rho_0} \approx \frac{\theta - \theta_0}{\theta_0} \quad , \tag{3.5.11}$$

in which ρ_1 and ρ_2 have been replaced by ρ_0 (the density at hydrostatic state) and by ρ respectively. (3.5.10) and (3.5.11) give rise to the buoyancy term in the momentum conservation equation (3.5.3).

3.5.3.2 Anelastic Approximation

The objective of the anelastic approximation is the same as the Boussinesq approximation, but it can be applied to non-acoustic atmospheric motions. The key point of the approximation is dropping the time derivative term in the continuity equation:

$$\frac{\partial \rho}{\partial t} \ll \vec{\nabla} \cdot (\rho \, \vec{v}) \tag{3.5.12}$$

3.6 Urban Atmospheric Modelling

Several important phenomena are not accounted for when likening the urban tissue to a rough surface with modified thermal properties, which is the traditional approach usually adopted in mesoscale models. First, vertical building surfaces induce drag forces accompanied with an associated loss of momentum. Then, building structures create shadowing zones as well as radiation trapping areas, leading to modifications in the heat flux. Finally, they generate additional turbulence in the kinetic energy.

In addition, the traditional approach will locate the sink of momentum solely at the lowest level of the model. Yet this sink should be distributed through the urban canopy levels.

3.6.1 Description

The urban module presented hereafter was proposed by Martilli (2001; 2002) and represents the city as a combination of street canyons. Each urban class is defined by a set of building rows characterized by:

- a given width of roads (W);
- a given broadness of buildings (B);
- a given distribution of building heights ($\gamma(z)$);
- several street orientations;
- several material properties.

These canyons are represented in Figure 3.8 in which capital indexes refer to grid cell centres, small letters to grid cell faces. H stands for horizontal values, V for vertical, whereas U stands for urban values. F denotes any flux and S surfaces.

3.6.2 Calculation of Urban Effects

The module calculates every urban surface induced effect separately, in proportion to the corresponding surface fraction at each level of the urban grid.

For instance, even though the applicability of the Monin-Obukhov Similarity Theory in this case is questionable, the momentum loss is computed by means of classical surface layer theory (Louis, 1979), aside from the fact that the loss is distributed

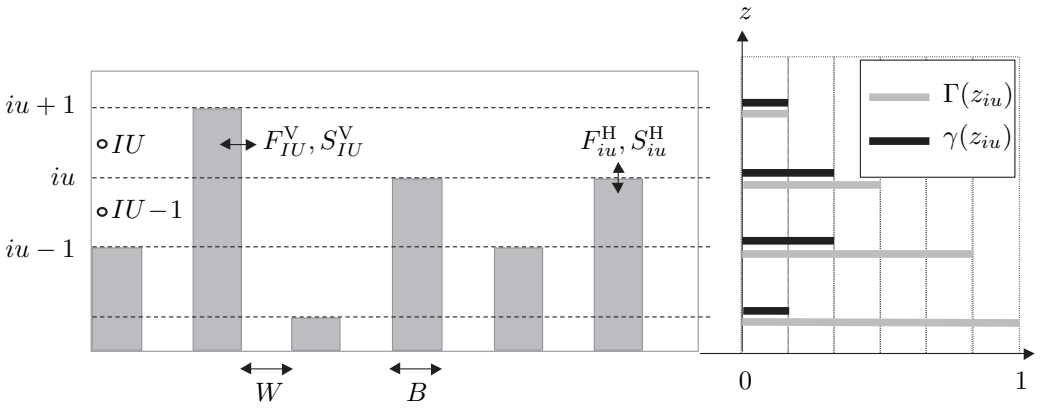

Figure 3.8: Schematic representation of the numerical grid in the urban module. Where W is streets width, B is buildings width, iu are the face and IU centre of the urban model levels, $\gamma(z_{iu})$ density of building of height z_{iu} and $\Gamma(z_{iu})$ density of buildings higher than z_{iu}. After Martilli (2001).

amidst the canopy levels. Horizontal and vertical surfaces are processed separately as well as for the purpose of heat flux modifications. The heat diffusion obeys to constant user-defined soil and wall temperatures[4].

As regards shadowing and radiation trapping effects, view factors are computed for each urban grid layer while multiple reflections of the incident solar radiation and long-wave reemission between walls and canyon floors are considered at each urban grid level (see Figure 3.9, left-hand side).

The urban module computes the D-terms in the conservations equations (3.5.3) to (3.5.5) while taking into account the reduction by the presence of buildings of both the initial air volume of the grid cells and the initial interface of two neighbouring cells. Thus, any of these D-terms (of mesoscale grid cell I) is given by:

$$D_{AI} = \frac{F^{\mathrm{H}}_{a\ I} + F^{\mathrm{V}}_{a\ I}}{V_{AI}} \tag{3.6.1}$$

with $F^{\mathrm{H}}_{a\ I}$ the horizontal flux (streets and roofs) and $F^{\mathrm{V}}_{a\ I}$ the vertical flux (walls) of any variable A (temperature, wind speed or humidity). V_{AI} is the *reduced* air volume. Fluxes indexed by I are the average (interpolation to the grid of the mesoscale model) of the fluxes computed on the urban grid.

[4]It is planned in a future work to think of buildings as constructions exchanging air with their environment and having varying temperatures, in the same fashion as it was made for Urbvent.

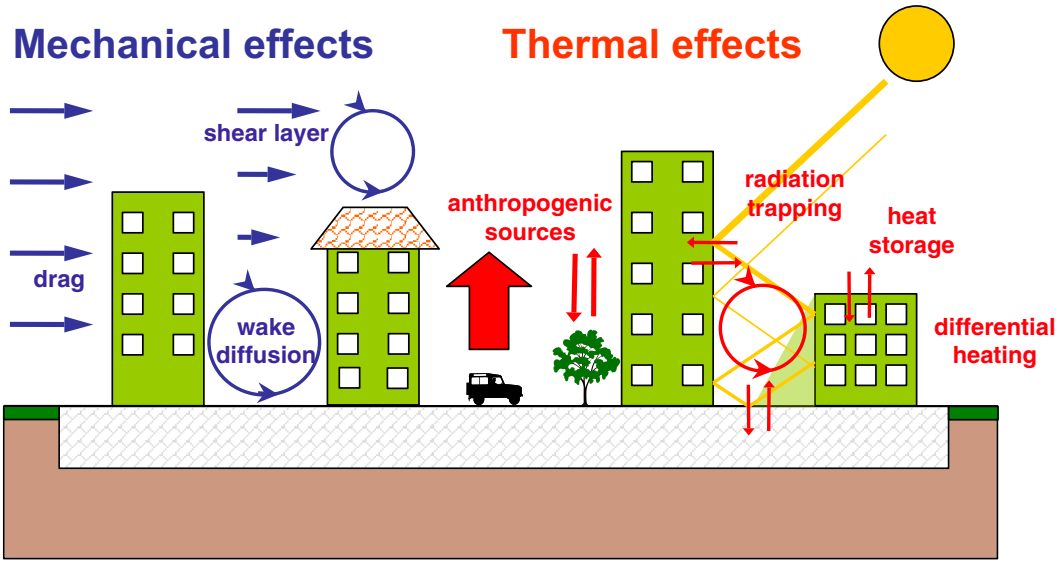

Figure 3.9: Main building effects. (Anthropogenic sources are not accounted for in the urban module.) Source: Air and Soil Pollution Laboratory (LPAS)

Concerning the areas of the horizontal air interfaces between any two cells, their reduction due to the presence of buildings has an impact on vertical turbulent transport. As less air surface area is available for vertical exchange between two cells, the turbulent transport is modified as follows:

$$\frac{\partial \rho \overline{wa'}}{\partial z} = \frac{1}{V_{AI}} \left(\rho \overline{wa'_i} S_{Ai} - \rho \overline{wa'_{i+1}} S_{Ai+1} \right) \tag{3.6.2}$$

where S_{Ai} is the area of the air interface between the grid cells I and $I-1$ (total surface area less the surface area occupied by buildings), ρ is the air density, and $\overline{wa'}$ is the vertical turbulent transport of a scalar A (temperature, wind speed or humidity).

3.6.3 Vegetation in Urban Zones

Vegetation areas present within urban zones (such as parks and gardens) are responsible for latent heat fluxes within these zones. It is very important to consider such vegetation areas in the calculations, since in the urban module, dry soils are assumed by default. The model needs landuse data as input, in order to determine whether a cell is urban or rural, and, thus, to calculate the corresponding fluxes. A modification in the model has been developed in the frame of Roulet's work (2004), in order to be able to consider mixed landuse within one cell. For a calculation of the associated heat

fluxes, each cell at ground is defined in terms of an urban class, a rural class, and a ratio of rural to urban soil coverage. For the mixed cells containing both urban and rural soil coverage, fluxes are first calculated separately for the two types of surface (with urban parameterisation for the urban part, and through the soil module of the mesoscale model for the rural part), and are then weighted according to the percentages of each soil coverage type:

$$\Phi = \alpha \cdot \phi_{\text{rural}} + (1 - \alpha) \cdot \phi_{\text{urban}} \tag{3.6.3}$$

where Φ represents a meteorological variable or flux in the mesoscale model, α is the percentage of rural soil coverage in the cell, ϕ_{rural} is the rural contribution, and ϕ_{urban} is the urban contribution to the scalar or flux considered.

Chapter 4

The URBVENT Method

4.1 Introduction

Natural ventilation potential (NVP) may be defined as the possibility of ensuring an acceptable indoor air quality through natural ventilation only. *Passive cooling potential* (PCP) can also be defined as the possibility of ensuring an acceptable indoor thermal comfort in summer by solely using natural ventilation.

The three objectives of natural ventilation in buildings are indoor air quality, thermal comfort and energy savings. The methodology proposed in this chapter provides an assessment of the natural ventilation potential for indoor air quality, while taking into consideration the other objectives. More precisely, 'comfort' requirements impose the appropriate ventilation strategies to be used for each given meteorological situation. On the basis of these strategies, the methodology evaluates the appropriateness of a given location to natural ventilation.

Ensuring an acceptable indoor air quality or cooling down the building structure by natural ventilation is subject to many conditions that depend upon the site *e.g.*:

- outdoor air quality;
- outdoor air temperature and moisture;
- outdoor noise;
- local winds or global winds;
- urban structure

or upon the building *e.g.*:

- indoor pollutant sources;

- indoor heat sources and stored heat;
- indoor air quality requirements;
- position and size of ventilation openings;
- indoor temperature;
- orientation of building;
- internal air-path distribution.

Since the details of the building needed for airflow estimation cannot be known until the project is well advanced, it is interesting to assess the natural ventilation potential of the site itself, regardless of the building. In this way, an analysis of the results can provide the type of ventilation to which a given site, as well as the type of building that should be built or how to refurbish an existing one.

4.2 Driving Forces of Natural Ventilation

4.2.1 Wind Pressure

As mentioned in sections 2.2.5 and 3.2.1.1, one of the driving forces of natural ventilation for a building exposed to wind is the wind pressure, given by:

$$\Delta p_{\text{wind}} = \frac{1}{2} C_{\text{p}} \rho v^2 \tag{4.2.1}$$

where C_{p} is a pressure coefficient depending upon the wind direction and upon the considered surface of the building envelope, ρ is the air density expressed in kilograms per cubic metre (kg/m^3) and v is the wind speed expressed in metres per second (m/s). Pressure coefficients are determined either experimentally, in wind tunnels, or numerically, using computational fluid dynamics.

4.2.1.1 Surface Winds

One problem in the assessment of natural ventilation potential is the weather data. Measurements are available only at meteorological stations and at airports. An alternative is to use data obtained from weather models that are used for forecasting. These models give good results and have the advantage that values are available for relatively high resolution (of the order of kilometres). The inaccuracy introduced by the model

is smaller than the inaccuracy introduced by data transfer in a homogeneous site. The wind data used in the URBVENT project come from the archive of the Swiss Federal Office of Meteorology and Climatology, hereafter referred to as MeteoSwiss. These data provide the wind speed and direction at an altitude of 10 meters above the ground for 125 125 points across Europe with a spatial resolution of 7 kilometres and a temporal resolution of four times per day. The model that the data come from, called the *Lokal-Modell* (LM), is a prediction model that solves the primitive hydro-thermodynamical equations describing compressible non-hydrostatic flow in a moist atmosphere by using the finite difference method (see section 3.4). The predictions, which have proved to fit the measurements well, use continuously new initial conditions and have been archived for several years, making it possible to carry out a statistical analysis of the data.

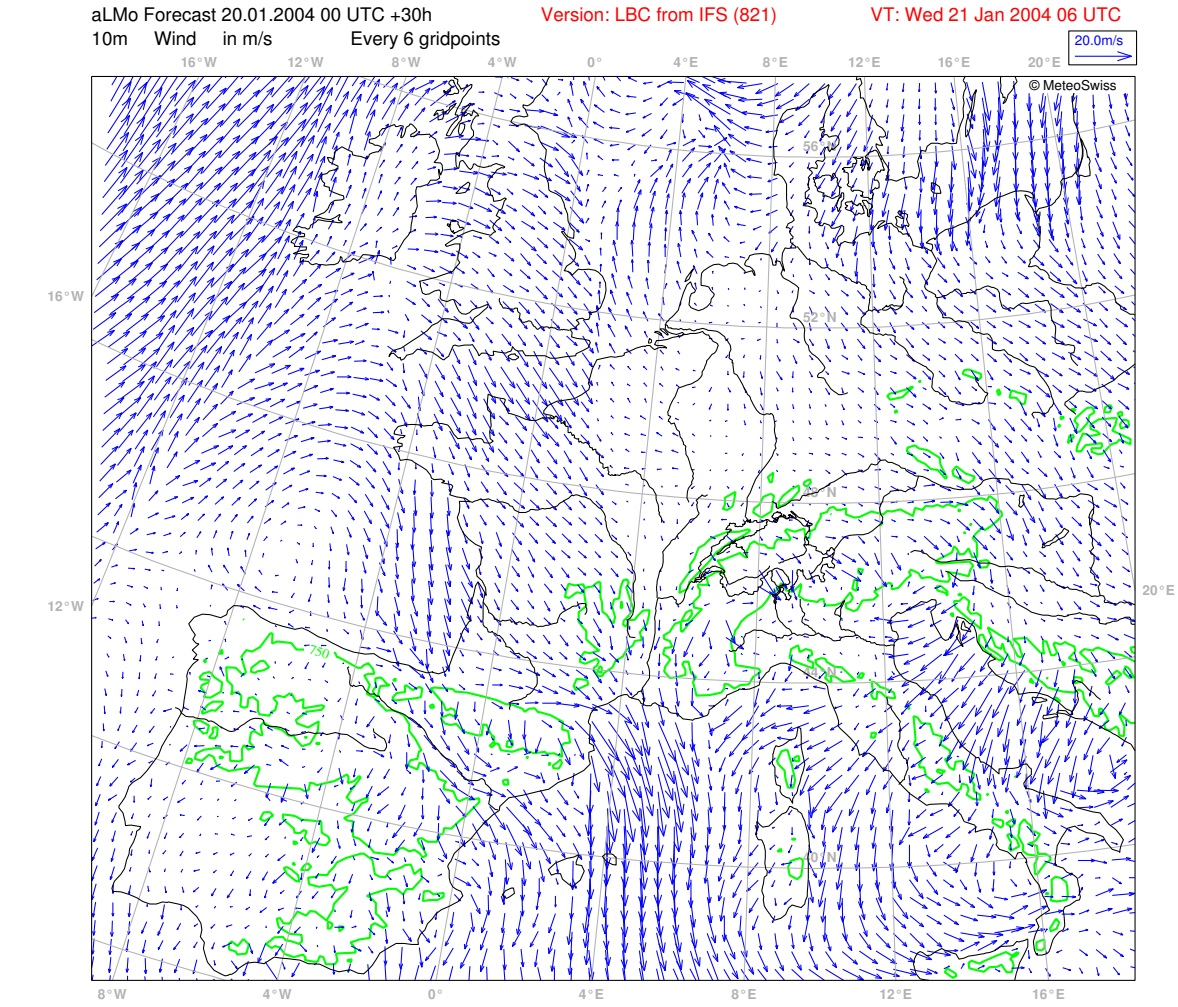

Figure 4.1: Wind field at 10 metres height calculated by the LM model. Source: `http://www.MeteoSwiss.ch`

4.2.1.2 Influence of the Urban Environment on the Local Wind Speed

The LM model takes into account the variation of altitude, but not the presence of buildings, by introducing roughness in the terrain. The wind speed estimated at 10 metres above the surface should be transformed when the site of interest is located in an urban canyon. The local wind speed is influenced by the following parameters: the speed of the undisturbed (surface) wind, the orientation of the undisturbed wind compared with the canyon orientation, the width W, the height H and the length L

of the canyon (Georgakis & Santamouris, 2005).

An algorithm devised by Georgakis & Santamouris (2005) and described in Figure 4.2 is applied to assess the wind speed within a canyon.

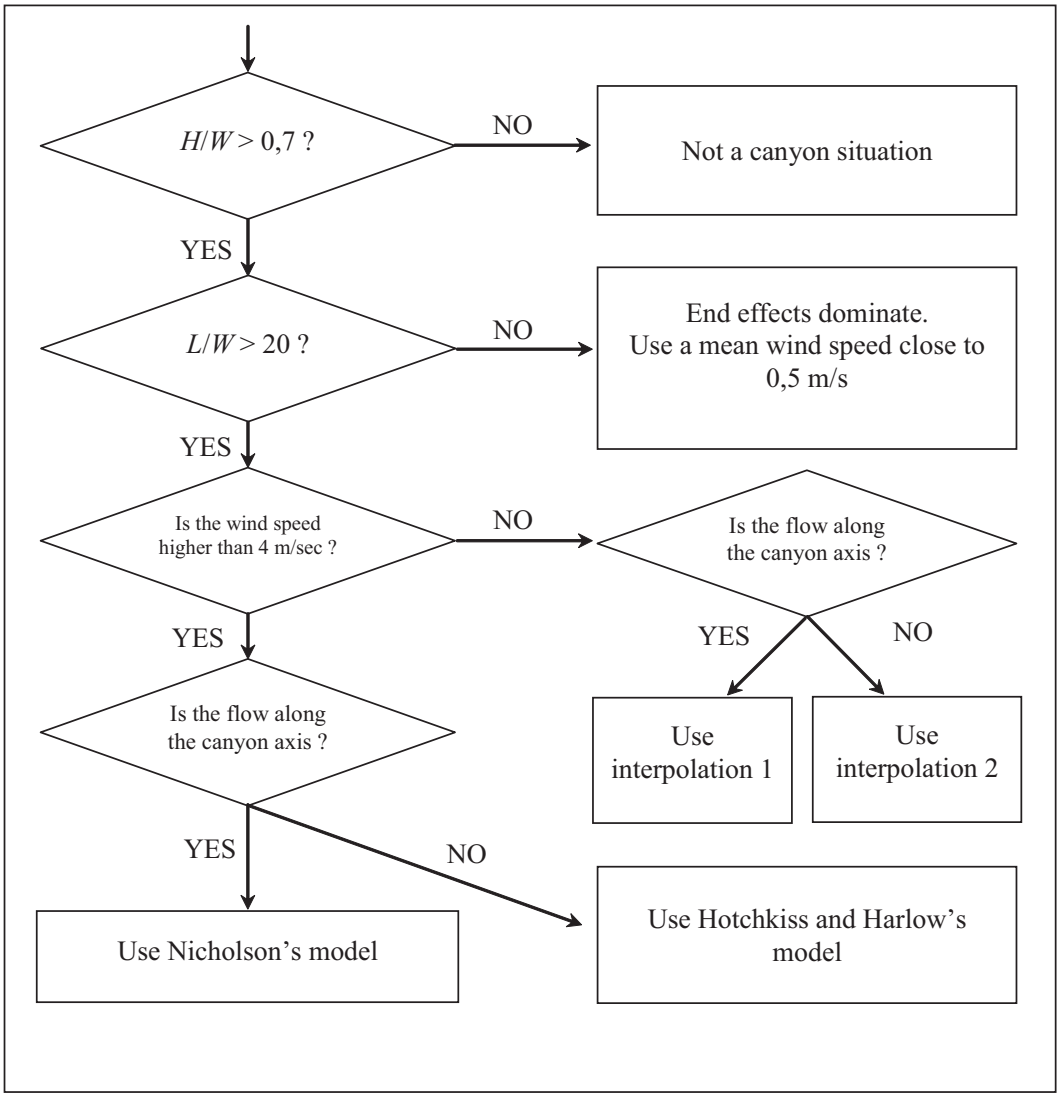

Figure 4.2: Algorithm for assessing wind speed inside the canyon (Georgakis & Santamouris, 2005).

In other cases (i.e. when the site of interest is located outside a canyon; see 'Not a canyon situation' in Figure 4.2), a simple rule of thumb[1] can be applied:

$$v^{\text{local}} = TCF \cdot v^{\text{undisturbed}} \tag{4.2.2}$$

[1]This rule can seem—with good reason—to be very crude. The method described in section 3.6 is by far more sophisticated and satisfactory.

where is a terrain correction factor whose values are given in Table 4.1.

Table 4.1: Terrain correction factor for wind speed (Chandra *et al.*, 1983).

Terrain type	Terrain correction factor (TCF)
Rural or suburban	0.85
Urban	0.67
City centre	0.47

The models used in the algorithm (see Figure 4.2) are described in (Georgakis & Santamouris, 2005). The resulting local wind speeds, v^{local} , are used in the subsequent equations (4.5.8) and (4.5.28).

4.2.2 Buoyancy Pressure

The other driving force of natural ventilation is stack pressure, or pressure due to buoyancy. It is induced by density differences between the indoor and outdoor air. The Bernoulli equation, combined with the ideal gas equation of state (see section 3.2.1.2), leads to the stack pressure difference between two openings separated by a vertical distance H:

$$\Delta p_{\text{ stack}} = \rho_{\text{i}}\, g\, H \left| \frac{T_{\text{i}} - T_{\text{e}}}{T_{\text{e}}} \right| \tag{4.2.3}$$

where ρ_{i} is the internal air density, g is the acceleration of gravity, T_i and T_e are the internal and external air temperatures. In the absence of wind, when $T_{\text{i}} > T_{\text{e}}$, the air enters through the lower openings and goes out through the upper ones (upward flow). A downward flow takes place when $T_{\text{i}} < T_{\text{e}}$. If both openings are of same area, A, and of same discharge coefficient, C_{d}, then the airflow is given by:

$$\dot{m} = \rho_{\text{i}}\, A\, C_{\text{d}} \sqrt{2\, g\, H \left| \frac{T_{\text{i}} - T_{\text{e}}}{T_{\text{i}} + T_{\text{e}}} \right|} \tag{4.2.4}$$

4.3 Constraints to Natural Ventilation

The two constraints to natural ventilation retained here are noise and pollution. Others exist, such as compromising the safety of the building while leaving windows open, or the fact that the occupants do not interact in a proper way; but they are only briefly mentioned.

4.3.1 Noise Pollution

Noise is a constraint to natural ventilation especially when the building is occupied. The definition of the acceptability of noise used in the current methodology is inspired by the Swiss federal regulation, which resorts to degrees of sensitivity:

- high: zones requiring an increased protection against noise, such as relaxation areas;
- medium: zones where no disturbing company is allowed, such as residential areas and areas restricted to public facilities;
- low: zones where disturbing companies are allowed, such as industrial, agricultural and craft areas.

Table 4.2 supplies a correspondence between qualitative levels—used in the current methodology—and quantitative levels in function of the degrees of sensitivity. These levels are inspired by the Swiss noise regulation (OPB, 1986).

Table 4.2: Equivalent sound pressure levels (Leq) expressed in dB(A): Table of correspondence between qualitative and quantitative levels.

		silent		acceptable		unacceptable	
		daytime	night time	daytime	night time	daytime	night time
degree of sensitivity	high	[0, 50 [	[0, 40 [	[50, 65 [	[40, 60 [	[65, ∞ [	[60, ∞ [
	medium	[0, 55 [	[0, 45 [	[55, 70 [	[45, 65 [	[70, ∞ [	[65, ∞ [
	low	[0, 60 [	[0, 50 [	[60, 70 [	[50, 65 [	[70, ∞ [	[65, ∞ [

4.3.2 Atmospheric Pollution

In order to assess outdoor air quality, the following pollutants are usually considered:

- nitrogen dioxide (NO_2);
- sulphur dioxide (SO_2);
- carbon monoxide (CO);
- ozone (O_3);

- volatile organic components (VOCs).

These pollutants each have long-term and short-term limiting values, or both. For instance, the Swiss environment protection law (LPE) imposes for nitrogen dioxide a daily limiting value of 80 $\mu g/m^3$, whereas the annual limiting value is 30 $\mu g/m^3$. To be mentioned are odours, dust and pollens, which cause direct inconvenience to the occupants.

4.4 Assumptions of the Methodology

The first assumption is that the building is built or will be built in a way that secures the most from natural ventilation. This also applies to refurbishment.

The second assumption is that the building's occupants are aware of natural ventilation and open the windows or *ad hoc* openings accordingly. It is thus assumed that occupants apply the best ventilation strategy. This is important because there is no sense in assessing the potential for natural ventilation if occupants subsequently do not operate the system correctly (*e.g.* by sealing all the openings and making the building airtight).

In addition, we assume that wind and buoyancy never counteract each other. As proven by Li and Delsante (2001), this opposition can occur, but can always be avoided by designing the building and by opening the apertures correctly.

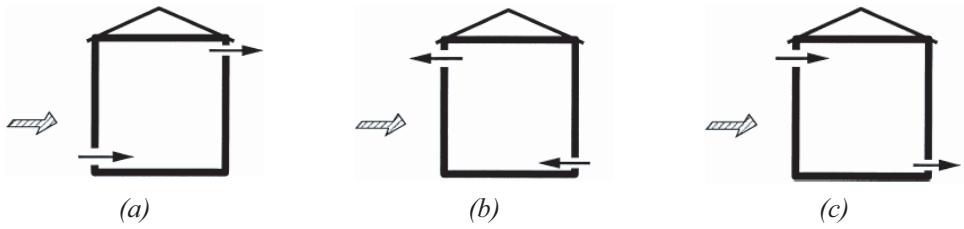

Figure 4.3: Situations when $T_i > T_e$: (a) assisting wind force; (b) opposing wind force with upward flow; (c) opposing wind force with downward flow (Li & Delsante, 2001).

The fourth assumption is that, given two city locations with different local wind speeds, wind-driven natural ventilation will be more effective at the location having the highest wind speed. It is provided that natural ventilation is assessed in the same

type of building in both locations. In other words, we suppose that the airflow rate is a monotonic increasing function of the wind speed. This is generally fulfilled if wind and stack have no opposed effects (this condition is met in accordance with the previous assumption) and if the wind direction is constant.

This assumption on wind will also be valid in the present method for the three last criteria, which are stack effect, noise and pollution (obviously as *decreasing* monotonic functions for the last two, since they are constraints instead of driving forces).

4.5 Climatic Suitability

Climatic suitability of a heating, ventilating and air-conditioning (HVAC) system is a measure of the energy needed for heating and for mechanical cooling, as well as a measure of the energy saved for cooling when ventilation is used. The climate should be taken into account in relation to the building's thermal behaviour and the anticipated thermal comfort. Constraints on comfort are important because they impose the ventilation strategy to be used.

4.5.1 Indoor Temperature of a Free-running Building

The *free-running temperature* is defined as the indoor temperature of the building in thermal balance with the outdoor environment when neither heating nor cooling is used. Furthermore, it is assumed that the free-running temperature is defined for the minimum ventilation rate required for indoor air quality, which implies that the building is almost airtight. With these assumptions, it may be accepted that, for a given month of the year, the indoor temperature of the free-running building is a function of the hour of the day. This temperature is calculated in the current method by means of a thermal simulation program and depends upon internal gains, solar gains, thermal inertia and thermal insulation.

4.5.2 Adaptive Comfort

The thermal comfort exhibits a neutral zone. In Figure 4.4, this zone is delimited by a lower comfort limit, T_{cl}, and an upper comfort limit, T_{cu}. These limits vary with the

mean outdoor temperature, resulting in an adaptation of the comfort criteria to the season.

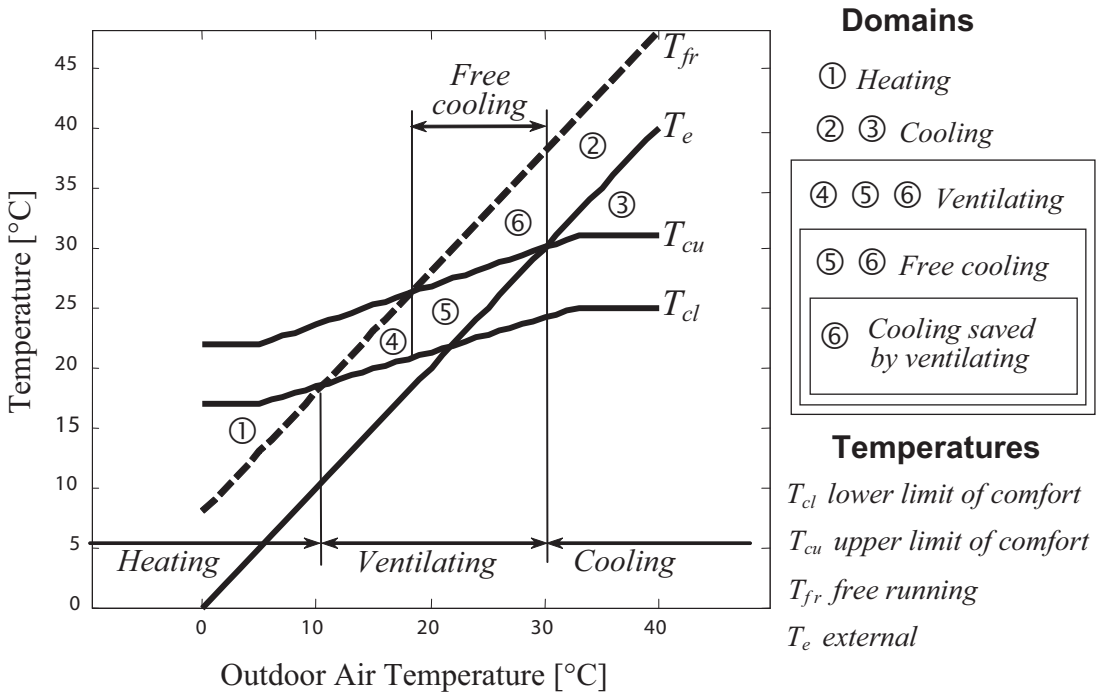

Figure 4.4: Heating, ventilation and cooling domains. (Ghiaus, 2003)

It is argued that thermal comfort in naturally ventilated buildings has larger seasonal differences than assumed by ISO 7730 and ASHRAE 55 Standards (Fountain *et al.*, 1996; Brager & de Dear, 1998; Sayigh & Marafia, 1998; De Dear & Brager, 1999; Nicol, 2001). Comfort ranges are much narrower when air-conditioning is used.

4.5.3 Domains for Heating, Cooling and Ventilation

Using the indoor temperature of the free-running building, the outdoor temperature and the comfort zone, the domains for heating, cooling and ventilation can be expressed by binary value functions (δ). Heating is needed when the free-running temperature is below the lower limit of comfort zone:

$$\delta_{\mathrm{h}} = \begin{cases} 1 & \text{when } T_{\mathrm{fr}} < T_{\mathrm{cl}}, \\ 0 & \text{otherwise.} \end{cases} \tag{4.5.1}$$

Mechanical cooling is required when both outdoor temperature and free-running temperature are larger than the upper limit of the comfort zone:

$$\delta_{\mathrm{c}} = \begin{cases} 1 & \text{when } T_{\mathrm{fr}} > T_{\mathrm{cu}} \text{ and } T_{\mathrm{e}} > T_{\mathrm{cu}}, \\ 0 & \text{otherwise.} \end{cases} \tag{4.5.2}$$

Ventilation may be used between heating and cooling. When mechanical or natural ventilation supply larger airflow rates than the minimum needed for indoor air quality, the indoor temperature may be varied from T_{fr} to $\max(T_{\mathrm{e}}, T_{\mathrm{cl}})$. This solution may be applied in situations corresponding to zones ③ to ⑤ in Figure 4.4. In zone ⑤, if the building were maintained airtight, then mechanical cooling would be needed. But, by using ventilation, the indoor temperature may be decreased by increasing the airflow, approaching the outdoor air temperature if the air exchange becomes very large. By controlling the airflow rate, the indoor temperature may be varied in the interval defined by the temperature for a free-running building (that corresponds to the situation when the building is airtight) and the outdoor temperature. Zone ⑤, defined by:

$$\delta_{\mathrm{fc}} = \begin{cases} 1 & \text{when } T_{\mathrm{e}} \leq T_{\mathrm{cu}} \text{ and } T_{\mathrm{fr}} > T_{\mathrm{cu}}, \\ 0 & \text{otherwise.} \end{cases} \tag{4.5.3}$$

corresponds to mechanical cooling saved by ventilation (or free cooling).

4.5.4 Degree Hours

Degree hours are a representative indication of the energy consumption for heating and cooling, as well as an indication of the energy saved for cooling by natural ventilation. For heating, they are defined as the sum of the differences between the lower limit of comfort temperature and the free-running temperature, when $T_{\mathrm{fr}} < T_{\mathrm{cl}}$:

$$DH_{\mathrm{h}} = \frac{1}{N} \sum_{i=1}^{N} (T_{\mathrm{cl}i} - T_{\mathrm{fr}i}) \delta_{\mathrm{h}i} \ , \tag{4.5.4}$$

where δ_{h} is defined in (4.5.1) and N is the number of moments in the considered period. In our case, we considered four daily instants during two years; thus $4 \cdot 2 \cdot 365 = 2\,920$ instants. If the degree days have to be considered for a given month j and a given hour k, then the summation is done exclusively on the instants belonging to that month

and that hour:

$$DH_{\mathrm{h}_{jk}} = \frac{1}{N_{jk}} \sum_{\substack{i=1 \\ i \in E_{jk}}}^{N_{jk}} (T_{\mathrm{cl}i} - T_{\mathrm{fr}ijk}) \delta_{\mathrm{h}ijk} \ , \tag{4.5.5}$$

where E_{jk} is the set of instants i belonging to month j and to hour k.

Similarly, the degree hours for cooling represent the sum of the differences between the free-running temperature and the upper limit of comfort, when $T_{\mathrm{fr}} > T_{\mathrm{cu}}$ and $T_{\mathrm{e}} > T_{\mathrm{cu}}$:

$$DH_{\mathrm{c}} = \frac{1}{N} \sum_{i=1}^{N} (T_{\mathrm{fr}i} - T_{\mathrm{cu}i}) \delta_{\mathrm{c}i} \ , \tag{4.5.6}$$

where δ_{c} is defined in (4.5.2).

Finally, the degree days of energy saved by natural ventilation for cooling is the same sum, when $T_{\mathrm{e}} \leq T_{\mathrm{cu}}$ and $T_{\mathrm{fr}} > T_{\mathrm{cu}}$:

$$DH_{\mathrm{fc}} = \frac{1}{N} \sum_{i=1}^{N} (T_{\mathrm{fr}i} - T_{\mathrm{cu}i}) \delta_{\mathrm{fc}i} \ , \tag{4.5.7}$$

where δ_{fc} is defined in (4.5.3). In other words, a contribution is brought to the sum only if it is too warm inside when the building is airtight and if it is cool enough outside.

Usually, the factor $\frac{1}{N}$ does not appear in these definitions. It has been included here to make degree hours independent of the number i of instants considered.

4.5.5 Criteria for Natural Ventilation

Criteria for natural ventilation can be defined similarly to the degree hours.

4.5.5.1 Criterion Related to Wind

For the criterion related to wind pressure, the following definition is proposed:

$$WH \overset{\text{def.}}{=} \frac{1}{N} \sum_{i=1}^{N} v_i^{\mathrm{local}} \tag{4.5.8}$$

where v^{local} is the local wind speed; *WH* stands for *wind hours*.

Note that as the current evaluation is ordinal (see section 4.6.6) and as the same building is supposed to be built at all sites (see the fourth assumption made in section 4.4), the coefficient $(\frac{1}{2} C_{\mathrm{p}} \rho)$ of equation (4.2.1) can be set aside, bypassing, in so doing, the problem of the pressure coefficients inaccuracy.

4.5.5.2 Criterion Related to Stack Effect

The criterion related to stack effect is defined as:

$$SH \overset{\text{def.}}{=} \frac{1}{N} \sum_{i=1}^{N} \left| \frac{T_{\mathrm{i}i} - T_{\mathrm{e}i}}{T_{\mathrm{e}i}} \right| \tag{4.5.9}$$

where T_{i} and T_{e} are the internal and external air temperatures respectively; *SH* stands for *stack hours*.

As was the case when it came to the wind-related criterion, the coefficient $(\rho_{\mathrm{i}}\, g\, H)$ of equation (4.2.3) can be set aside.

According to the cases of Figure 4.4, the internal temperature can be written as:

$$T_{\mathrm{i}} = \begin{cases} T_{\mathrm{cl}} & \text{if } T_{\mathrm{fr}} < T_{\mathrm{cl}} \\ T_{\mathrm{fr}} & \text{if } T_{\mathrm{cl}} \leq T_{\mathrm{fr}} \leq T_{\mathrm{cu}} \\ T_{\mathrm{cu}} & \text{if } T_{\mathrm{e}} \leq T_{\mathrm{cu}} \text{ and } T_{\mathrm{fr}} > T_{\mathrm{cu}} \\ \frac{1}{2}(T_{\mathrm{fr}} + T_{\mathrm{e}}) & \text{if } T_{\mathrm{fr}} > T_{\mathrm{cu}} \text{ and } T_{\mathrm{e}} > T_{\mathrm{cu}} \end{cases} \tag{4.5.10}$$

The following assumptions have been made here:

- if $T_{\mathrm{fr}} < T_{\mathrm{cl}}$: the heating system ensures that the indoor temperature never falls below the lower limit of the comfort temperature.
- if $T_{\mathrm{cl}} \leq T_{\mathrm{fr}} \leq T_{\mathrm{cu}}$: the internal temperature can be anything between T_{cl} and T_{cu} depending upon the airflow rate. If the flow rate is zero, then $T_{\mathrm{i}} = T_{\mathrm{fr}}$. At all events, the flow should not exceed a critical value in order to prevent the internal temperature from falling below the lower limit of comfort, but should always be high enough to ensure a good internal air quality.
- if $T_{\mathrm{e}} \leq T_{\mathrm{cu}}$ and $T_{\mathrm{fr}} > T_{\mathrm{cu}}$: free cooling is used to make sure that the internal temperature is, at the most, at the upper limit of the comfort temperature.
- if $T_{\mathrm{fr}} > T_{\mathrm{cu}}$ and $T_{\mathrm{e}} > T_{\mathrm{cu}}$: the assumption is made that no air-conditioning system is used. The internal temperature can be anything between T_{e} and T_{fr} depending upon the airflow rate. If wind is absent, an equilibrium temperature between both of these values will be reached because, on the one hand, if the airflow drops, T_{i} will tend towards T_{fr} and the stack effect will then induce a flow due to the difference between T_{i} and T_{e}. On the other hand, an increasing flow will bring T_{i} closer to T_{e}, decreasing the stack-induced flow. Both trends balance each other out towards an equilibrium temperature well approximated by $\frac{1}{2}(T_{\mathrm{fr}} + T_{\mathrm{e}})$.

By defining δ_{v} as:

$$\delta_{\mathrm{v}} = \begin{cases} 1 & \text{when } T_{\mathrm{cl}} \leq T_{\mathrm{fr}} \leq T_{\mathrm{cu}}, \\ 0 & \text{otherwise,} \end{cases} \tag{4.5.11}$$

and by considering (4.5.10), the internal temperature can be written as follows:

$$T_{\mathrm{i}} = T_{\mathrm{cl}}\ \delta_{\mathrm{h}} + T_{\mathrm{fr}}\ \delta_{\mathrm{v}} + T_{\mathrm{cu}}\ \delta_{\mathrm{fc}} + \tfrac{1}{2}(T_{\mathrm{fr}} + T_{\mathrm{e}})\ \delta_{\mathrm{c}} \tag{4.5.12}$$

This expression can be inserted in (4.5.9) in order to calculate ST.

4.5.5.3 Criterion Related to Noise Pollution

The criterion related to noise pollution is defined here as:

$$NH \overset{\text{def.}}{=} 10 \cdot \log_{10}\Big(\frac{1}{N}\sum_{i=1}^{N} 10^{\ L_{\mathrm{noise}\,i}/10}\Big) \tag{4.5.13}$$

where L_{noise} is the noise level. NH stands for *noise hours*. This definition is close to the definition of the *equivalent sound pressure level*, which is the steady sound level that, over a specified period of time, would produce the same energy equivalence as the fluctuating sound level actually occurring.

4.5.5.4 Criterion Related to Atmospheric Pollution

The criterion related to atmospheric pollution reads:

$$PH \overset{\text{def.}}{=} \frac{1}{N}\sum_{i=1}^{N} L_{\mathrm{pollution}_i} \tag{4.5.14}$$

where $L_{\mathrm{pollution}}$ is the qualitative pollution level. PH stands for *pollution hours*.

4.5.6 Frequency Distributions

Degree hours can be calculated as soon as we know the monthly variation of daily mean temperature (time series). However, this approach has two disadvantages: the data are not easily available and, if accessible, they should be available for numerous years (typically 5 to 20 years) in order to be statistically significant. An alternative to using time series of daily mean temperature is to use the probability distribution

of daily mean temperature. The probability distribution is obtained on measurements achieved during long periods of time. The same goes for wind speed distributions.

Let X a random variable. The expectation value $\mathbb{E}(f(X))$ of a function $f(X)$ of X is given by:

$$\mathbb{E}(f(X)) = \lim_{N\to\infty} \frac{1}{N} \sum_{i=1}^{N} f(x_i). \tag{4.5.15}$$

where x_i $(i = 1, \ldots, N)$ are the values taken by X trough time. On the other hand:

$$\mathbb{E}(f(X)) = \int_{\mathbb{R}} f(x) f_X(x) \mathrm{d}x \tag{4.5.16}$$

where $f_X(X)$ is the probability density function of variable X. When N is large, this yields:

$$\frac{1}{N} \sum_{i=1}^{N} f(x_i) \approx \int_{\mathbb{R}} f(x) f_X(x) \mathrm{d}x \tag{4.5.17}$$

In the case where function $f(x)$ and this probability density function $f_X(x)$ depend upon the month j and the hour k, the previous equation reads:

$$\frac{1}{N_{jk}} \sum_{\substack{i=1 \\ i\in E_{jk}}}^{N_{jk}} f_{jk}(x_i) \approx \int_{\mathbb{R}} f_{jk}(x) f_{X\,jk}(x) \mathrm{d}x \tag{4.5.18}$$

4.5.6.1 Degree Hours

When the random variable is the external temperature T_e, the probability density function is well approximated by the normal law:

$$f_{T_\mathrm{e}}(T_\mathrm{e}) = \frac{1}{\sigma\sqrt{2\pi}} \exp(-\frac{1}{2}(\frac{T_\mathrm{e} - \mu}{\sigma})^2) \tag{4.5.19}$$

where μ is the mean and σ^2 is the variance of variable T_e.

Replacing $f_{jk}(x_i)$ by $(T_{\mathrm{cl}i} - T_{\mathrm{fr}ijk})\delta_{\mathrm{h}ijk}$ in (4.5.18) yields:

$$\frac{1}{N_{jk}} \sum_{\substack{i=1 \\ i\in E_{jk}}}^{N_{jk}} (T_{\mathrm{cl}i} - T_{\mathrm{fr}ijk})\delta_{\mathrm{h}ijk} \approx \int_{\mathbb{R}} (T_\mathrm{cl}(T_\mathrm{e}) - T_{\mathrm{fr}jk}(T_\mathrm{e}))\delta_{\mathrm{h}jk}(T_\mathrm{e}) f_{T_\mathrm{e}jk}(T_\mathrm{e}) \mathrm{d}T_\mathrm{e} \tag{4.5.20}$$

According to (4.5.5), the left-hand side of this equation is equal to $DH_{\mathrm{h}_{jk}}$, so that degree hours for heating can be expressed as:

$$\boxed{DH_{\mathrm{h}_{jk}} \approx \int_{\mathbb{R}} (T_\mathrm{cl}(T_\mathrm{e}) - T_{\mathrm{fr}jk}(T_\mathrm{e}))\delta_{\mathrm{h}jk}(T_\mathrm{e}) f_{T_\mathrm{e}jk}(T_\mathrm{e}) \mathrm{d}T_\mathrm{e}} \tag{4.5.21}$$

with

$$f_{T_{\mathrm{e}}jk}(T_{\mathrm{e}}) = \frac{1}{\sigma_{jk}\sqrt{2\pi}} \exp(-\frac{1}{2}(\frac{T_{\mathrm{e}} - \mu_{jk}}{\sigma_{jk}})^2) \tag{4.5.22}$$

Similarly, degree hours for cooling and degree hours of energy saved by natural ventilation for cooling can be rewritten respectively as:

$$\boxed{DH_{\,\mathrm{c}_{jk}} \approx \int_{\mathbb{R}} (T_{\mathrm{fr}}(T_{\mathrm{e}}) - T_{\mathrm{cu}jk}(T_{\mathrm{e}}))\delta_{\,\mathrm{c}jk}(T_{\mathrm{e}}) f_{T_{\mathrm{e}}jk}(T_{\mathrm{e}})\mathrm{d}T_{\mathrm{e}}} \tag{4.5.23}$$

$$\boxed{DH_{\mathrm{fc}_{jk}} \approx \int_{\mathbb{R}} (T_{\mathrm{fr}}(T_{\mathrm{e}}) - T_{\mathrm{cu}jk}(T_{\mathrm{e}}))\delta_{\mathrm{fc}jk}(T_{\mathrm{e}}) f_{T_{\mathrm{e}}jk}(T_{\mathrm{e}})\mathrm{d}T_{\mathrm{e}}} \tag{4.5.24}$$

4.5.6.2 Criterion Related to Wind

When the random variable is the wind speed v, the probability density function is well approximated by the Weibull distribution law:

$$f_v(v) = \begin{cases} a\, b\, v^{b-1} \exp(-av^b) & \text{if } v > 0 \\ 0 & \text{if } v \leq 0 \end{cases} \tag{4.5.25}$$

where a and b are two strictly positive parameters. Note that the second case arises only when $v = 0$ as wind speed is never strictly negative.

Following a reasoning similar to the above-mentioned, one can write:

$$\frac{1}{N_{jk}} \sum_{\substack{i=1 \\ i \in E_{jk}}}^{N_{jk}} f_{jk}(v_i) \approx \int_{\mathbb{R}} f_{jk}(v) f_{vjk}(v)\mathrm{d}v \tag{4.5.26}$$

By replacing $f_{jk}(v_i)$ by the local wind speed—the local wind speed being indeed a function of the undisturbed wind speed:

$$\frac{1}{N_{jk}} \sum_{\substack{i=1 \\ i \in E_{jk}}}^{N_{jk}} v_i^{\mathrm{local}} \approx \int_{\mathbb{R}} v_{\mathrm{local}}(v) f_{vjk}(v)\mathrm{d}v \tag{4.5.27}$$

the expression for *wind hours* reads:

$$\boxed{WH_{jk} \approx \int_{\mathbb{R}} v_{\mathrm{local}}(v) f_{vjk}(v)\mathrm{d}v} \tag{4.5.28}$$

4.5.6.3 Criterion Related to Stack Effect

If $f_{jk}(x_i)$ in (4.5.18) is replaced by $\left|(T_{\mathrm{i}ijk} - T_{\mathrm{e}i})/T_{\mathrm{e}i}\right|$, one gets:

$$\frac{1}{N_{jk}} \sum_{\substack{i=1 \\ i \in E_{jk}}}^{N_{jk}} \left| \frac{T_{\mathrm{i}ijk} - T_{\mathrm{e}i}}{T_{\mathrm{e}i}} \right| \approx \int_{\mathbb{R}} \left| \frac{T_{\mathrm{i}jk}(T_{\mathrm{e}}) - T_{\mathrm{e}}}{T_{\mathrm{e}}} \right| f_{T_{\mathrm{e}}jk}(T_{\mathrm{e}}) \mathrm{d}T_{\mathrm{e}} \tag{4.5.29}$$

Therefore, the expression for *stack hours* reads:

$$\boxed{SH_{jk} \approx \int_{\mathbb{R}} \left| \frac{T_{\mathrm{i}jk}(T_{\mathrm{e}}) - T_{\mathrm{e}}}{T_{\mathrm{e}}} \right| f_{T_{\mathrm{e}}jk}(T_{\mathrm{e}}) \mathrm{d}T_{\mathrm{e}}} \tag{4.5.30}$$

with $f_{T_{\mathrm{e}}jk}(T_{\mathrm{e}})$ given by (4.5.22) and $T_{\mathrm{i}jk}(T_{\mathrm{e}})$ given by (4.5.12).

4.5.6.4 Criterion Related to Noise Pollution

As solely one value is assigned for the noise level for daytime and one for night time throughout the year, equation (4.5.13) can simply be written as:

$$\boxed{NH = 10 \cdot \log_{10} \left(\frac{10^{\,L_{\mathrm{noise}}^{\mathrm{daytime}}/10} + 10^{\,L_{\mathrm{noise}}^{\mathrm{night\text{-}time}}/10}}{2} \right)} \tag{4.5.31}$$

4.5.6.5 Criterion Related to Atmospheric Pollution

For the same reasons, equation (4.5.14) can simply be written as:

$$\boxed{PH = \frac{L_{\mathrm{pollution}}^{\mathrm{daytime}} + L_{\mathrm{pollution}}^{\mathrm{night\text{-}time}}}{2}} \tag{4.5.32}$$

4.6 Multi-criteria Analysis

Multi-criteria analysis is a technique devoted to simplifying a decision problem and to solving it. The problem is made up of several possibly conflicting objectives, translated into criteria. An example is given in section 4.6.6 ('Principles of the Multi-criteria Analysis Method *Qualiflex*') below. The expected result of a multi-criteria evaluation is an action or a group of actions to be taken (Schärlig, 1990a; Schärlig, 1990b). In our case, the actions are 'to build in a given place' and the decision is 'where to build.' This is why *action* and *location* have the same meaning in the following text.

It is noteworthy to mention that the way multi-criteria analysis is used here is rather original, because it would generally be applied in decision processes in which pure physics is not involved, such as politics or establishment choice projects.

4.6.1 Why multi-criteria analysis ...

Three main reasons led to the choice of multi-criteria analysis as a tool for evaluating the potential for natural ventilation. First, the driving forces and constraints mentioned above make up several criteria that are not commensurable (Schärlig, 1990a). In other words, except, perhaps, wind and stack pressure translated into airflow rates, they cannot be reduced to a single criterion. Multicriteria analysis allows to overcome this 'uncommensurability'.

Second, the intention is to be exhaustive and thus to take into account the entire set of criteria involved in natural ventilation—namely, in our case, wind and stack pressure, noise and pollution.

Moreover, the airflow due to wind depends upon numerous parameters seldom known with sufficient precision (see, for instance, the remark on pressure coefficients in section 2.2.5). In fact, one of the advantages of multi-criteria analysis applied here is that the airflow does not need to be known precisely: stating that a higher wind speed (and, thus, a larger wind-induced airflow) will be present in a given location will suffice. This, of course, is valid only under the assumption that the airflow rate is an increasing function of the wind speed.

As a matter of fact, a general property of multicriteria aggregation methods is their 'monotonicity', that is to say that if any of the criteria improves (respectively worsens), then the global evaluation improves (respectively worsens). In our case, if for example, wind blows stronger in a second situation than in a first one (without changing the other criteria), then the global evaluation of the natural ventilation potential will be better in the second situation. Similarly, if a location is noisier in a second situation than in a first one, then the global evaluation of the natural ventilation potential will be better in the first situation. This 'monotonicity' is fully coherent with the fourth assumption mentioned in section 4.4 ('Assumptions of the Methodology').

4.6.2 . . . rather than traditional models ?

This way of reasoning suits the philosophy according to which approximately correct results are preferable to exactly wrong ones. Traditional 'exact' modelling, such as computational fluid dynamics (CFD) and zonal models (see *e.g.* Feustel and Dieris (1992)), give results that are very sensitive to input data (Fürbringer, 1994). Moreover, these data are not readily available with sufficient accuracy. The models present the following additional drawbacks:

- They do not process qualitative knowledge.
- The results depend strongly upon the user, who should be an expert in the field.
- They do not provide directly and automatically the uncertainty of the outcomes.

Moreover, each of these models has a restricted field of application and none of them allows a global and systemic approach. For example, none of them is able to completely model natural ventilation as the combined effect of wind and temperature gradients in a multi-zone building with large openings.

One of the reasons to use multi-criteria analysis is to obtain a pre-design tool. Computational fluid dynamics, zonal models and so on are design tool which can be used during the advanced stages of designing a building; they are not suitable for the first steps of pre-designing a building.

4.6.3 General Procedure for Evaluating a Site

In order to evaluate a site from the natural ventilation potential point of view, the intention was to avoid simply assigning a 'mark' to it. The results of the evaluation will be a ranking of the site in comparison with other well-known sites, referred to as *base sites*. The potential for natural ventilation of these sites is known, so that the ranking amongst them of the site to be assessed will provide its potential. In a sense, the *base sites* supply a scale of values.

The *base sites* are to be entered by an expert user, leaving the assessment (strictly speaking) to the 'normal' (end) user. In addition, meaningful results will be provided together with this ranking.

4.6.4 Procedure for Choosing *Base Sites*

The whole evaluation process relies on a set of well-known base sites. Several such sites are delivered with the tool which was developed as part of this work (see section 4.7); but the user may like to add some more—for example, in order to make the ranking more accurate, or to compare the assessed site with others that are well known to the user. The criteria such sites should fulfil are defined below. The following characteristics should be available:

- natural ventilation potential for this site, known from experience or from indoor air quality (IAQ) in existing, naturally ventilated buildings;
- location (climatic data is provided by the program from this location);
- urban fabric typology (*e.g.* open field, suburb, dense buildings, canyon, etc.);
- noise environment (silent, acceptable, unacceptable) during the day and night;
- outdoor air quality (clean, acceptable, unacceptable)—*i.e.* if pollution hinders natural ventilation or not.

The set of base sites should be distributed within the whole five-dimension volume defined by the five variables mentioned above. An evaluation could be performed with only two base sites (*e.g.* a rather good and a rather poor site from the natural ventilation potential point of view); but the evaluation will be more accurate if more buildings are included. Ideally, between 20 and 40 base cases will be useful for each climatic zone: two different natural ventilation potentials, four urban typologies, and two noise and two pollution levels. However, a set of few sites could be defined using an optimal design, provided that such specified sites exist. Table 4.3 shows an example of such a minimum set of sites, based upon a Plackett-Burman design (Plackett & Burman, 1943).

Table 4.3: Example of the characteristics of a minimal but optimal set of base sites.

site	1	2	3	4	5	6
NVP	low	low	good	good	low	low
urban fabric	suburban	urban	urban	suburban	suburban	urban
exposed to wind	yes	no	yes	no	no	no
outside temperature	cold	warm	cold	cold	warm	cold
noise	noisy	noisy	silent	silent	silent	noisy
pollution	polluted	clean	clean	clean	polluted	polluted

4.6.5 Selected Multi-criteria Analysis Method

Since some criteria are qualitative, particularly pollution (see section 4.7.1.4), the selected multi-criteria analysis method must be qualitative. The method *Qualiflex* was chosen. This method ranks locations as a function of their ranking in each single criterion. This method has been adapted for its use in the current methodology with regard to weights (see section 4.6.7, 'Adaptive Weights').

4.6.6 Principles of the Multi-criteria Analysis Method *Qualiflex*

The principles of *Qualiflex* (Paelinck, 1976, 1978, 1979) are explained hereafter in a simplified way as a result of an example made up of three actions a_1, a_2, a_3 (three sites in our case) and three criteria c_1, c_2, c_3. Let us assume that each action (each site in our case) is assigned a rank for each criterion and that each criterion is assigned a weight. Figures in italics in Table 4.4 represent the ranking matrix elements.

Table 4.4: Input table. The ranking matrix elements are represented by figures in italics.

	c_1	c_2	c_3
weight	5	4	1
a_1	*1*	*2*	*3*
a_2	*2*	*1*	*3*
a_3	*2*	*3*	*2*

In this example, for the first criterion (whose weight is 5), a1 is better placed than a_2 and a_3, which, in turn, are equally placed. The next step consists in considering all of the possible action rankings R_i, for $i = 1, \ldots, (3!)$:

$$
\begin{aligned}
R_1&: \quad (a_1, \quad a_2, \quad a_3) \\
R_2&: \quad (a_2, \quad a_1, \quad a_3) \\
R_3&: \quad (a_3, \quad a_1, \quad a_2) \\
R_4&: \quad (a_3, \quad a_2, \quad a_1) \\
R_5&: \quad (a_2, \quad a_3, \quad a_1) \\
R_6&: \quad (a_1, \quad a_3, \quad a_2)
\end{aligned}
$$

For each ranking R_i and for each criterion, the concordance with the ranking matrix must be checked by comparing every couple of actions. Each time the relative position

is the same in the ranking matrix of the problem data and in the ranking R_i, a so-called concordance index is incremented by one; when the relative position is different, the concordance index is decremented by one.

In our example, let us consider ranking R_4 and criterion c_2. For each couple of actions:

1. R_4 causes a_2 to be better placed than a_1; so does the matrix for criterion c_2. As a result, the concordance index is incremented.

2. R_4 causes a_3 to be better placed than a_1. The matrix causes a_1 to be better placed than a_3 for criterion c_2. The concordance index is thus decremented.

3. R_4 causes a_3 to be better placed than a_2. The matrix causes a_2 to be better placed than a_3 for criterion c_2. The concordance index is thus decremented.

Therefore, the value of the concordance index for R_4 and c_2 is $1 - 1 - 1 = -1$[2]. By repeating this operation for every couple (R_i, c_j), $i = 1, \ldots, 6$ and $j = 1, \ldots, 3$ the concordance indices take the values given in Table 4.5.

Table 4.5: Matrix of concordance indices.

	c_1	c_2	c_3
weight	5	4	1
R_1	2	1	-2
R_2	0	3	-2
R_3	-2	1	0
R_4	-2	-1	2
R_5	0	-3	2
R_6	2	-1	0

A so-called global concordance index is then calculated for every ranking by adding the concordance indices of the ranking, beforehand multiplied by the corresponding weight. For example, the global concordance index of R_4 is: $-2 \cdot 5 - 1 \cdot 4 + 2 \cdot 1 = -12$. The resulted rankings are given in Table 4.6.

If these indices are considered, the first ranking R_1 accords best with the data of the problem (Table 4.4). Therefore, the ranking R_1, which causes a_1 to be better placed than a_2, and a_3 to be better placed than a_2, will be chosen.

[2] A minor modification has been brought to this procedure: the concordance index of a given ranking is decremented also if the ranking matrix gives two actions equally placed for a criterion and if the actions differ of more then one position in this given ranking.

Table 4.6: Global concordance indices

	global concordance index
R_1	12
R_2	10
R_3	−6
R_4	−12
R_5	−10
R_6	6

4.6.7 Adaptive Weights

The weights that appear in a multi-criteria analysis method represent, in a way, the importance of the related criterion. Usually, when a set of weights has to be drawn up, a committee of experts is brought together and comes to an agreement. Occasionally, an agreement is not even found and several multi-criteria analyses are carried out with the various sets of weights (hoping that the outcome is the same).

Frequently, weights are subjective and can depend upon the value system of the decision-maker(s), especially when the decision is of a political nature. In our case, some inhabitants may be more tolerant of noise in a given country than in another, and will assign a lower weight to this criterion.

With regard to the wind and stack effect criteria, the weights should not be subjective at all since physical phenomena are involved.

This weight problem has been solved in the current methodology by considering things in a reverse way: the set of weights results from the ranking of the locations and from the ranking matrix. Put another way, all of the weights contained between two chosen values are enumerated until one set is compatible with the mentioned ranking. The compatibility is checked by running Qualiflex each time. The sites ranked in this way are referred to as base sites. Clearly, an infinite number of sets are possible. The first encountered can be arbitrarily selected.

The ranking has to be worked out by an expert user who knows the base sites from a natural ventilation potential point of view and can create new base sites. If the case arises, the expert will rank a new site against the other base sites and launch a new search for weights. Base sites may also be removed, if required. Once the set of weights is fixed, it can be used for the initial purpose of the method—namely, to assess a new site.

Let us consider the example given above in which we try to find a set of weights and suppose that the expert proposes the following ranking: a_1, a_3, a_2. By enumerating all of the weights from 5 down to 0, we start with $w_1 = 5$, $w_2 = 5$ and $w_3 = 5$. With this set and with the ranking matrix given in Table 10.1, Qualiflex provides the following ranking: (a_1, a_2, a_3).

Since this is not the ranking chosen by the expert, the set of weights ($w_1 = 5$, $w_2 = 5$, $w_3 = 5$) has to be discarded. The same ranking comes out with the subsequently enumerated sets:

- $(w_1 = 5, w_2 = 5, w_3 = 4)$;
- $(w_1 = 5, w_2 = 5, w_3 = 3)$;
- $(w_1 = 5, w_2 = 5, w_3 = 2)$;
- $(w_1 = 5, w_2 = 5, w_3 = 1)$.

These must thus be discarded, as well. With the subsequent set ($w_1 = 5$, $w_2 = 4$, $w_3 = 5$), Qualiflex provides the ranking (a_1, a_3, a_2). Since this is the ranking chosen by the expert, the following weights are retained:

$$w_1 = 5, w_2 = 4, w_3 = 5.$$

These can then be used in a 'normal' multi-criteria analysis, as presented in section 4.6.6 ('Principles of the Multi-criteria Analysis Method *Qualiflex*') for evaluating a fourth action, say a_4.

Note that if the user of the tool is not satisfied with this procedure for getting weights, the possibility is left to choose user-defined weights.

4.7 Software Tool

In its 'Description of Work', the URBVENT project demanded 'a methodology, embedded in *software*, to assess the potential and feasibility, and to design optimal façades for natural ventilation in urban environment, accessible to architects, designers and decision makers.'

The present section presents the mentioned software tool, based upon the above-described methodology. However, this section is not meant to be a user's guide. Instead, it describes the purpose of the steps encountered during the execution of the program.

The user has two possibilities at the beginning of the execution: he can either:

- *add a new base site* or;
- *assess the potential for natural ventilation of a new site.*

In both cases, a new row of the ranking matrix (see section 4.6.6, 'Principles of the Multi-criteria Analysis Method *Qualiflex*') has to be filled for the new site.

In the first case (*add a new base site*), once the new row of the ranking matrix is filled out, the user must provide a ranking of the base sites and start a search for a set of weights, which has to be compatible with both the ranking matrix and the user-provided ranking. The base sites and the weights are stored in a database.

In the second case (*assess the potential for natural ventilation of a new site*), once the ranking matrix is filled, the program supplies a ranking drawn up with the previously established weights.

4.7.1 Filling Out the Ranking Matrix

Several frames (questionnaires) appear during the program execution in order to collect information from the user:

4.7.1.1 Undisturbed Wind

The user is asked to enter the location of interest (see Figure 4.5). The coordinates are then used to determine the undisturbed wind speed and direction through time thanks to MeteoSwiss' data.

4.7.1.2 Local Wind

The user is asked to enter the environment of the place of interest and the characteristics of the canyon located there, if any (see Figure 4.6). These inputs, along with the undisturbed wind features, are used to assess the local wind speed and direction.

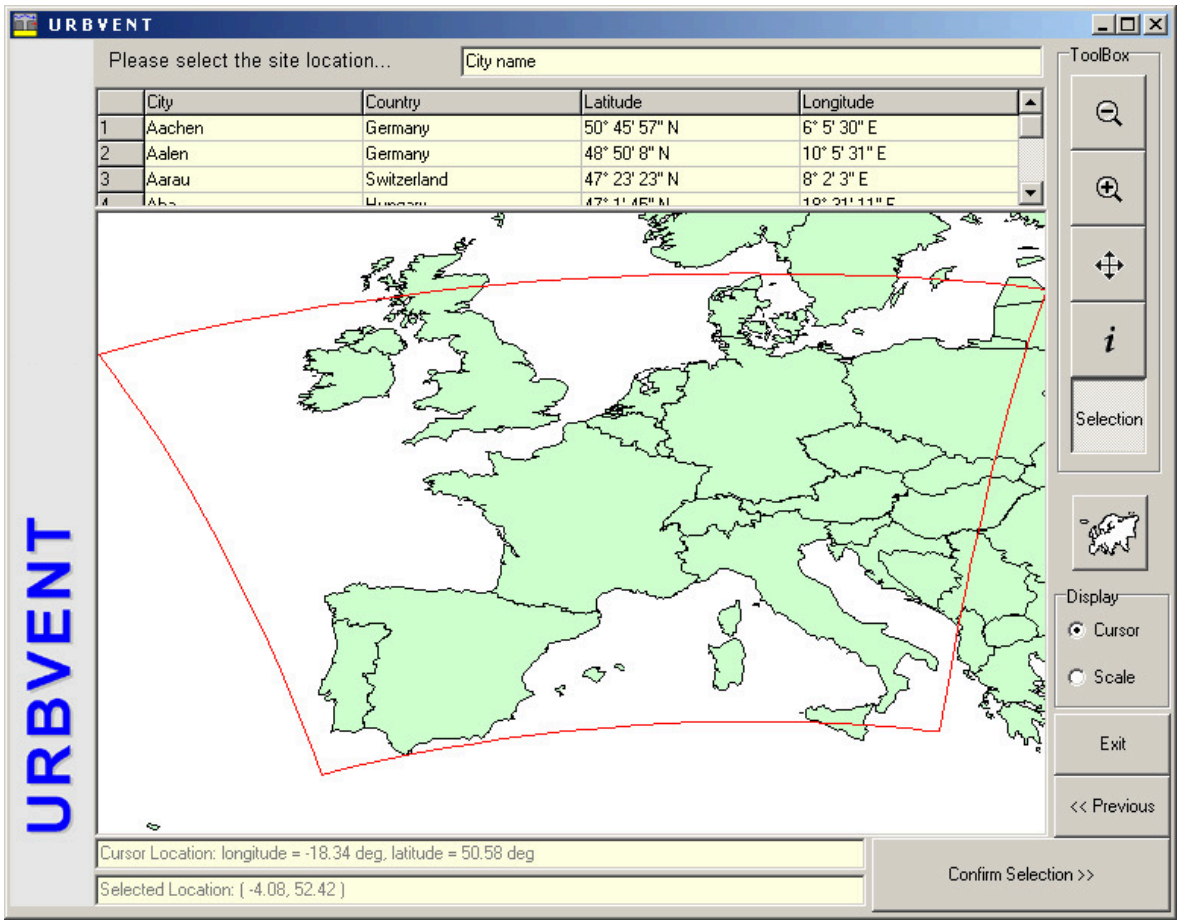

Figure 4.5: Location selection form

4.7.1.3 Temperatures

Outdoor temperatures are retrieved in MeteoSwiss' data due to the location entered by the user as for the undisturbed wind speed. In order to determine *internal temperatures*, the software tool asks the user the type of building (see Figure 4.7), which is used by a thermal simulation tool named *Ecotect* [3] to assesses the indoor-outdoor temperature difference as a function of the thermal mass, façade orientation and occupancy[4].

[3] See `http://www.ecotect.com`. *Ecotect* is based upon the *CIBSE Admittance Method* (CIBSE, 1999).

[4] The indoor-outdoor temperature differences are in fact pre-calculated for the $3 \cdot 4 \cdot 2 = 24$ possibilities. However, the use can put his/her own building.

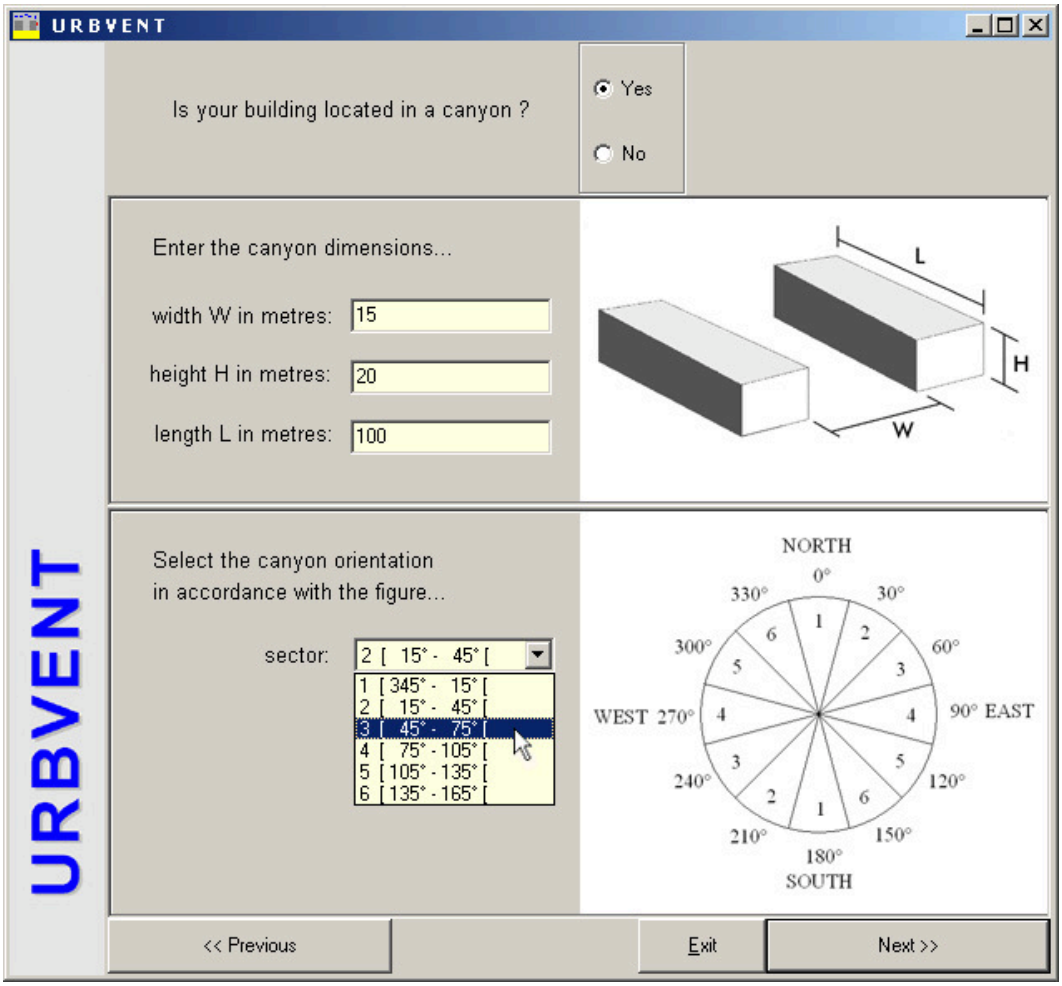

Figure 4.6: Canyon selection form

4.7.1.4 Noise and Pollution Levels

The user then enters qualitative daytime and night-time noise levels (see Figure 4.8) in accordance with Table 4.2.

Finally, the user is asked to enter qualitative pollution levels. Pollution levels can be selected only qualitatively. The reason for this is that quantitative pollution levels would require substantial numbers of measurements from the user. Moreover, long-term *and* short-term limiting values exist for the pollutants of interest: nitrogen dioxide, sulphur dioxide, carbon monoxide, ozone and volatile organic components amongst other pollutants. Finally, the transport and transformation of pollutants is complex (Clappier *et al.*, 2000). However, it can be conceived to use pollution maps.

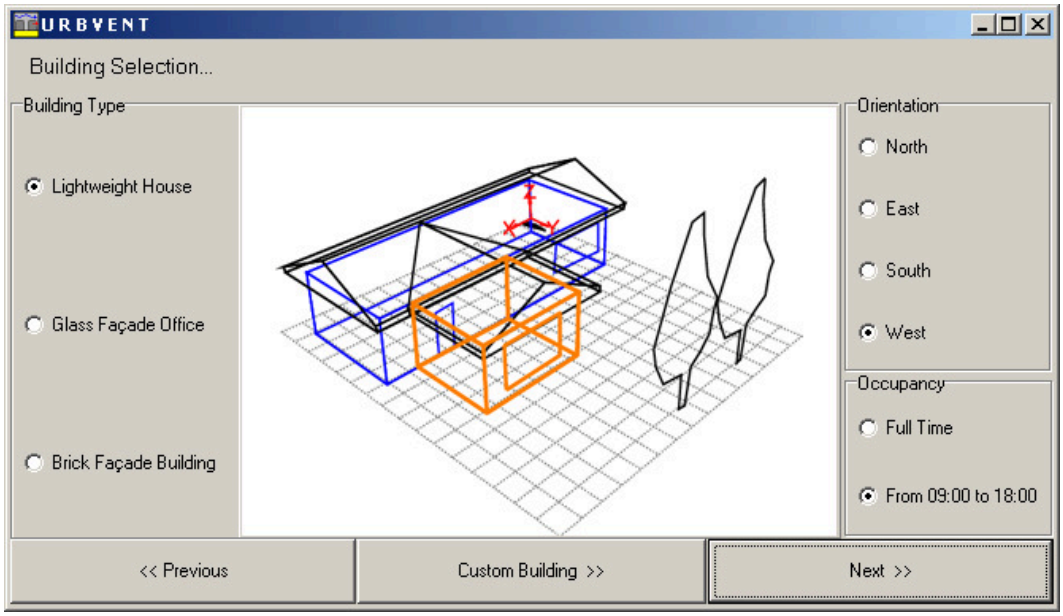

Figure 4.7: Selecting the type of building, the orientation of the façade and the occupancy schedule

These maps do not yet cover Europe. Values of sections 4.7.1.2 to 4.7.1.4 are then used to calculate the criteria for the multi-criteria analysis, as well as degree-hours and airflow rates.

4.7.2 Example

Let us consider the example given in the user's guide of the software tool. The following base sites are put in the database with the ranking given in Table 4.7 with the same convention as in Table 4.4. It turns out that every criterion is found to have a weight of 5.

Table 4.7: Ranking matrix before *Lausanne*'s entry.

	wind hours	stack hours	noise hours	pollution hours
weight	5	5	5	5
La Rochelle	*1*	*3*	*2*	*1*
Brussels	*2*	*1*	*2*	*3*
London	*3*	*2*	*1*	*3*
Porto	*4*	*4*	*2*	*2*

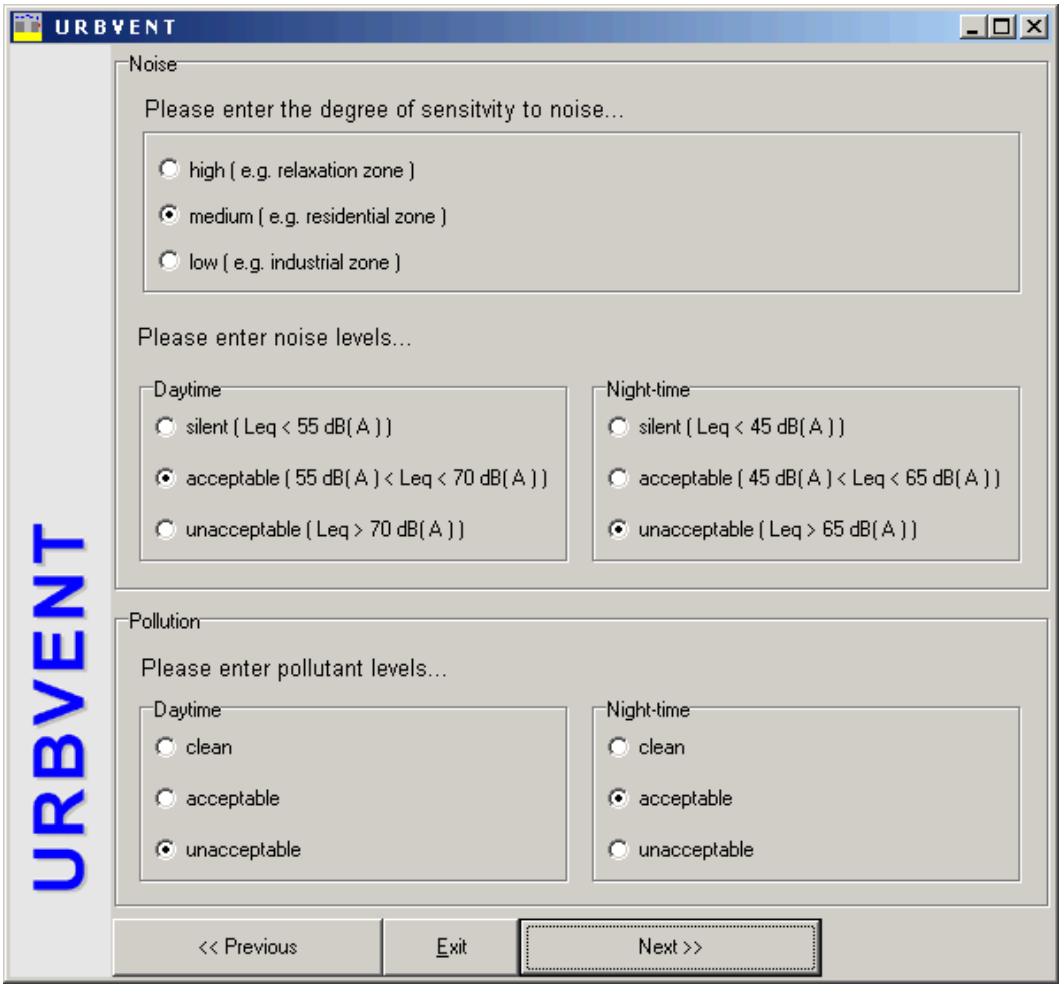

Figure 4.8: Noise and pollution selection form

In the example, a new site (*Lausanne*) is assessed and ranked by the multi-criteria analysis in third position (see Table 4.8).

Rather than assign a mark to the new site, the user can state that it is better than Porto (that has been rated by the expert as *poor* according to Figure 4.10) and not as good as London (that has been rated by the expert as *medium*) from the natural ventilation potential point of view.

The program also provides a set of graphs.

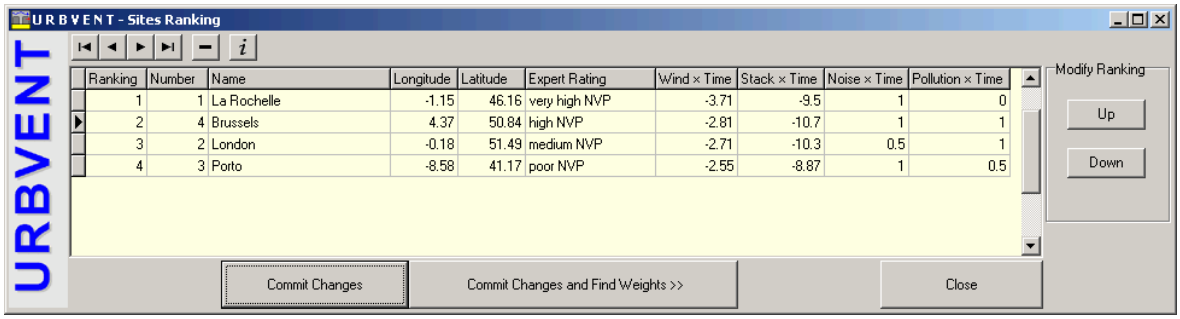

Figure 4.9: Expert's ranking form. Screenshot of the URBVENT software corresponding to Table 4.7

Table 4.8: Ranking matrix after *Lausanne*'s entry.

	wind hours	stack hours	noise hours	pollution hours
weight	5	5	5	5
La Rochelle	*1*	*3*	*2*	*1*
Brussels	*3*	*1*	*2*	*3*
London	*4*	*2*	*1*	*3*
Lausanne	*2*	*4*	*2*	*3*
Porto	*5*	*5*	*2*	*2*

4.7.3 Natural Ventilation Potential Graphs

The graphs hereafter provide more information on the natural ventilation potential by showing why a site is good or poor. Three graphs have been retained for this topic:

1. the average squared wind speed;
2. the average stack temperature difference;
3. the fraction of time when free (passive) cooling is possible.

The first two graphs correspond to the first two criteria used in the multi-criteria analysis and are strictly associated with (hygienic) ventilation potential and not with any passive cooling potential. Indoor temperatures have been determined on the basis of the ventilation strategy to be applied, in accordance with equation (4.5.12).

The third graph provides the *fraction of time when free cooling is possible*, given by:

$$\frac{1}{N}\sum_{i=1}^{N}\delta_{\mathrm{fc}\,i} \tag{4.7.1}$$

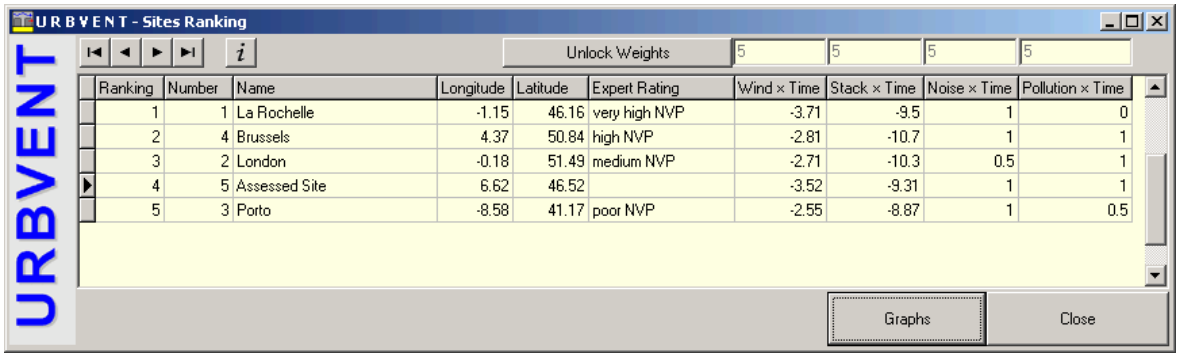

Ranking	Number	Name	Longitude	Latitude	Expert Rating	Wind × Time	Stack × Time	Noise × Time	Pollution × Time
1	1	La Rochelle	-1.15	46.16	very high NVP	-3.71	-9.5	1	0
2	4	Brussels	4.37	50.84	high NVP	-2.81	-10.7	1	1
3	2	London	-0.18	51.49	medium NVP	-2.71	-10.3	0.5	1
4	5	Assessed Site	6.62	46.52		-3.52	-9.31	1	1
5	3	Porto	-8.58	41.17	poor NVP	-2.55	-8.87	1	0.5

Figure 4.10: Sites ranking form. Screenshot of the URBVENT software corresponding to Table 4.8

with:

$$\delta_{\mathrm{fc}} = \begin{cases} 1 & \text{when } T_{\mathrm{fr}} > T_{\mathrm{cu}} \text{ and } T_{\mathrm{e}} \leq T_{\mathrm{cu}}, \\ 0 & \text{otherwise.} \end{cases} \tag{4.7.2}$$

The summation counts, amongst N instants, the occurrences when free cooling is possible—that is, when both the following conditions are met:

1. the air is too warm indoors[5] ($T_{\mathrm{fr}} > T_{\mathrm{cu}}$);

2. the outside air is cool enough to cool down the building ($T_{\mathrm{e}} \leq T_{\mathrm{cu}}$).

This kind of situation is encountered especially during the night-time hours of summer if the building has a large thermal inertia.

Remark

Criteria related to a passive cooling potential (PCP, see section 4.1) could be defined by weighting the terms of the summation in (4.7.1) by the terms encountered in the criteria related to wind (4.5.8), to stack effect (4.5.9), to noise (4.5.13) and to pollution

[5] in absence of heating, ventilation and cooling

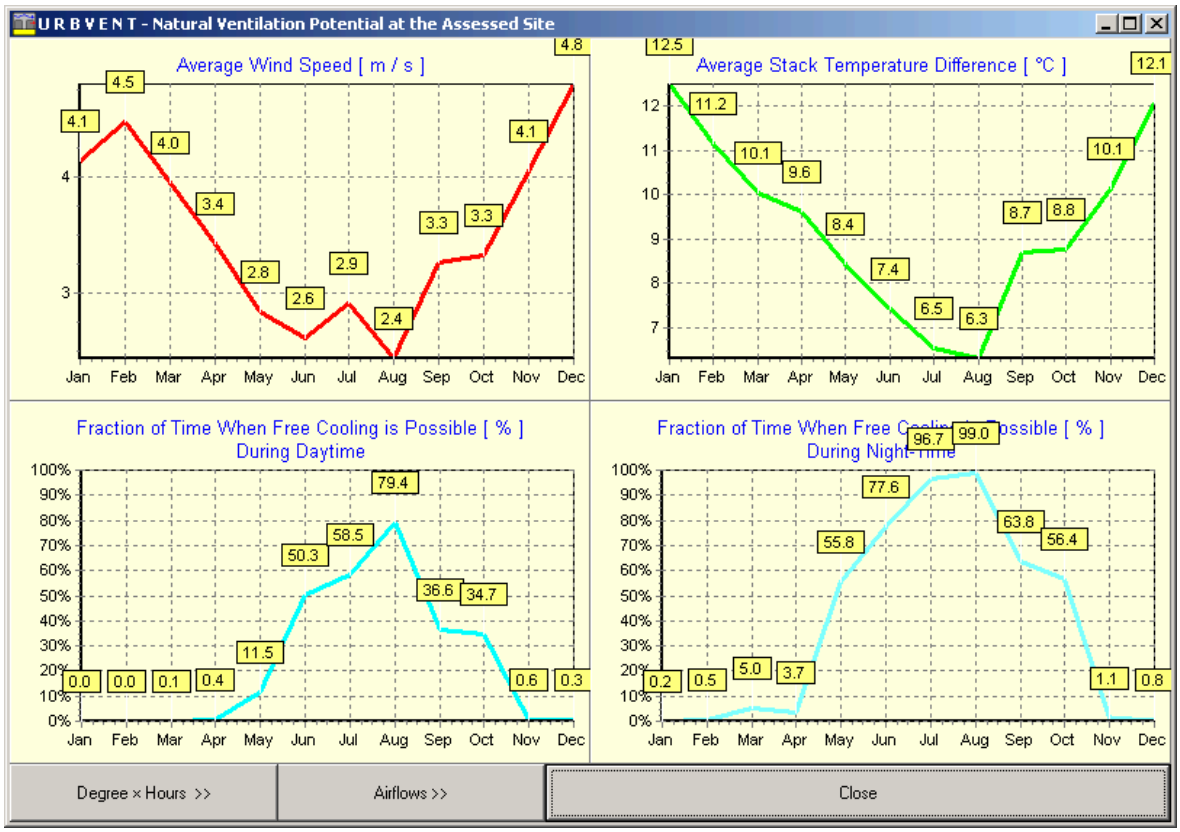

Figure 4.11: Natural ventilation potential graphs (situation in Lausanne, Switzerland)

(4.5.14). These criteria would take the following form:

$$WH_{\mathrm{PCP}} \overset{\mathrm{def.}}{=} \frac{1}{N} \sum_{i=1}^{N} v_i^{\mathrm{local}} \; \delta_{\mathrm{fc}i} \tag{4.7.3}$$

$$SH_{\mathrm{PCP}} \overset{\mathrm{def.}}{=} \frac{1}{N} \sum_{i=1}^{N} \left| \frac{T_{\mathrm{i}i} - T_{\mathrm{e}i}}{T_{\mathrm{e}i}} \right| \; \delta_{\mathrm{fc}i} \tag{4.7.4}$$

$$NH_{\mathrm{PCP}} \overset{\mathrm{def.}}{=} 10 \cdot \log_{10} \left(\frac{1}{N} \sum_{i=1}^{N} 10^{\; L_{\mathrm{noise}i} \; \delta_{\mathrm{fc}i}/10} \right) \tag{4.7.5}$$

$$PH_{\mathrm{PCP}} \overset{\mathrm{def.}}{=} \frac{1}{N} \sum_{i=1}^{N} L_{\mathrm{pollution}_i} \; \delta_{\mathrm{fc}i} \tag{4.7.6}$$

However, this passive cooling potential will not be addressed here.

4.7.4 Graphs of Degree Hours

These graphs (see Figure 4.12 (a)) represent the degree hours associated with:

1. the heating demand;
2. the cooling saved by ventilation; and
3. the cooling demand.

These degree hours can also be obtained in a distribution form, as shown in Figure 4.12 (b). This is very useful for sizing heating or cooling systems.

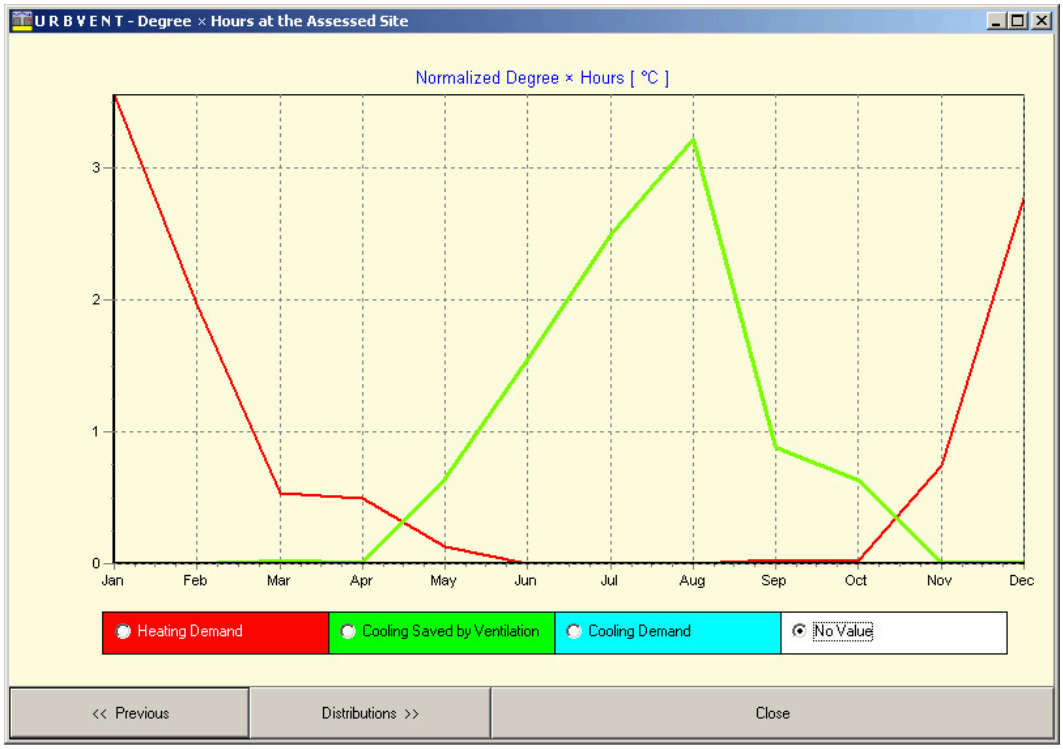

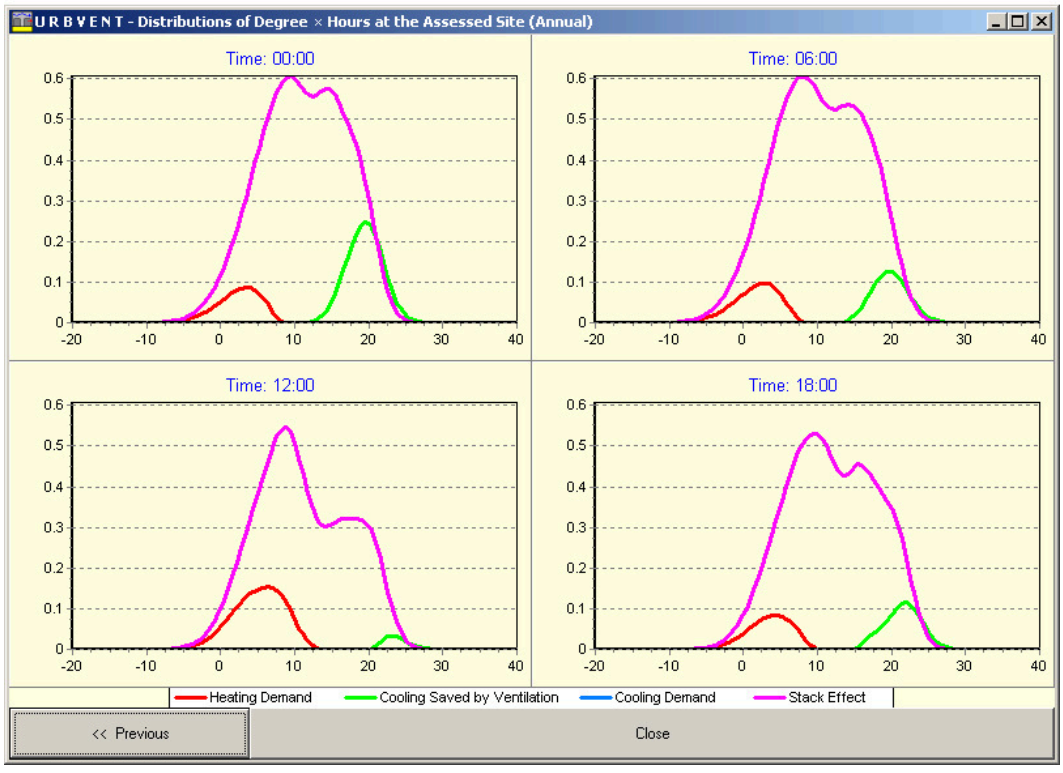

Figure 4.12: **(a)** Degree hours graphs (situation in Lausanne, Switzerland). **(b)** Degree hours distributions and inside–outside temperature difference ('stack effect') distributions (situation in Lausanne, Switzerland)

4.7.5 Airflow Graph

Only airflow due to stack effect is displayed (see Figure 4.13), without accounting for the effect of wind pressure. This graph presents airflow in a very simple example, comprising a room with two openings, as sketched in the top left corner. This is a monthly averaged value, which does not guarantee that the airflow is always sufficient. Both the apertures have the same area A and have a vertical distance of H. This airflow is calculated by means of (4.2.4).

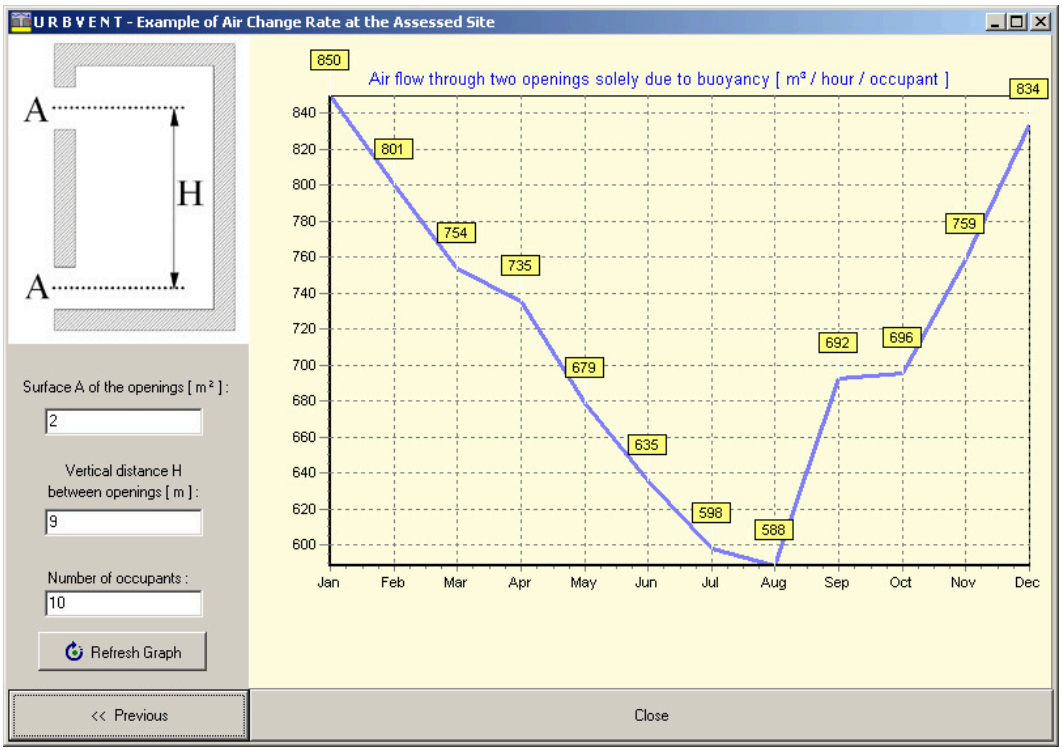

Figure 4.13: Airflow graph (situation in Lausanne, Switzerland))

4.7.6 Analysing the Graphs: An Example

This section gives an explanation of how to interpret the graphical results and how to stress the difference between months and between different locations in the example of Lausanne, Switzerland (see above) and Seville, Spain. Two distant sites have been selected for this case study in order to emphasize the differences encountered in the graphs. However, according to the situation, the user may need to compare different

sites in the same city. In this case, local factors, such as local street geometry or local noise conditions, prevail in the ranking process.

4.7.6.1 Natural Ventilation Potential Graphs

Figure 4.11 emphasizes the fact that stack effect is primarily due to temperature differences induced by the heating system. As one can see, the average stack temperature difference is higher during the heating season. Moreover, the assumption has been made that no cooling system is used, creating few stack effects during the 'cooling season'. If air-conditioning were used, the outside–inside temperature difference would induce buoyancy; but this would be useless for ventilation purposes anyway since air-conditioning already provides ventilation.

On the other hand, when considering the situation in Lausanne, Switzerland (see Figure 4.11), free (passive) cooling is almost only possible during summer, as one can expect. In fact, free cooling is possible only if the inside (free-running) temperature is higher than the upper limit of comfort *and* if the outside temperature is lower than this limit. This configuration is met especially during summer night-time hours of summer in Lausanne. The situation in Seville, Spain (Figure 4.14) is quite different in the sense that free cooling is also possible during spring and autumn.

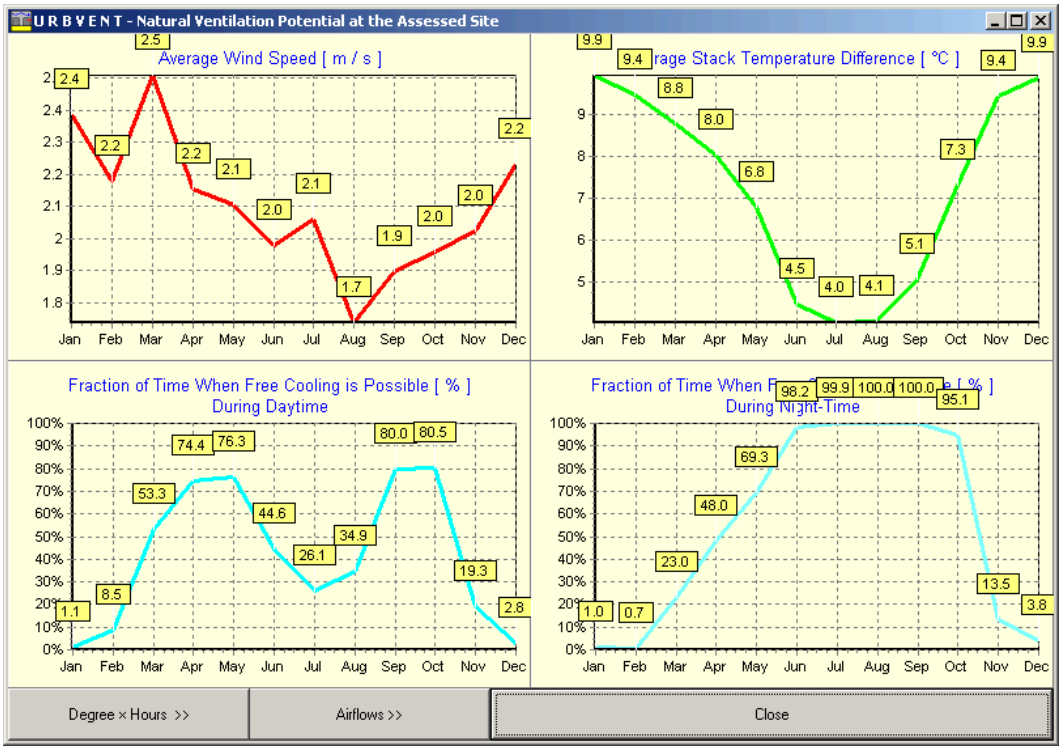

Figure 4.14: Natural ventilation potential graphs (situation in Seville, Spain)

4.7.6.2 Degree Hours Graphs

When comparing the situations in Lausanne (see Figure 4.12) and in Seville (see Figure 4.15), it comes out—without surprise—that the heating demand is higher in Lausanne and that the cooling demand is higher in Seville. Regarding the cooling demand, it should be stressed here that it concerns a *cooling requirement when free cooling is not possible*, as opposed to cooling saved by ventilation. Thus, considering a specific moment, either a contribution is brought to the 'cooling saved by ventilation' graph, or to the 'cooling demand' graph, but never to both simultaneously.

Expressed another way, the cooling demand can only be fulfilled by mechanical cooling. However, the decision can be made to avoid mechanical cooling and to tolerate higher temperatures in the building (or to adapt oneself to them). According to Figure 4.12 (a), this situation is never encountered in Lausanne and this is corroborated by the fact that air-conditioning is very seldom used in that city.

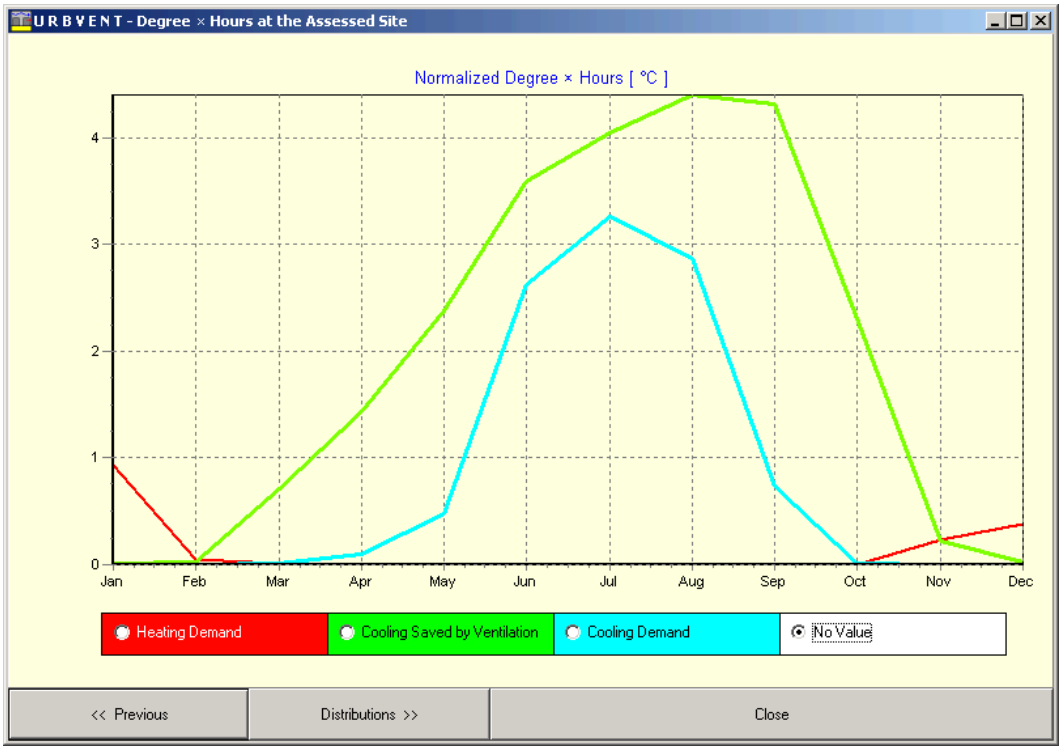

Figure 4.15: Degree hours graphs (situation in Seville, Spain)

4.7.6.3 Airflow Graph

The minimal airflow requirements are fulfilled as soon as pollutants concentrations in the room are acceptable. Most of the time, the larger airflow needs come from odours and carbon dioxide evacuation and range approximately from 10 to 30 cubic metres per hour and per occupant.

As shown in Figure 4.13, these rates are largely exceeded.

4.8 Software Verification

This verification—or validation against a limited number of cases—concerns only the part of the software that ranks the sites in the aspect of the natural ventilation potential, regardless of the graphs. It is important to mention that this piece of software is almost impossible to validate because it assesses a potential (*i.e.* something pre-existing the building and that has to be capitalized by the building's architecture).

This is seldom entirely the case. In other words, the suppositions made in section 4.4 ('Assumptions of the Methodology') are hardly ever fulfilled. However, a verification has been carried out, bearing in mind that one should keep an open mind about its results.

4.8.1 Verification Method

The method chosen for the verification was based on a survey carried out within the frame of the European project Hope (Health Optimization Protocol for Energy-Efficient Buildings) (Bluyssen *et al.*, 2003), whose aim, amongst others, was to solve the conflict between strategies to reduce energy use and strategies to create healthy buildings. A substantial number of questionnaires have been distributed and perused. Amongst the questions, several have been considered relevant for the present verification. Some questions were related to indoor air quality and have been used here to describe the extent of the natural ventilation driving forces. These included the following:

- In winter, do you experience bad smells coming from furnishings, the kitchen or the stairway ?
- In summer, do you experience bad smells coming from furnishings, the kitchen or the stairway ?
- Is air odourless in winter ?
- Is air odourless in summer ?

Other questions, on external noise and external pollution, have been retained to describe the extent of the constraints. These were:

- Do you experience outside noise in winter ?
- Do you experience outside noise in summer ?
- Do you experience outside pollution in winter ?
- Do you experience outside pollution in summer ?

The answers to the first four questions and to the last four were aggregated separately. The two ensuing aggregation results were then aggregated, in turn, in order to provide a natural ventilation potential.

The aggregation method used here is *Hermione* (Flourentzou *et al.*, 2003). It allows several levels of aggregation (such as the ones just mentioned) and is completely independent of the method Qualiflex used until this point. In Hermione, the user assigns

each criterion to a class: Green + (best); Green ∘ ; Green – ; Yellow + ; Yellow ∘ ; Yellow – ; Red + ; Red ∘ ; Red – ; or Black (worst). In our case, each criterion corresponds to one of the eight above-mentioned questions. This process requires a strict correspondence table between the answers given for each question and a class (colour). The method then aggregates the criteria and assigns a class to the newly aggregated criterion following democratic rules. In our case, this final criterion is the natural ventilation potential.

4.8.2 Verification Results

4.8.2.1 Hermione Results

Nine sites across Europe with naturally ventilated homes were selected to validate the software. Table 4.9 shows their respective Hermione-assigned class according to the answers in the questionnaires. In so doing, a ranking of these nine sites could be drawn up (keeping in mind that this ranking is not unambiguous because sites can be permuted within a same Hermione class).

Table 4.9: HOPE sites and *Hermione* classes. URBVENT base sites are bracketed.

site	***Hermione* class**
[Switzerland 1] Switzerland 2	Green +
Germany 1 [Switzerland 3]	Green ∘
Switzerland 4	Green –
[Switzerland 5] Portugal 1 [Germany 2]	Yellow +
Italy 1	Yellow –

4.8.2.2 URBVENT Results

Among these nine sites, four were chosen as URBVENT base sites in order to provide a 'representative scale' of classes. These sites are written between square brackets in Table 4.9.

The four base sites were introduced in the software database following the procedure

described in section 4.7.1 (*'Filling Out the Ranking Matrix'*). Noise and pollution levels were entered in accordance with the answers given to the Hope questionnaires.

The following set of weights was found: (5, 3, 5, 5) (see section 4.6.7, *'Adaptive weights'*). These weights show that all of the criteria have roughly the same importance and that they are all relevant since none is equal to zero. Keeping these weights, the program finds the rankings for the five remaining sites, after their introduction (one by one) again by following the procedure of section 4.7.1; the results are given in Tables 4.10 to 4.14 .

Table 4.10: Ranking of Switzerland 2 compared with base sites (in squared brackets)

site
[Switzerland 1]
Switzerland 2
[Switzerland 3]
[Switzerland 5]
[Germany 2]

Table 4.11: Ranking of Germany 1 compared with base sites (in squared brackets)

site
[Switzerland 1]
Germany 1
[Switzerland 3]
[Switzerland 5]
[Germany 2]

Table 4.12: Ranking of Switzerland 4 compared with base sites (in squared brackets)

site
[Switzerland 1]
[Switzerland 3]
Switzerland 4
[Switzerland 5]
[Germany 2]

Table 4.13: Ranking of Portugal 1 compared with base sites (in squared brackets)

site
[Switzerland 1]
[Switzerland 3]
[Switzerland 5]
Portugal 1
[Germany 2]

Table 4.14: Ranking of Italy 1 compared with base sites (in squared brackets)

site
[Switzerland 1]
[Switzerland 3]
[Switzerland 5]
[Germany 2]
Italy 1

4.8.2.3 Comparison between URBVENT and Hermione

The sites have been introduced one by one in order to check whether each of them falls in the correct Hermione class. For instance, *Switzerland 2* is correctly ranked by URBVENT (see Table 4.10) because it is compatible with Table 4.9. In fact, had *Switzerland 2* been ranked in first position by URBVENT, the result would have been deemed to be correct because *Switzerland 1* and *Switzerland 2* are not discernible by Hermione (because they are in the same Hermione class). Therefore, the probability that this agreement is due to pure luck is $\frac{2}{5}$ because there are five possible positions for *Switzerland 2* amongst which two are in agreement with Table 4.9.

It can be noticed that each of the five rankings provided by the software tool is in full agreement with the ranking of Table 4.9. The probability that this agreement is due to chance for the entire set of rankings is (following the same reasoning as above) $\frac{2}{5} \cdot \frac{2}{5} \cdot \frac{1}{5} \cdot \frac{3}{5} \cdot \frac{1}{5} = \frac{12}{3125} = 0.384\,\%$.

4.9 Sensitivity Analysis

A sensitivity analysis has been conducted on the last ranking (see Table 4.14) to check the effect of small variations of the weight values on the ranking itself. For this purpose, a Plackett-Burman design (Plackett & Burman, 1943) has been carried out by varying the weights by –1 or +1. In order to lighten the notation, *Switzerland 1*, *Switzerland 3*, *Switzerland 5*, *Germany 2* and *Italy 1* have been assigned numbers 1, 2, 3, 4 and 5, respectively, so that the ranking of Table 4.14 can be written as (1, 2, 3, 4, 5).

Table 4.15 shows a Plackett-Burman design in eight runs. The weight variations are given in columns 2 to 5 and the resulting ranking is in column 6. By way of illustration, in the first run, weights 6, 4, 6 and 4 are assigned two of the four criteria, since the initial weights were 5, 3, 5 and 5.

The results show that the initial ranking (1, 2, 3, 4, 5) appears three times out of eight. A permanent feature is that site 1 (*Switzerland 1*) and site 5 (*Italy 1*) are always ranked in first and in last position, respectively.

Table 4.15: Plackett-Burman design Run Wind time Stack time Noise time Pollution time Ranking)

run	wind hours	stack hours	noise hours	pollution hours	ranking
1	+1	+1	+1	–1	(1, 2, 3, 4, 5)
2	+1	+1	–1	+1	(1, 4, 3, 2, 5)
3	+1	–1	+1	–1	(1, 2, 3, 4, 5)
4	–1	+1	–1	–1	(1, 4, 3, 2, 5)
5	+1	–1	–1	+1	(1, 3, 4, 2, 5)
6	–1	–1	+1	+1	(1, 2, 4, 3, 5)
7	–1	+1	+1	+1	(1, 2, 4, 3, 5)
8	–1	–1	–1	–1	(1, 2, 3, 4, 5)

4.10 Conclusion

It is important to conclude by emphasizing that the assessed natural ventilation potential is the potential of the site. Once a site with a good potential is found, the designer's task is to construct a building or to refurbish an existing one in a way that makes the most out of this potential. This is in accordance with the first assumption made is this chapter. In other words, both an appropriate site and an appropriate building are necessary conditions if natural ventilation is to be applied.

This is why this methodology is so difficult to validate: a proper validation would imply that buildings erected on the assessed site do take advantage of the best potential of those sites.

Chapter 5

FVM's Results

5.1 Introduction

As mentioned in section 3.5, the results of the mesoscale model FVM weren't applied in URBVENT's software. This is a consequence first of the large quantity of data required for forcing FVM: if the intention is to obtain representative enough data, at least a two-year period of 9 variable's hourly data over a domain of $8 \times 8 \times 45$ grid cells should be extracted from the *Lokal-Modell*'s results archive for each city. For a city such as Basel of Geneva only, this represents approximately three gigabytes of data. On top of that, a parametrization would have to be set up for each city in Europe, including building height distributions, street orientation distributions, albedos, material properties, landuses and the like. Eventually, highly time consuming simulations would have to be run for each city.

Consequently, the present chapter presents the results of solely a set of simulations launched over the region of Basel, Switzerland. The main objective is to determine whether the new urban modelling contributes to an improvement of wind and temperature simulation results.

5.2 The BUBBLE Project

Figure 5.1 represents both the LM and the FVM domains. (See section 3.5, 'Mesoscale Atmospheric Modelling'), as well as the domain covered by the *BUBBLE project* (Basel UrBan Boundary Layer Experiment).

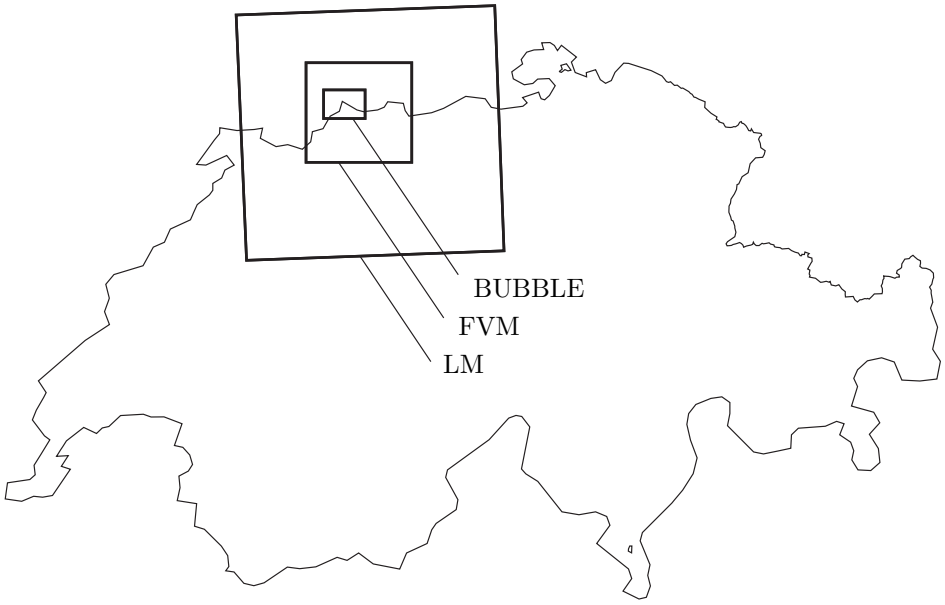

Figure 5.1: LM, FVM and BUBBLE domains over Basel's area.

The occurrence of this project in which on-site measurements were undertaken led to the choice of Basel for comparing LM's and FVM's outcomes with these measurements.

The BUBBLE project[1] consisted in a large urban Planetary Boundary Layer (PBL) experiment carried out under the auspices of the European COST 715 action. Its aim was that of investigating the exchange processes occurring near the urban surface as well as the flows occurring in the upper part of the Urban Boundary Layer (UBL). The tools used were surface and remote sensing instrumentation on the one hand, and a mesoscale meteorological model on the other hand.

From the 15th June until the 12th July 2002, a so-called *Intensive Operation Period* (IOP) took place during which a maximum number of measuring weather stations were in use, as shown in Figure 5.2. Therefore, a simulation covering three days has been realized within this period, namely from 25th June to 27th June (see section 5.4, 'FVM Simulation Results').

Weather stations are located either at rural, suburban or urban sites as can be seen in Figure 5.2. The fraction α of rural to urban coverage has been determined as

[1]Homepage of the project:
`http://www.unibas.ch/geo/mcr/Projects/BUBBLE/`

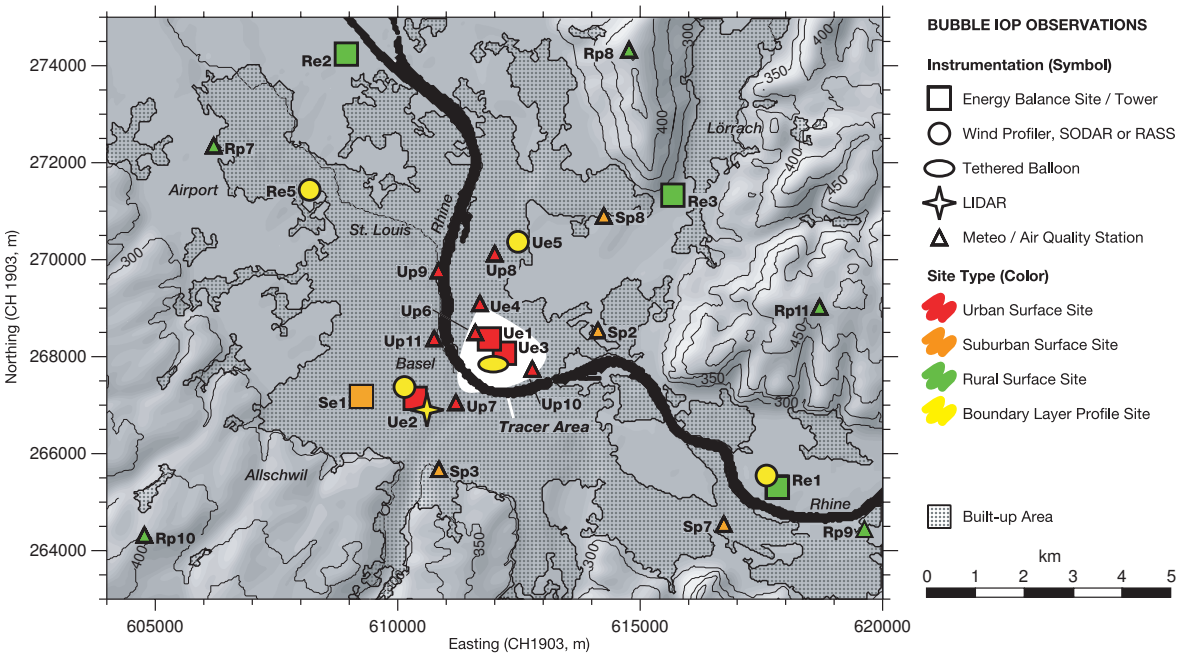

Figure 5.2: Map of the measurement stations during BUBBLE-IOP. (Some rural sites are out of map.) source: `http://www.unibas.ch/geo/mcr/Projects/BUBBLE/`

part of another project named KABA[2] (*Klimaanalyse der Region Basel*), whose main objective was "to design maps covering the trinational region of Basel (Switzerland, Germany and France) with a size of 51×33 km^2 ". This fraction α—corresponding to the one encountered in equation (3.6.3)—was assessed for each cell of FVM's domain.

Station Ue1 (Sperrstrasse) is of particular interest due to its location within an urban canyon. In addition, like in other stations, its measurements are made on several levels by means of a mast, along which psychrometers and cup anemometers are uniformly set (see Figure 5.3).

[2]Homepage of the project:
`http://www.unibas.ch/geo/mcr/Projects/KABA/`

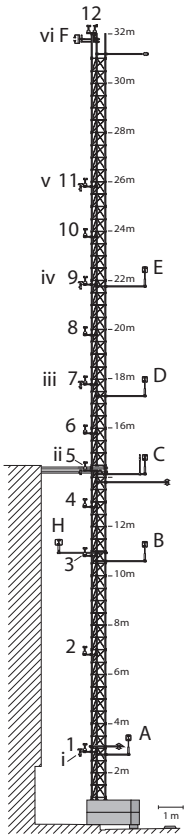

Figure 5.3: The 32-metre tower at Sperrstrasse (Ue1).

source: `http://www.unibas.ch/geo/mcr/Projects/BUBBLE/`

5.3 The Basel Area

Climate and wind regimes of the Basel area are mainly influenced by the Rhine valley. Globally, wind speeds are very low (below 4 m/s) and east-west oriented. Topographically, the region is surrounded noth-east by the German Black Forest (reach its highest point at 1 493 m a.s.l), south by the Jura range, and west by the French Vosges mountains. These surrounding mountains cause the formation of diurnal slope winds. This basin-like situation makes of Basel one of the warmest (and incidentally most polluted) regions of Switzerland.

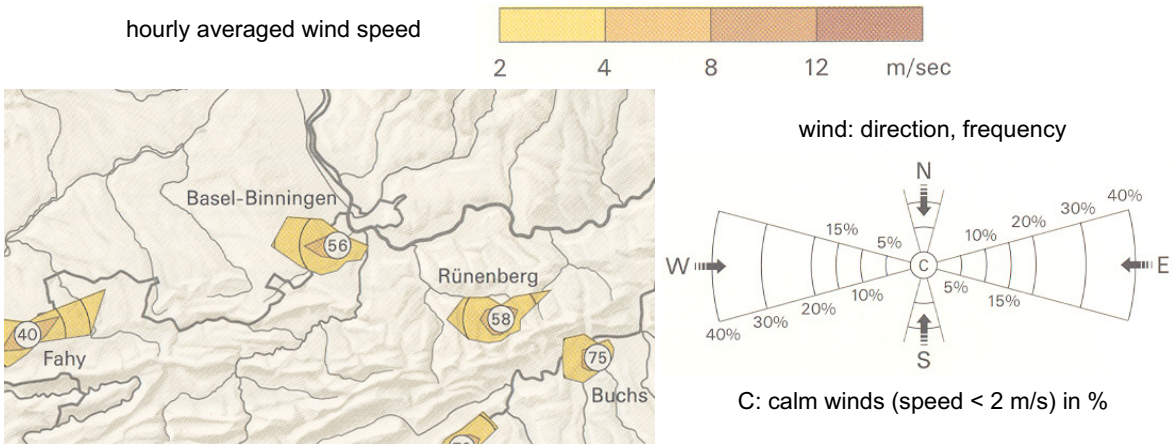

Figure 5.4: July's windrose in the region of Basel (MeteoSwiss, 1982-2000). Wind generally blows below 4 m/s in east-west direction. (This direction is still more pronounced during the rest of the year.)

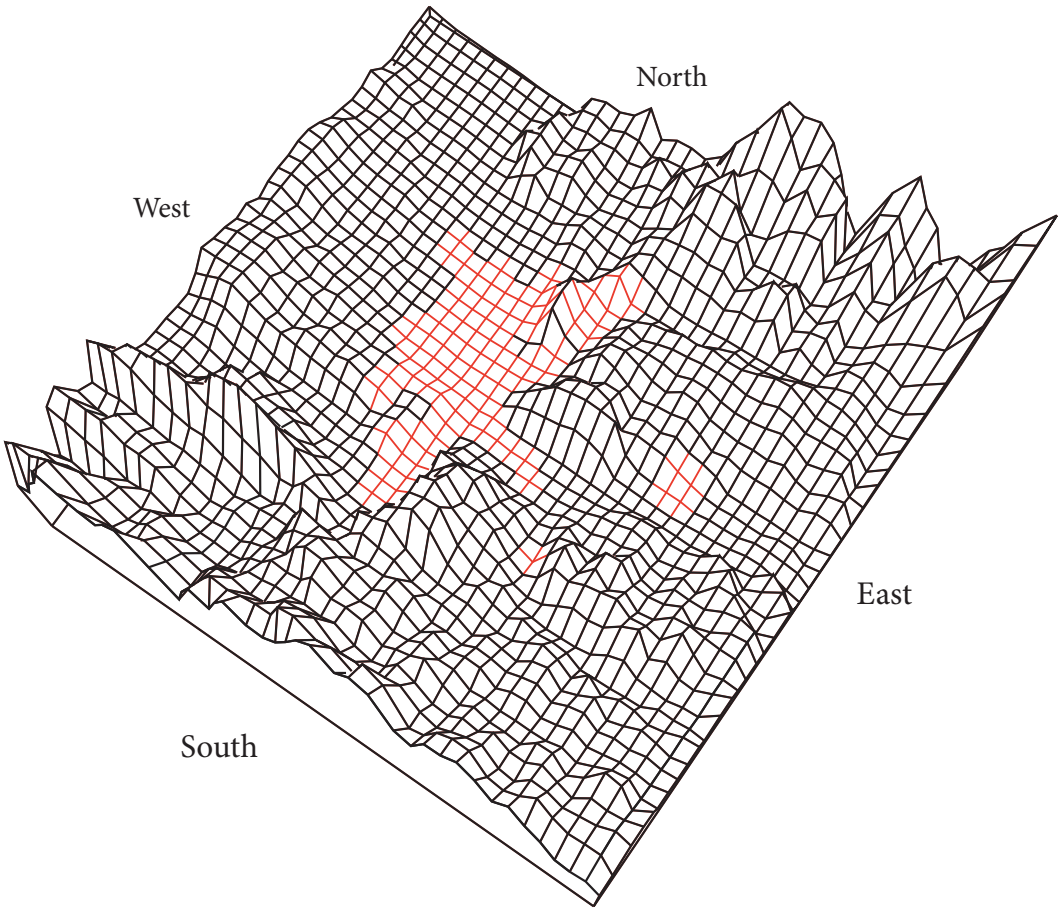

Figure 5.5: Topography of the 40 km × 40 km simulated domain. Red zones represent the built-up area of Basel. Extension of the simulated domain: longitude: 7.406–7.939°East, latitude: 47.363–47.723°North.

5.3.1 Forcing and Interpolation Techniques

In order to launch FVM's simulations, initial and boundary conditions must be provided. These conditions are supplied in the event by a larger-scale model. This process, referred to as *forcing*, is made possible in our case via the outputs of the *Lokal-Modell* (LM).

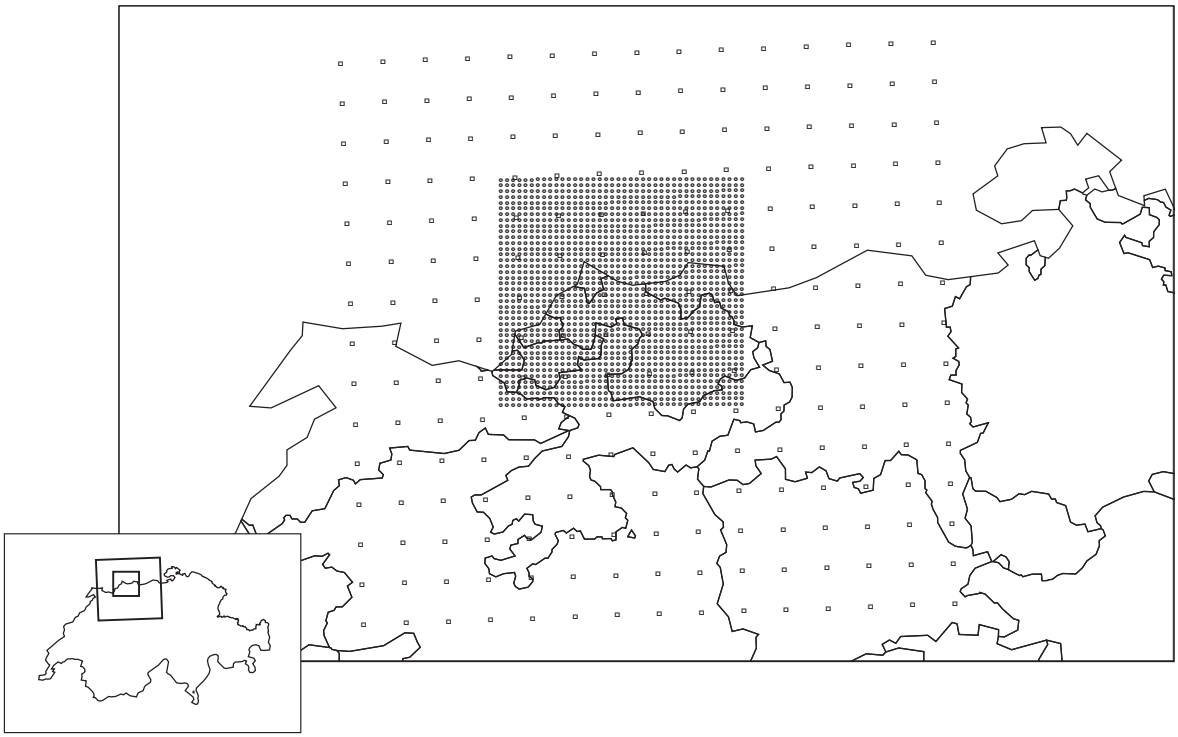

Figure 5.6: Nesting of FVM's grid (circles) in LM's grid (squares). Vignette: overview of both domains over Switzerland.

As both models have different grid definitions (see Figure 5.6), variables values at each grid point of FVM are obtained by interpolation of LM's values. More specifically, for each of FVM's grid point, LM's closest neighbours are used for the interpolation by means of an *inverse distance weighted* interpolation.

Inverse distance weighted (IDW) interpolation methods are based on the assumption that the interpolating point should be influenced most by the nearby points and less by the more distant points. The interpolating point is a weighted average of the neighbouring points and the weight assigned to each point diminishes as the distance from the interpolation point to this point increases.

The weights w are given by:

$$w(P_{\mathrm{FVM}}; P_{\mathrm{LM}i}) = \frac{\left[\frac{1}{\delta(P_{\mathrm{FVM}}; P_{\mathrm{LM}i})}\right]^{\alpha}}{\sum_{j=1}^{N}\left[\frac{1}{\delta(P_{\mathrm{FVM}}; P_{\mathrm{LM}j})}\right]^{\alpha}} \qquad \forall\, i \in \{1, \ldots, N\} \tag{5.3.1}$$

where $\delta(P_{\mathrm{FVM}}; P_{\mathrm{LM}i})$ (for $i = 1, \ldots, N$) are the distances from the interpolated point P_{FVM} to the N neighbouring interpolation points $P_{\mathrm{LM}i}$ (usually N equals eight or four). α is the (positive) interpolation exponent. In IDW, the exponent determines how much influence each point will have on the result. The higher the exponent the greater the influence closer points will have on the cell value. Exponents can range from 1 to 10. In the present work, a value of 2 was chosen.

The value of a variable $\psi(P_{\mathrm{FVM}})$ at the interpolated point P_{FVM} is then computed as:

$$\boxed{\psi(P_{\mathrm{FVM}}) = \sum_{i=1}^{N} w(P_{\mathrm{FVM}}; P_{\mathrm{LM}i}) \cdot \psi(P_{\mathrm{LM}i})} \tag{5.3.2}$$

where $\psi(P_{\mathrm{LM}i})$ (for $i = 1, \ldots, N$) are the values of variable ψ at the N neighbouring interpolation points of the larger-scale model.

An example of interpolation result is shown in Figure 5.7

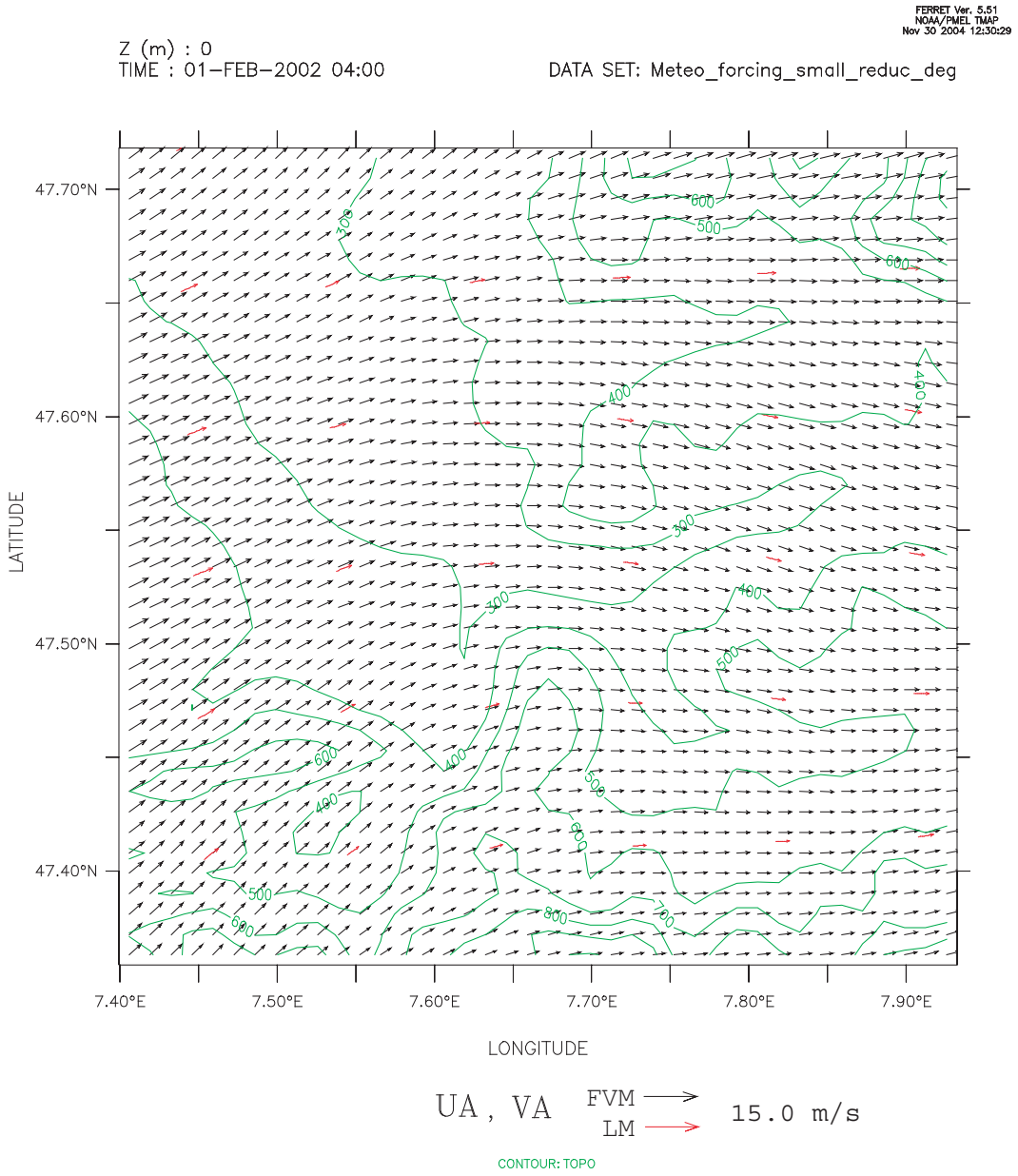

Figure 5.7: Example of interpolation of the wind field (black arrows) from the larger-scale model wind field (red arrows). Topography is displayed in green.

The forcing is carried out for wind and temperature at the boundaries of the simulated domain. As one goes deeper into the domain, the values calculated by FVM are mixed with the forcing (LM) values until encountering purely FVM-computed values (after say 5 km).

As far as solar radiation is concerned, the mesoscale model, unlike the *Lokal-Modell*, does not consider any condensation or cloud formation processes. Therefore, no feedback to the solar radiation calculation (attenuation through cloud episodes) is taken into account in the model. Since this phenomenon plays an important role for the amount of energy available for turbulence generation near the ground, and should therefore be included, solar radiation can be prescribed to the model by data input interpolation, rather than calculating it by the model itself. This constitutes an 'indirect' consideration of cloud formation in the model and improves the fit to local meteorological conditions.

Finally, pressures are interpolated as well.

5.4 FVM Simulation Results during the BUBBLE *Intensive Operation Period* (IOP)

The focus has been fixed on temperatures and wind speeds for these two parameters come into play in the URBVENT method. Several weather stations at which wind speeds and temperatures were recorded have been used to compare simulation results with.

5.4.1 Temperatures—Geographical Comparisons

The first comparisons are geographical. Weather FVM can catch local differences better than LM is what these comparisons are meant to determine. Note that in addition to the urban module, FVM uses a more detailed topography coming from the KABA project (see Figure 5.5).

In each of the following figures (Figures 5.8 to 5.12), the first shade plot (a) shows LM's simulation results, along with measurements coming from BUBBLE represented by small squares, whereas the second shade plot (b) provides FVM's simulation results, as well as the same on-site measurements—still represented by small squares.

Simulation results coming from either model are shown in these figures for an altitude of 10 metres above ground level. Yet the reader should bear in mind that the measurements from BUBBLE weren't made at the same height and that Figures 5.8 to 5.12 show the measured values closest to these 10 metres, according to Table 5.1.

Table 5.1: Type of environment and altitude above ground level of BUBBLE's measurement closest to 10 m.

weather station	type	altitude in metres of the measurement a.g.l.	
		temperature	wind velocity
Re1 Grenzach	rural	1.5	30
Re2 Village-Neuf	rural	0.5	5
Re3 Lange Erlen	rural	10	10
Rp10 Schoenenbuch	rural	3	10
Rp11 St-Chrischonaturm	rural	2	250
Se1 Allschwil	suburban	15	8.3
Sp3 Binningen	suburban	2	17
Sp7 Schweizerhalle	suburban	32	40
Ue1 Sperrstrasse	dense urban	13.9	11.3
Ue4 Horburg	urban	17.2	18.4
Up11 St-Johann	urban	2.8	25

Results are shown for five instants (at noon or midnight) during the Intensive Operation Period. The large rectangle stands for the BUBBLE area whereas the built-up areas are represented by a shape overlapping this area (see legend in Figure 5.8 (a)).

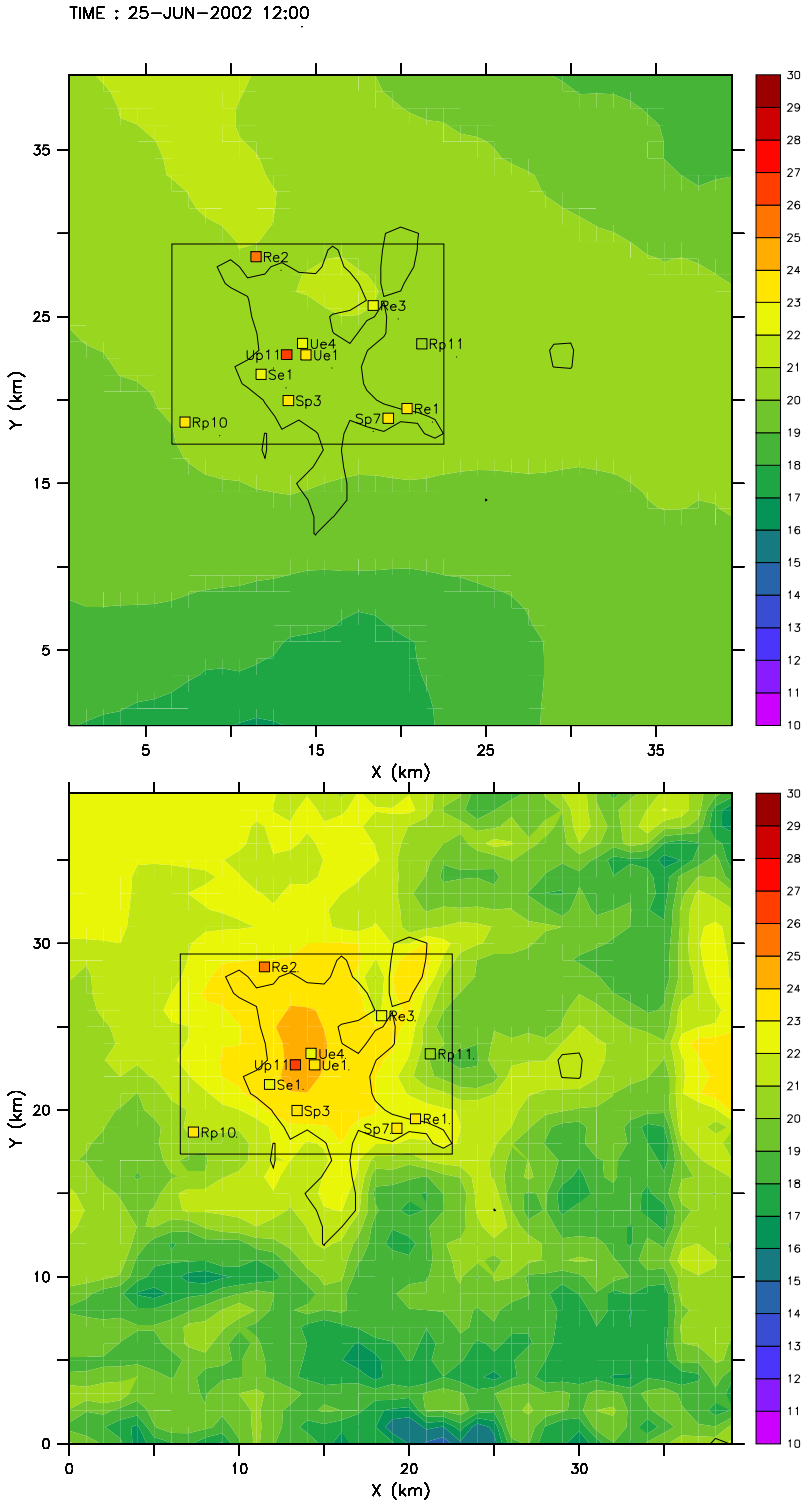

Figure 5.8: Temperatures on 25th June 2002, 12:00 UTC time

(a) Comparison of LM's results (at 10 m a.g.l.) with BUBBLE's measurements (squares).

(b) Comparison of FVM's results (at 10 m a.g.l.) with BUBBLE's measurements (squares).

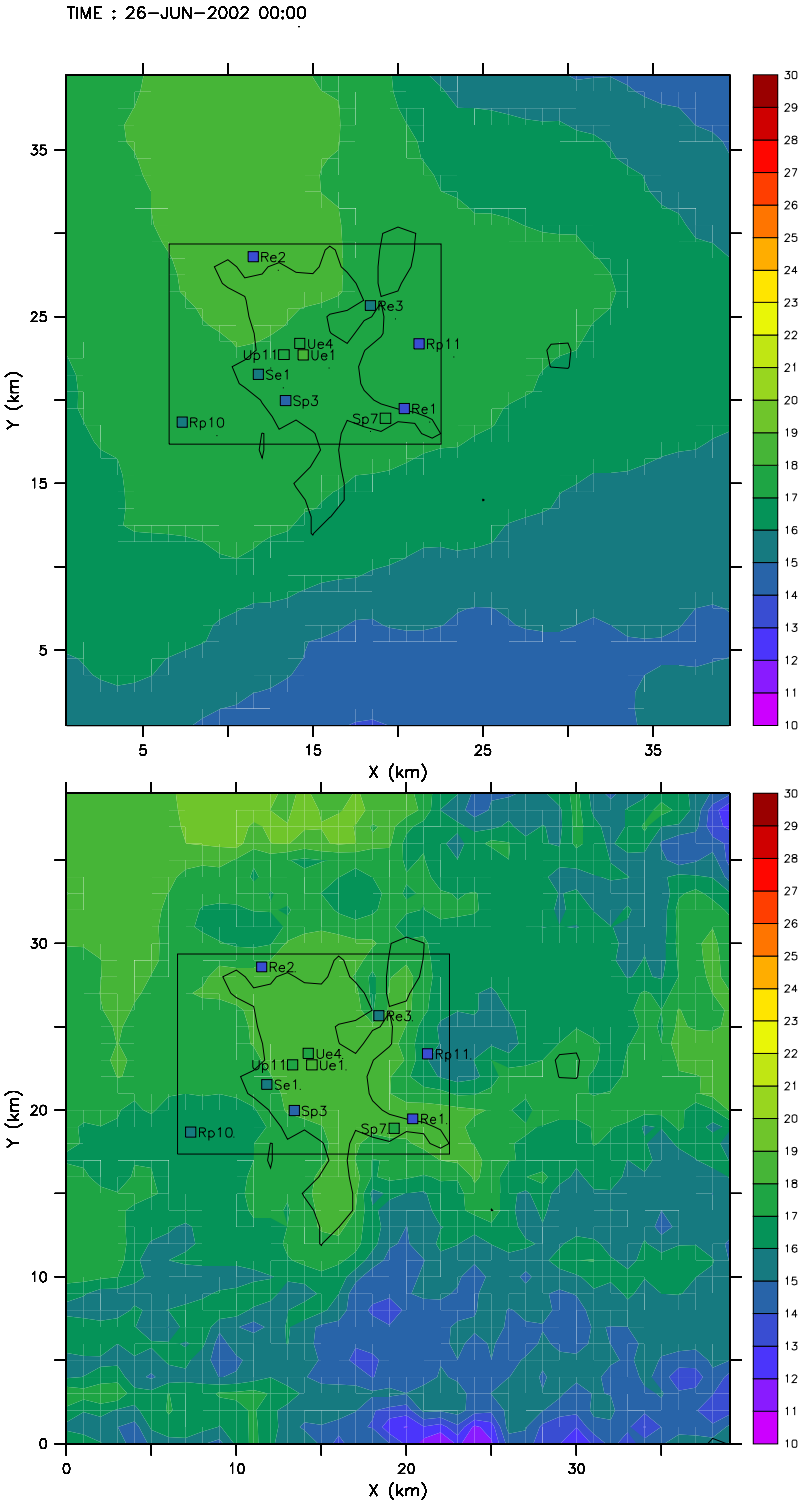

Figure 5.9: Temperatures on 26th June 2002, 00:00 UTC time

(a) Comparison of LM's results (at 10 m a.g.l.) with BUBBLE's measurements (squares).

(b) Comparison of FVM's results (at 10 m a.g.l.) with BUBBLE's measurements (squares).

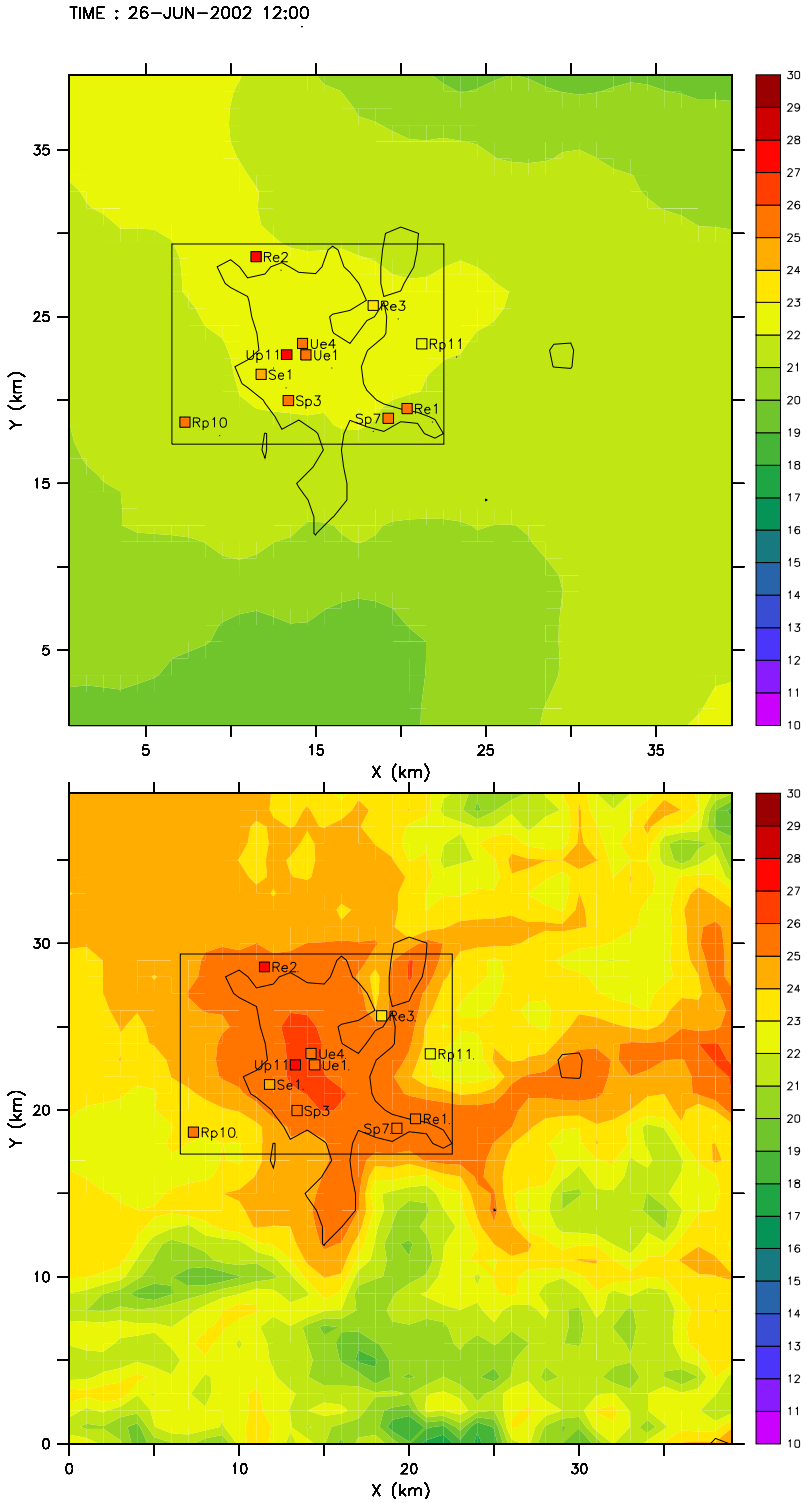

Figure 5.10: Temperatures on 26th June 2002, 12:00 UTC time

(a) Comparison of LM's results (at 10 m a.g.l.) with BUBBLE's measurements (squares).

(b) Comparison of FVM's results (at 10 m a.g.l.) with BUBBLE's measurements (squares).

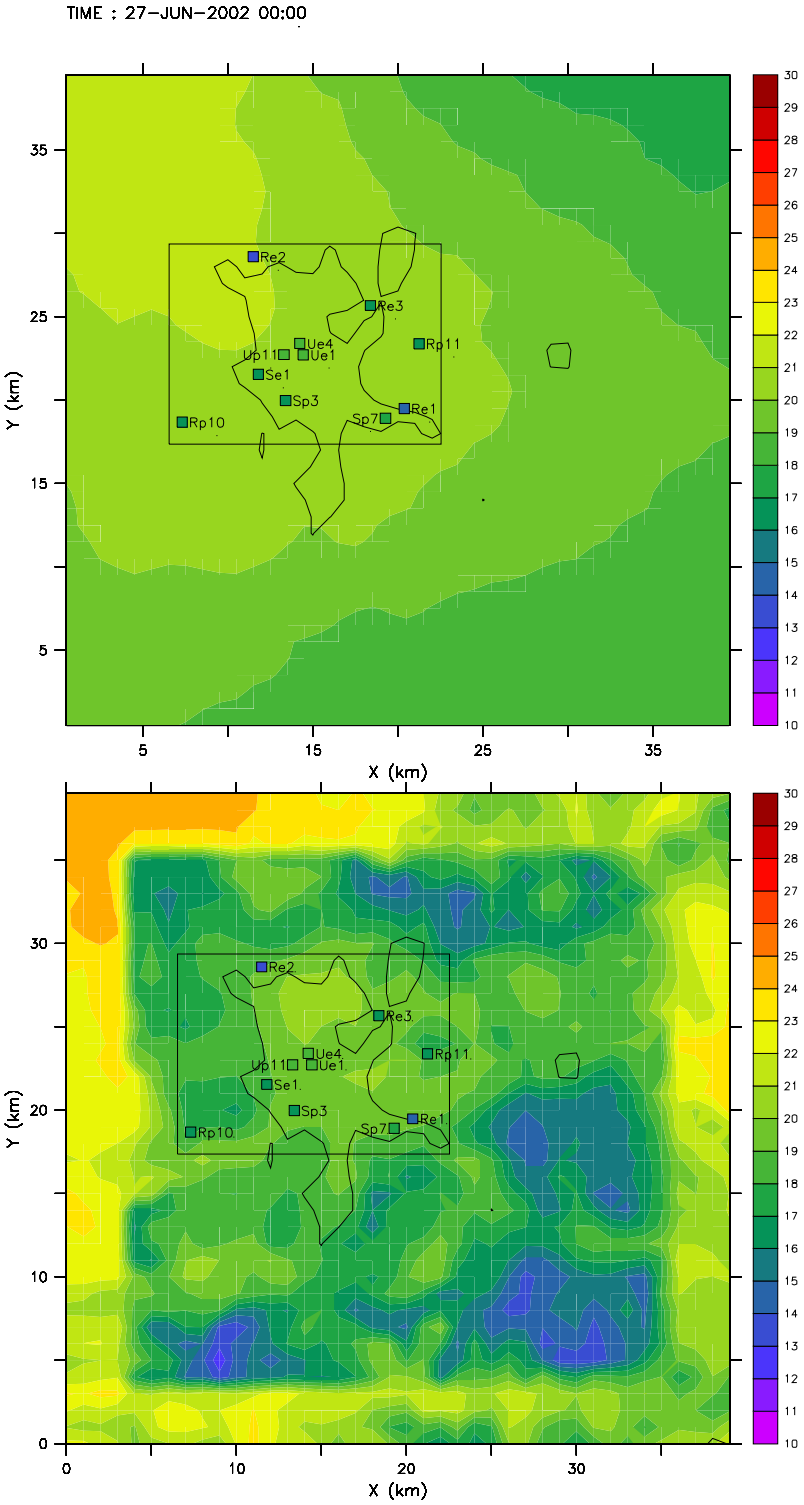

Figure 5.11: Temperatures on 27th June 2002, 00:00 UTC time

(a) Comparison of LM's results (at 10 m a.g.l.) with BUBBLE's measurements (squares).

(b) Comparison of FVM's results (at 10 m a.g.l.) with BUBBLE's measurements (squares).

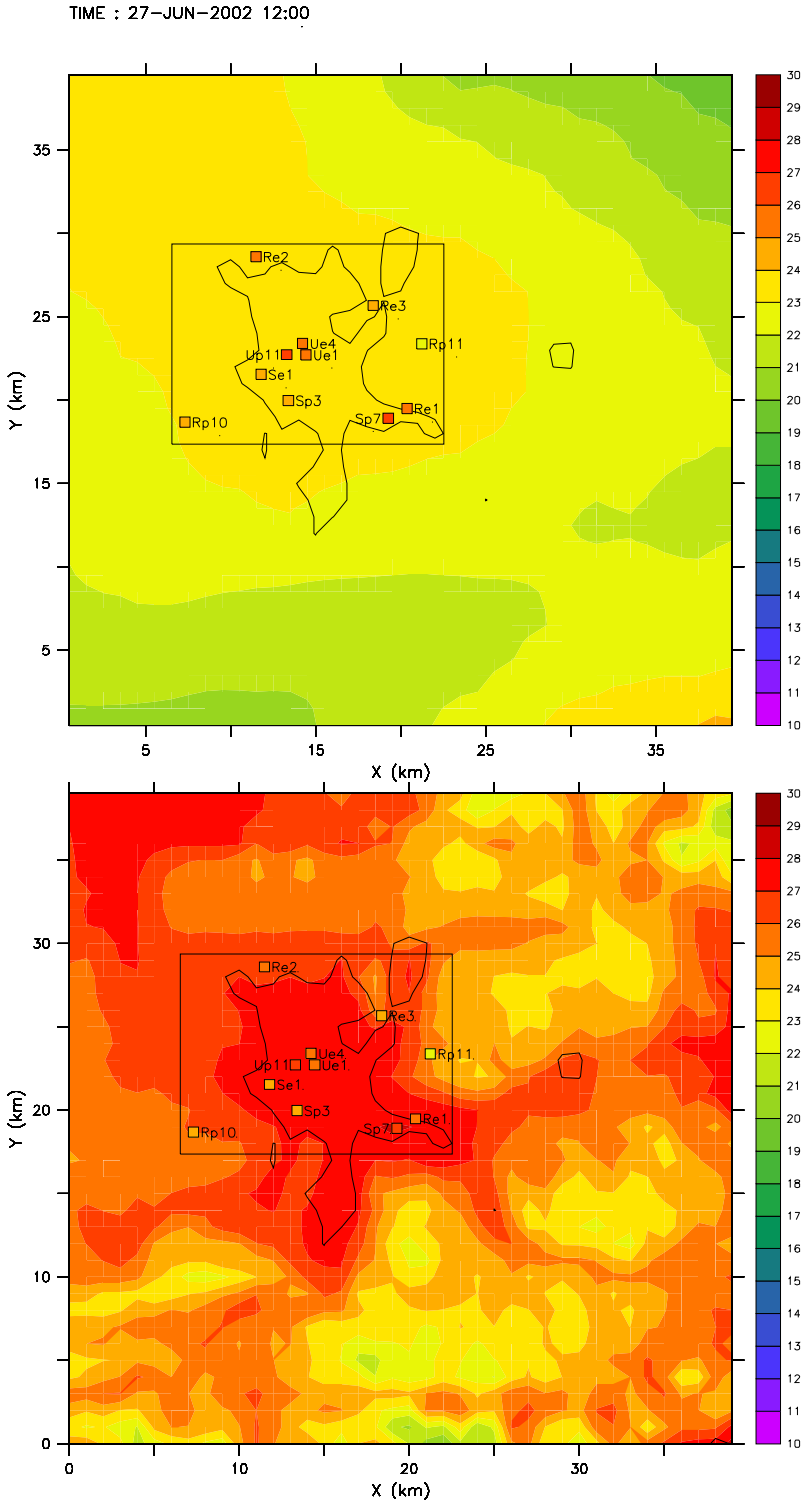

Figure 5.12: Temperatures on 27th June 2002, 12:00 UTC time

(a) Comparison of LM's results (at 10 m a.g.l.) with BUBBLE's measurements (squares).

(b) Comparison of FVM's results (at 10 m a.g.l.) with BUBBLE's measurements (squares).

5.4.2 Temperatures—Local Comparisons

The second comparisons are local in that they regard the evolution of temperatures during the IOP at each meteorological station provided by measurements on the one hand, and by LM and FVM on the other hand, respectively represented by black, red and green lines in Figures 5.13 to 5.15.

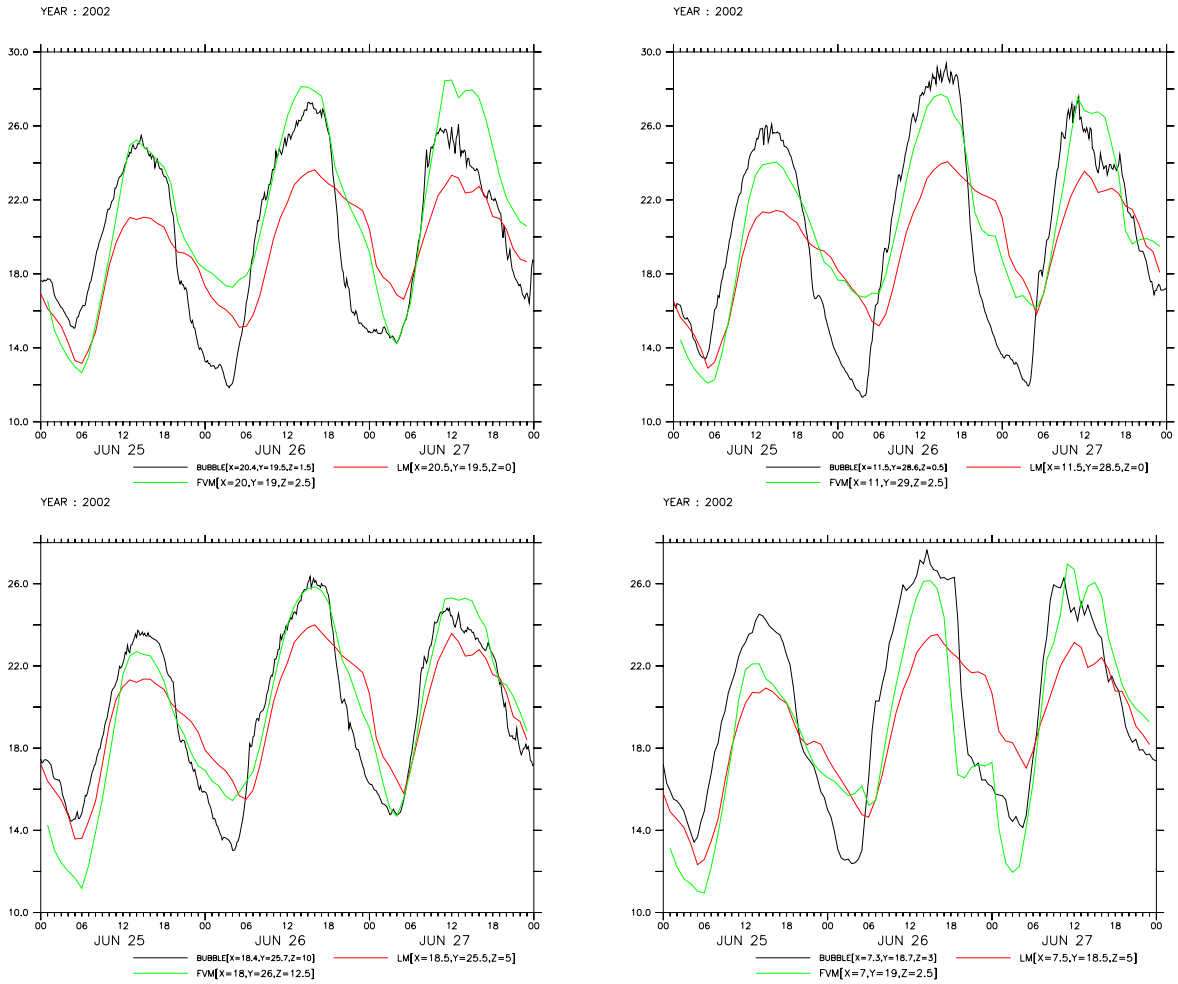

Figure 5.13: Comparison of the evolution of the temperatures (in Degrees Celsius) between BUBBLE's measurements (black line), LM's simulation results (red line) and FVM's simulation results (green line).

(a) Re1 Grenzach (measurement's altitude a.g.l.: 1.5 m)

(b) Re2 Village-Neuf (0.5 m)

(c) Re3 Lange Erlen (10 m)

(d) Rp10 Schoenenbuch (3 m)

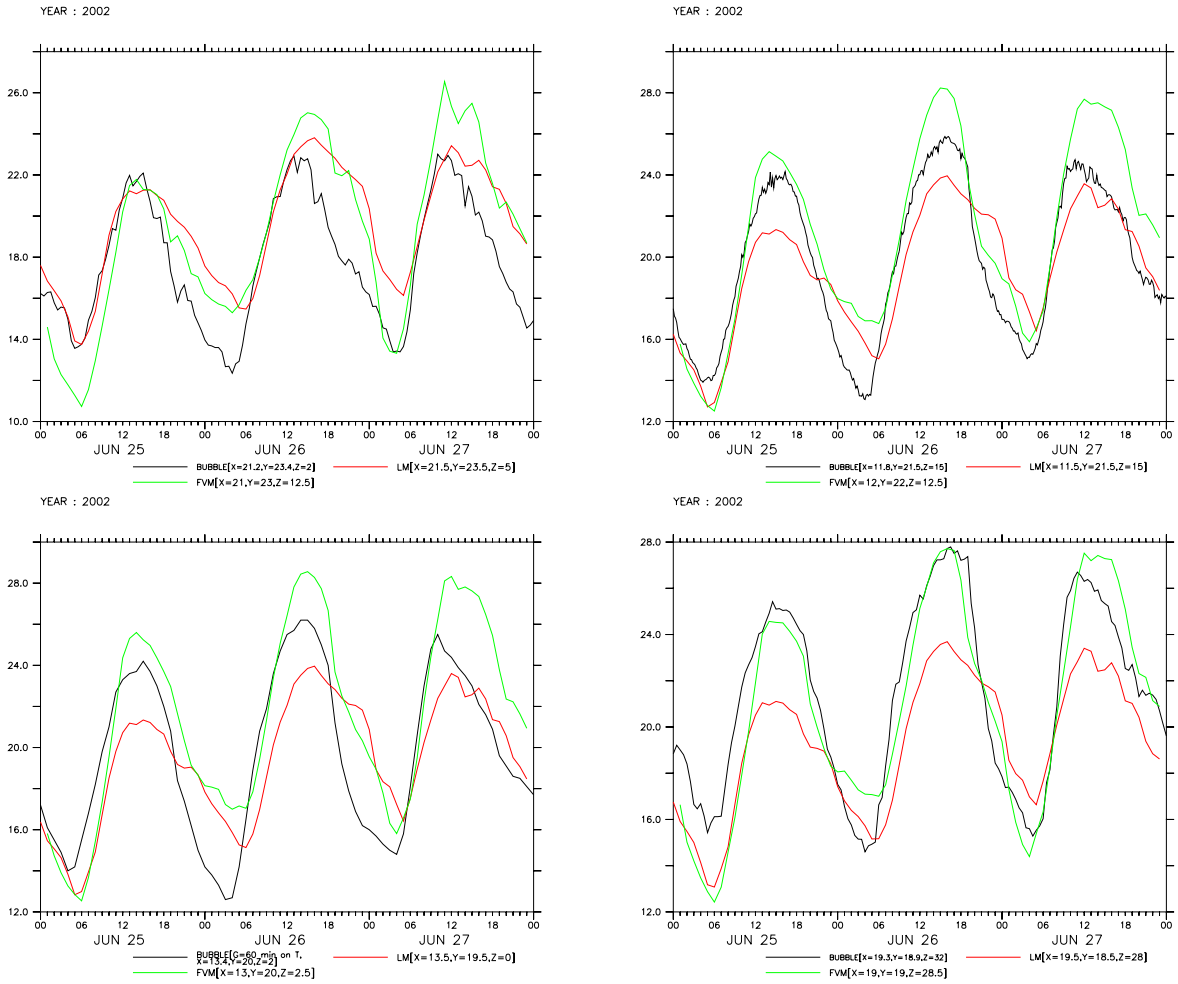

Figure 5.14: Comparison of the evolution of the temperatures (in Degrees Celsius) between BUBBLE's measurements (black line), LM's simulation results (red line) and FVM's simulation results (green line).

(a) Rp11 St-Chrischonaturm (measurement's altitude a.g.l.: 2 m)

(b) Se1 Allschwil (15 m)

(c) Sp3 Binningen (2 m)

(d) Sp7 Schweizerhall (32 m)

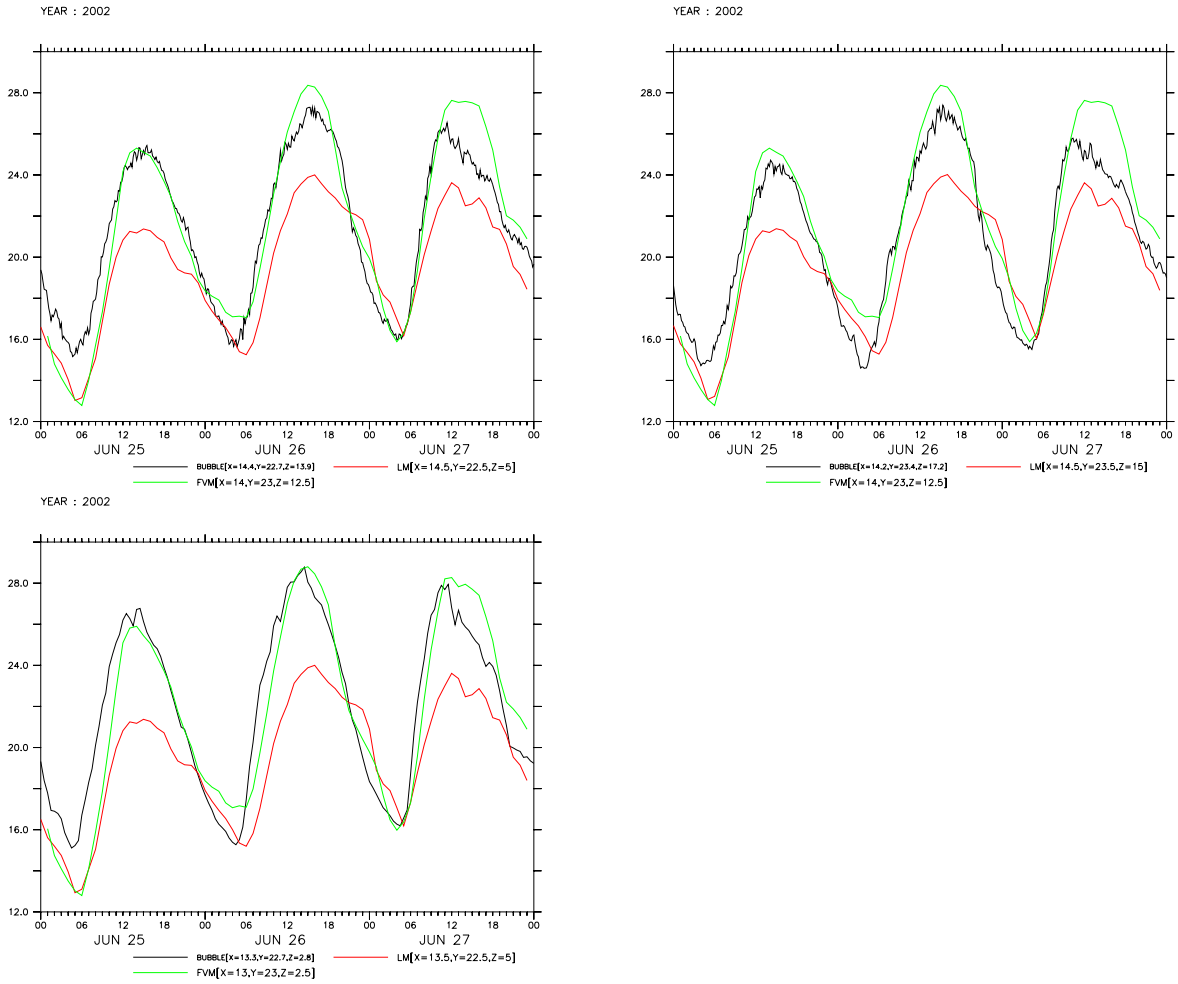

Figure 5.15: Comparison of the evolution of the temperatures (in Degrees Celsius) between BUBBLE's measurements (black line), LM's simulation results (red line) and FVM's simulation results (green line).

(a) Ue1 Sperrstrasse (measurement's altitude a.g.l.: 13.9 m)

(b) Ue4 Horburg (17.2 m)

(c) Up11 St-Johann (2.8 m)

With a view to giving more quantitative comparisons between measurements and each of the model results, the percent change $\%\Delta x_{\text{model}}$ has been computed for each hour of the IOP by way of equation (5.4.1) in which the subscript 'model' designates either LM or FVM.

$$\%\Delta x_{\text{model}} = \left| \frac{x_{\text{reference}} - x_{\text{model}}}{x_{\text{reference}}} \right| \tag{5.4.1}$$

where x is any variable[3].

[3]To be more mathematically rigorous, the so-called *arithmetic-geometric mean* between x_{model} and $x_{\text{reference}}$ should be written in the denominator instead of $x_{\text{reference}}$, but this is not very important since $x_{\text{reference}}$ is the same for either model.

The time-averaged percent changes for temperature are supplied in Table 5.2. The fourth column states whether this average change is smaller in FVM than in LM. It comes out that the case arises eight times out of eleven. The fifth column provides the altitude above ground level of BUBBLE's measurements. The level corresponding to this altitude has been selected in both models results to make the comparisons.

Table 5.2: Averaged percent changes in temperatures. BUBBLE's values are taken as starting (reference) values according to (5.4.1). The fifth column provides the altitude above ground level of BUBBLE's measurement.

weather station	$\%\Delta T_{\mathrm{LM}}$	$\%\Delta T_{\mathrm{FVM}}$	$\%\Delta T_{\mathrm{LM}} > \%\Delta T_{\mathrm{FVM}}$?	altitude a.g.l.
Re1 Grenzach	14.4	12.7	YES	1.5 m
Re2 Village-Neuf	17.7	13.8	YES	0.5 m
Re3 Lange Erlen	9.05	7.77	YES	10 m
Rp10 Schoenenbuch	13.5	11.7	YES	3 m
Rp11 St-Chrischonaturm	11.8	13.1	NO	2 m
Se1 Allschwil	8.53	9.26	NO	15 m
Sp3 Binningen	11.9	13.2	NO	2 m
Sp7 Schweizerhalle	11.4	7.12	YES	32 m
Ue1 Sperrstrasse	9.88	5.29	YES	13.9 m
Ue4 Horburg	8.86	6.41	YES	17.2 m
Up11 St-Johann	12.1	6.58	YES	2.8 m

5.4.3 Temperatures—Vertical Profiles

As two met stations had several measurement heights for temperature and wind—namely Re3 and Ue1—vertical profiles have been represented at five given instants at these stations. The temperature profiles are shown in Figures 5.16 and 5.17.

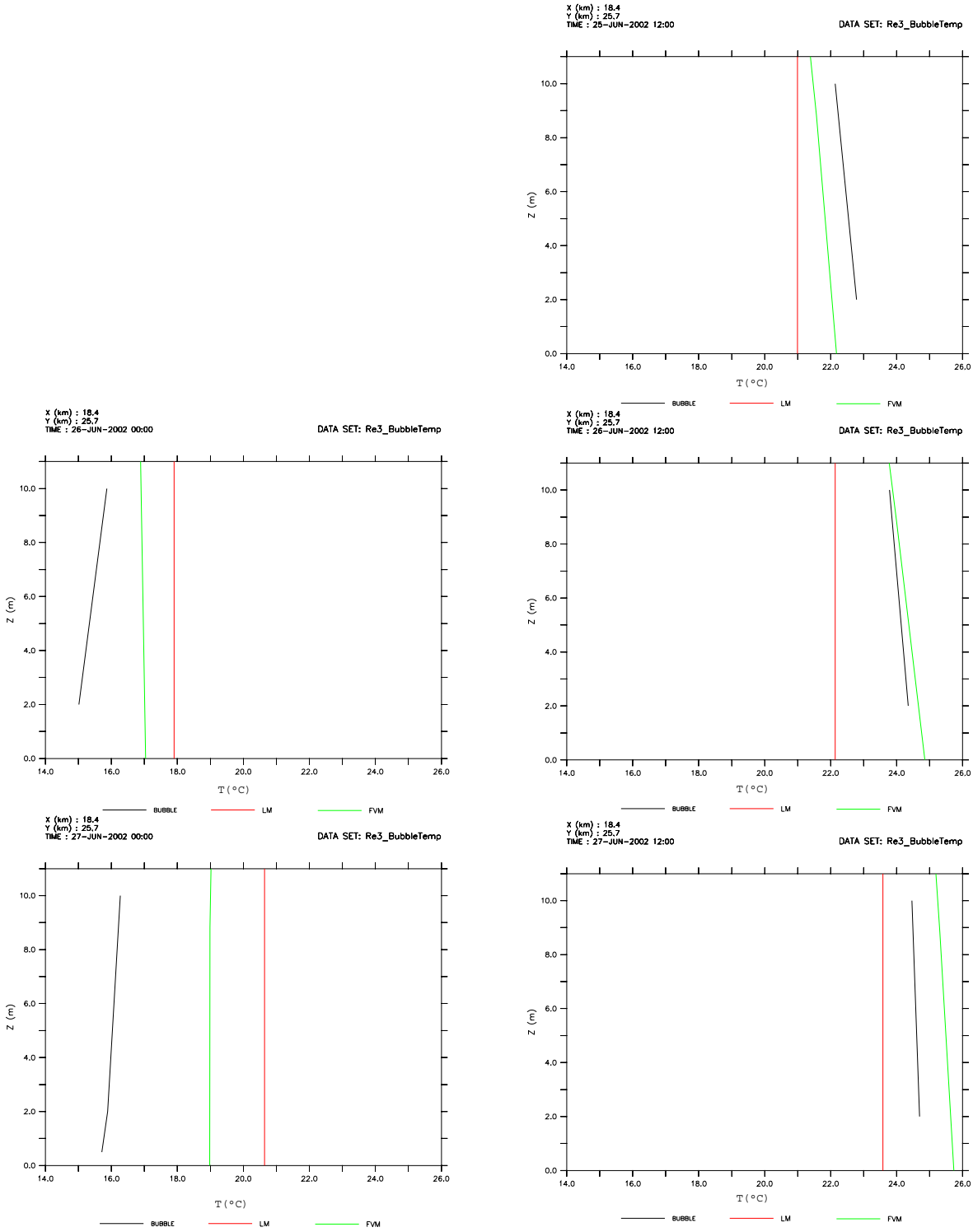

Figure 5.16: Vertical temperature profiles in Lange Erlen (Re3) during the IOP. Comparison (in Degrees Celsius) between BUBBLE's measurements (black lines), LM's simulation results (red lines) and FVM's simulation results (green lines).

(a) 25th June 2002, 12:00 UTC time

(b) 26th June 2002, 00:00 UTC time

(c) 26th June 2002, 12:00 UTC time

(d) 27th June 2002, 00:00 UTC time

(e) 27th June 2002, 12:00 UTC time

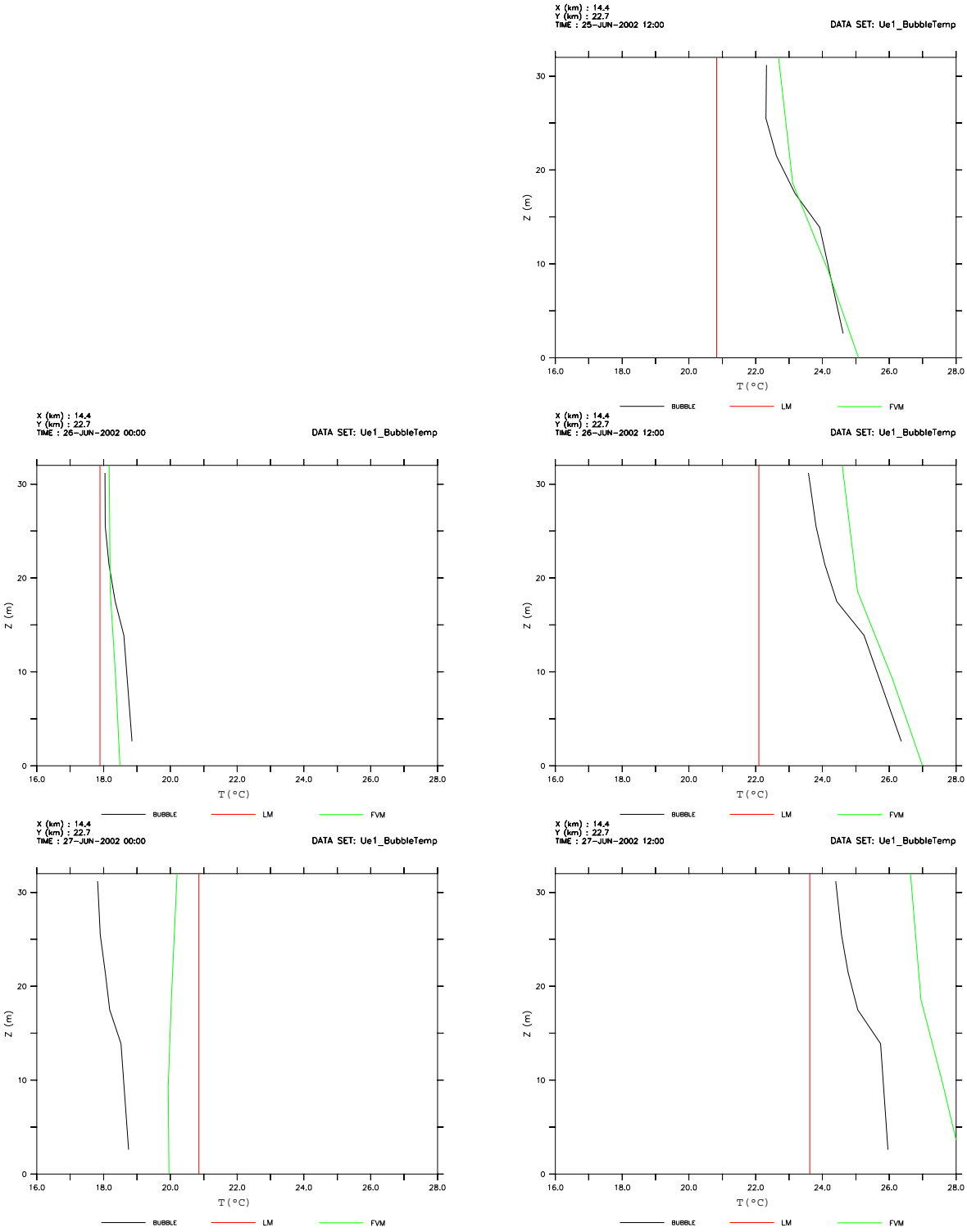

Figure 5.17: Vertical temperature profiles in Sperrstrasse (Ue1) during the IOP. Comparison (in Degrees Celsius) between BUBBLE's measurements (black lines), LM's simulation results (red lines) and FVM's simulation results (green lines).

(a) 25th June 2002, 12:00 UTC time

(b) 26th June 2002, 00:00 UTC time

(c) 26th June 2002, 12:00 UTC time

(d) 27th June 2002, 00:00 UTC time

(e) 27th June 2002, 12:00 UTC time

5.4.4 Wind Speeds—Geographical Comparisons

The comparisons made in section 5.4.1, this time for the horizontal wind speeds, are shown in Figures 5.18 to 5.22.

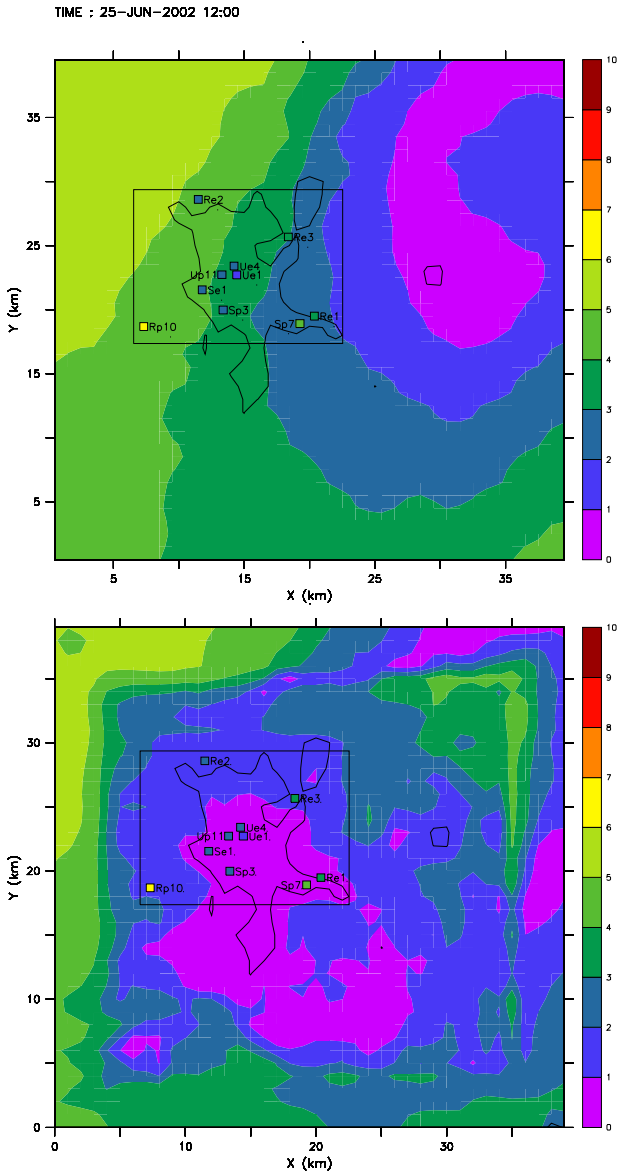

Figure 5.18: Horizontal wind speeds on 25th June 2002, 12:00 UTC time

(a) Comparison of LM's results (at 10 m a.g.l.) with BUBBLE's measurements (squares).

(b) Comparison of FVM's results (at 10 m a.g.l.) with BUBBLE's measurements (squares).

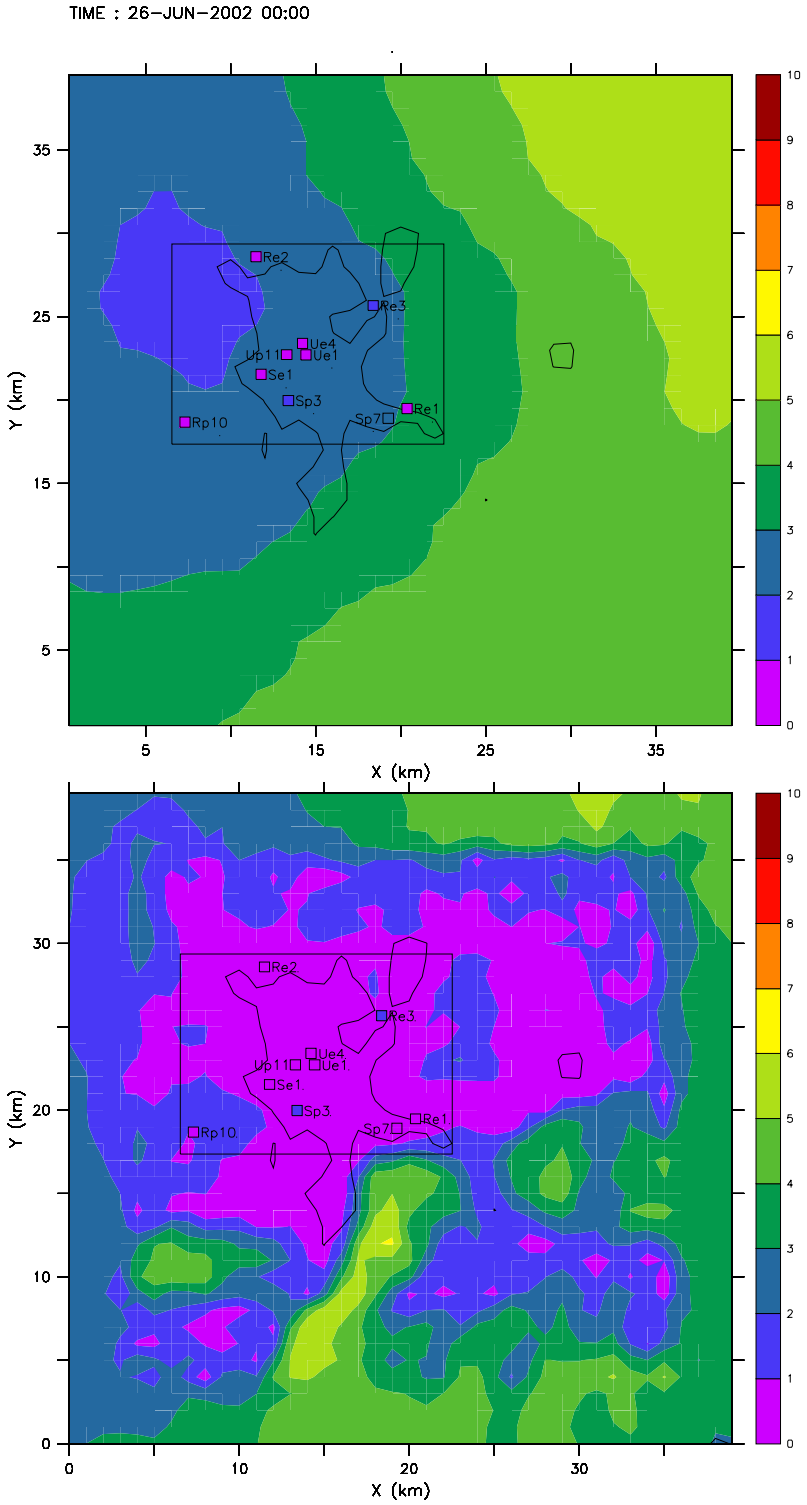

Figure 5.19: Horizontal wind speeds on 26th June 2002, 00:00 UTC time

(a) Comparison of LM's results (at 10 m a.g.l.) with BUBBLE's measurements (squares).

(b) Comparison of FVM's results (at 10 m a.g.l.) with BUBBLE's measurements (squares).

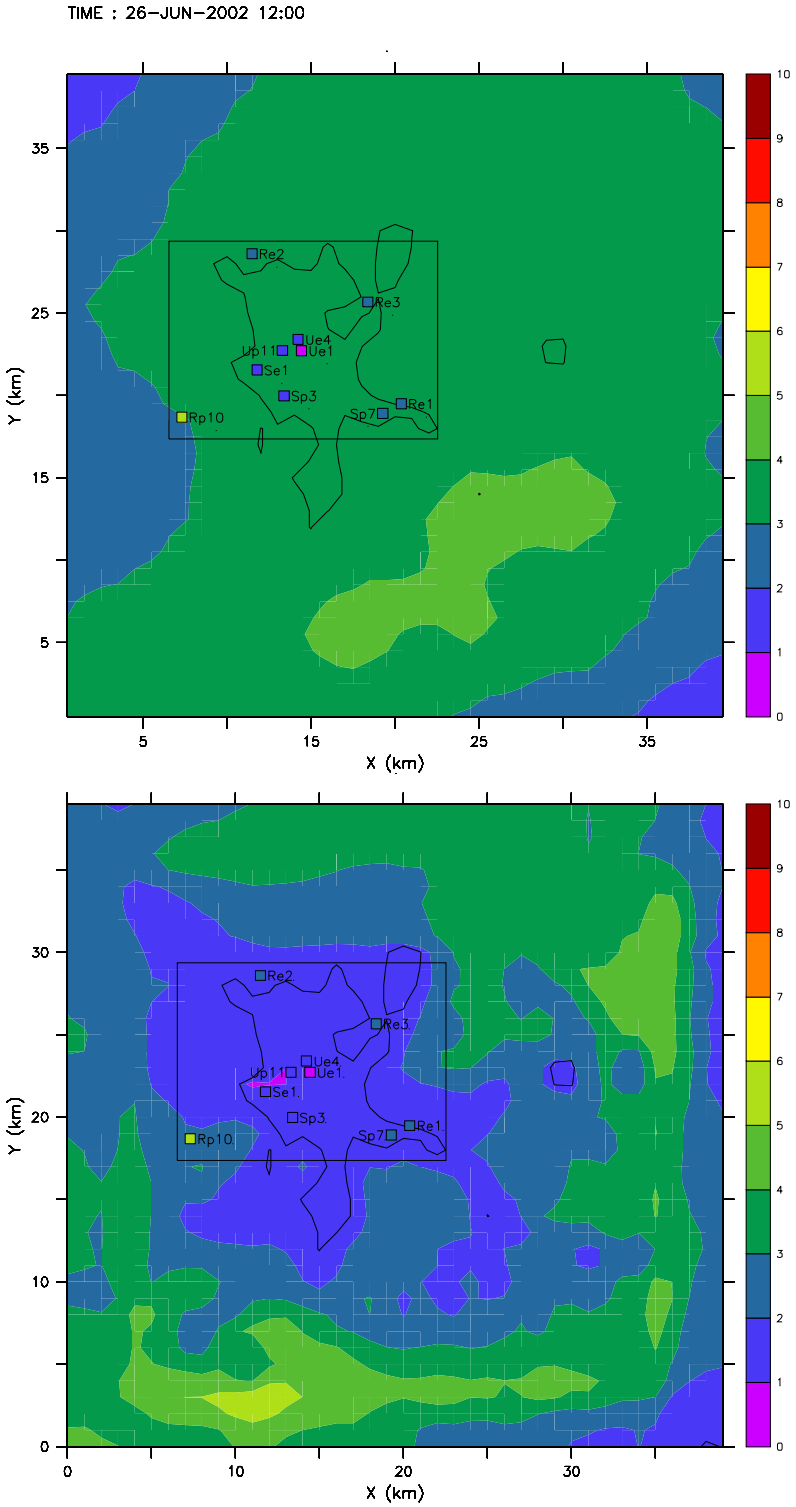

Figure 5.20: Horizontal wind speeds on 26th June 2002, 12:00 UTC time

(a) Comparison of LM's results (at 10 m a.g.l.) with BUBBLE's measurements (squares).

(b) Comparison of FVM's results (at 10 m a.g.l.) with BUBBLE's measurements (squares).

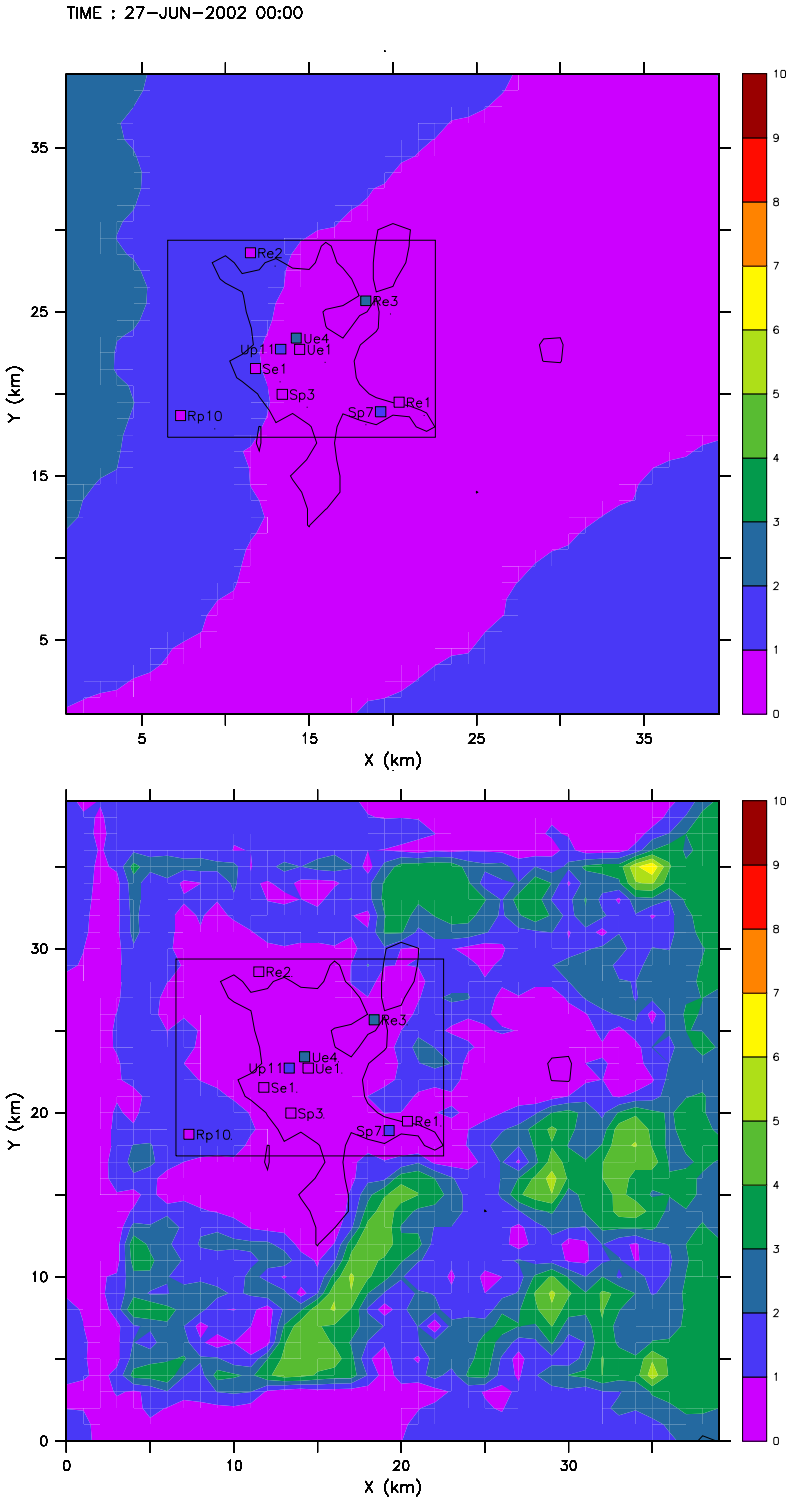

Figure 5.21: Horizontal wind speeds on 27th June 2002, 00:00 UTC time

(a) Comparison of LM's results (at 10 m a.g.l.) with BUBBLE's measurements (squares).

(b) Comparison of FVM's results (at 10 m a.g.l.) with BUBBLE's measurements (squares).

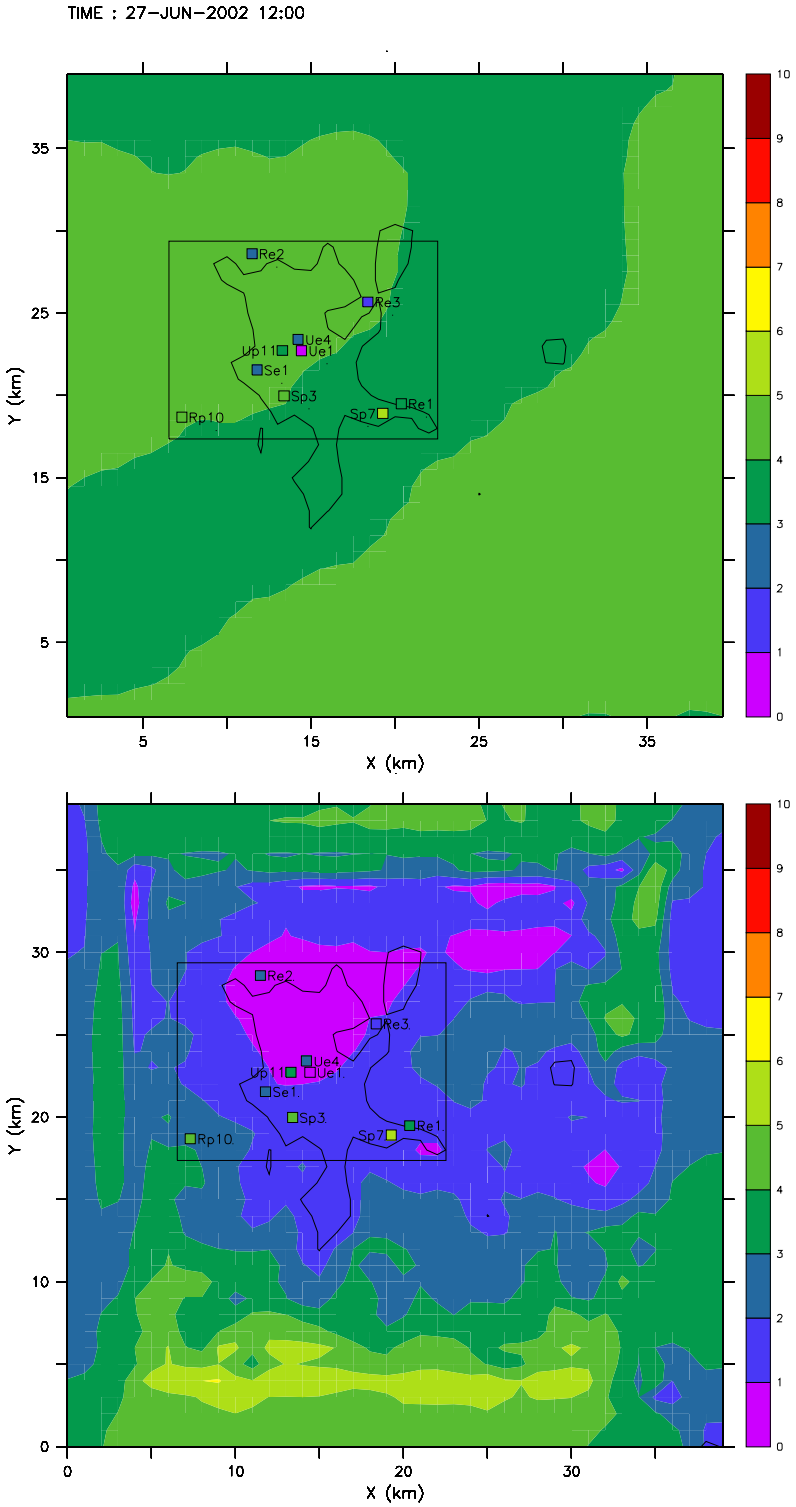

Figure 5.22: Horizontal wind speeds on 27th June 2002, 12:00 UTC time

(a) Comparison of LM's results (at 10 m a.g.l.) with BUBBLE's measurements (squares).

(b) Comparison of FVM's results (at 10 m a.g.l.) with BUBBLE's measurements (squares).

5.4.5 Wind Speeds—Local Comparisons

The comparisons akin to those made in section 5.4.2, but this time for the horizontal wind speeds, are shown in Figures 5.23 and 5.24.

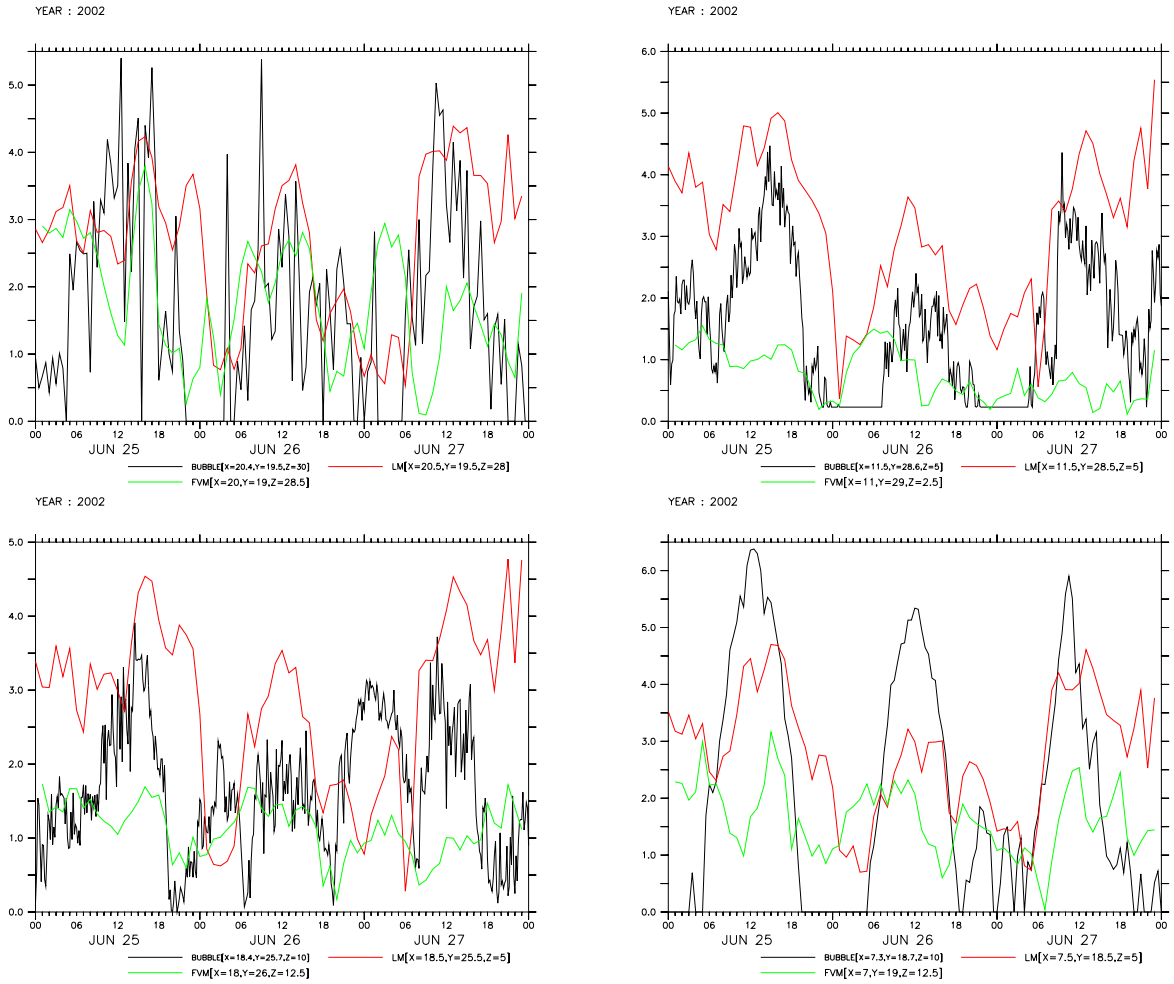

Figure 5.23: Comparison of the evolution of the horizontal wind speeds (in metres per second) between BUBBLE's measurements (black line), LM's simulation results (red line) and FVM's simulation results (green line).

(a) Re1 Grenzach (measurement's altitude a.g.l.: 30 m)

(b) Re2 Village-Neuf (5 m)

(c) Re3 Lange Erlen (10 m)

(d) Rp10 Schoenenbuch (10 m)

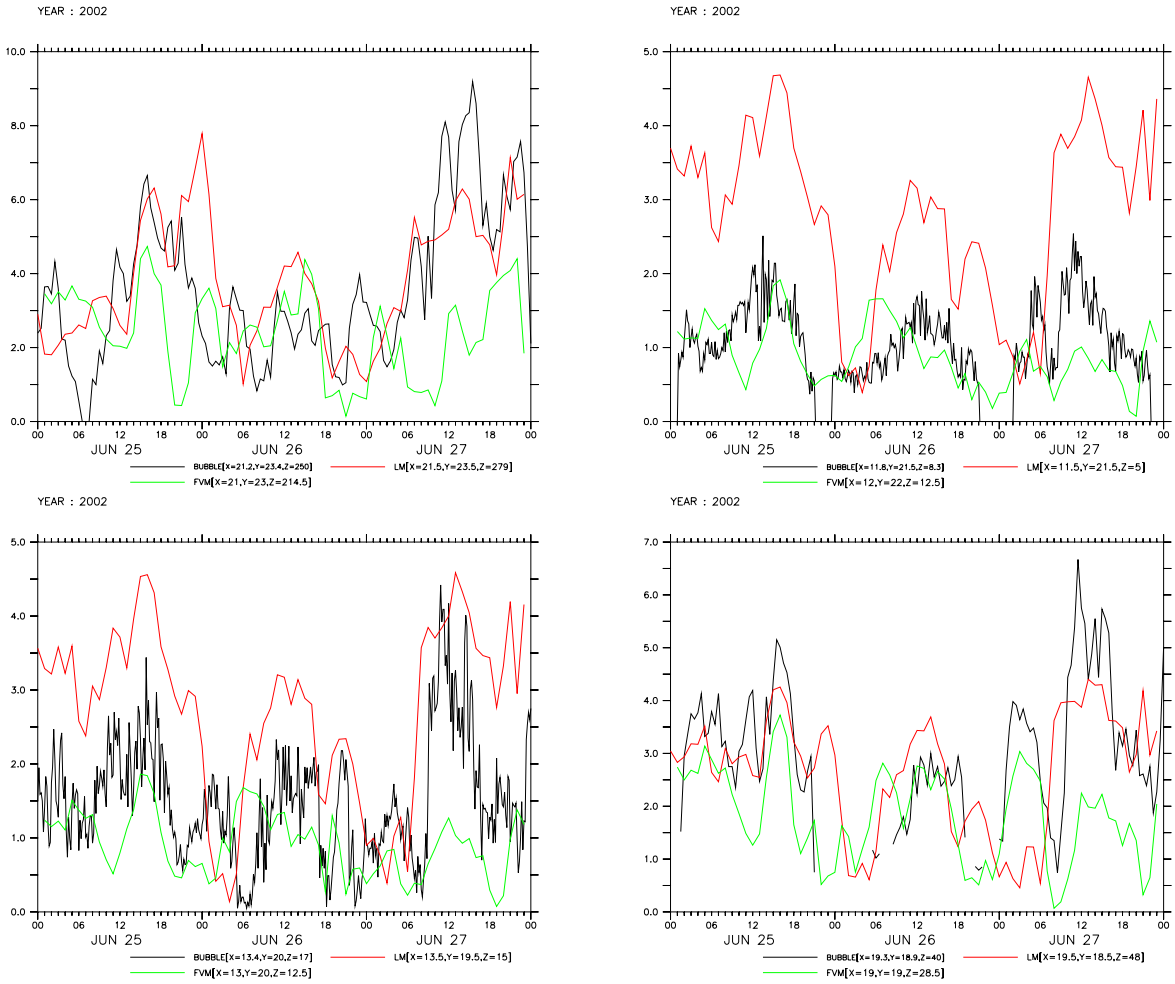

Figure 5.24: Comparison of the evolution of the horizontal wind speeds (in metres per second) between BUBBLE's measurements (black line), LM's simulation results (red line) and FVM's simulation results (green line).

(a) Rp11 St-Chrischonaturm (measurement's altitude a.g.l.: 250 m)

(b) Se1 Allschwil (8.3 m)

(c) Sp3 Binningen (17 m)

(d) Sp7 Schweizerhall (40 m)

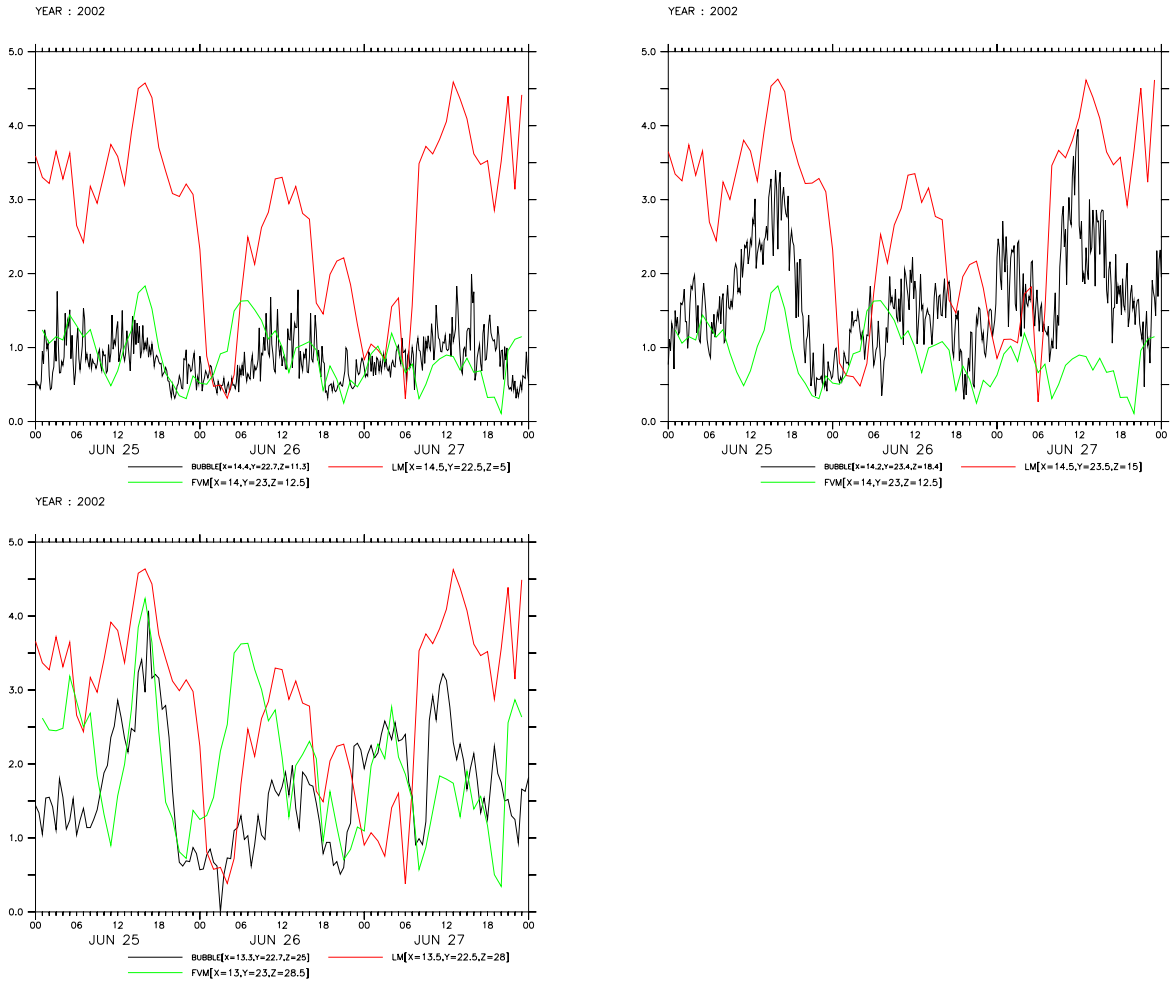

Figure 5.25: Comparison of the evolution of the horizontal wind speeds (in metres per second) between BUBBLE's measurements (black line), LM's simulation results (red line) and FVM's simulation results (green line).

(a) Ue1 Sperrstrasse (measurement's altitude a.g.l.: 11.3 m)

(b) Ue4 Horburg (18.4 m)

(c) Up11 St-Johann (25 m)

The time-averaged percent changes for horizontal wind speeds appear in Table 5.3. All but one of FVM's percent changes happen to be smaller than LM's. Even so, the latter are rather large.

Table 5.3: Averaged percent changes in horizontal wind speeds. BUBBLE's values are taken as starting values according to (5.4.1). The fifth column provides the altitude above ground level of BUBBLE's measurement.

weather station	$\%\Delta v_{\mathrm{LM}}$	$\%\Delta v_{\mathrm{FVM}}$	$\%\Delta v_{\mathrm{LM}} > \%\Delta v_{\mathrm{FVM}}$?	altitude a.g.l.
Re1 Grenzach	117.2	103.4	YES	30 m
Re2 Village-Neuf	256.4	91.14	YES	5 m
Re3 Lange Erlen	242.0	71.94	YES	10 m
Rp10 Schoenenbuch	81.59	60.82	YES	10 m
Rp11 St-Chrischonaturm	54.58	62.04	NO	250 m
Se1 Allschwil	178.3	44.77	YES	8.3 m
Sp3 Binningen	148.1	69.42	YES	17 m
Sp7 Schweizerhalle	62.88	52.30	YES	40 m
Ue1 Sperrstrasse	244.5	48.08	YES	11.3 m
Ue4 Horburg	115.9	47.22	YES	18.4 m
Up11 St-Johann	107.6	64.33	YES	25 m

5.4.6 Wind Speeds—Vertical Profiles

In the same fashion as what was made for temperatures (see section 5.4.3, 'Temperatures—Vertical Profiles'), the vertical profiles of horizontal wind speeds have been reported in Figures 5.26 and 5.27.

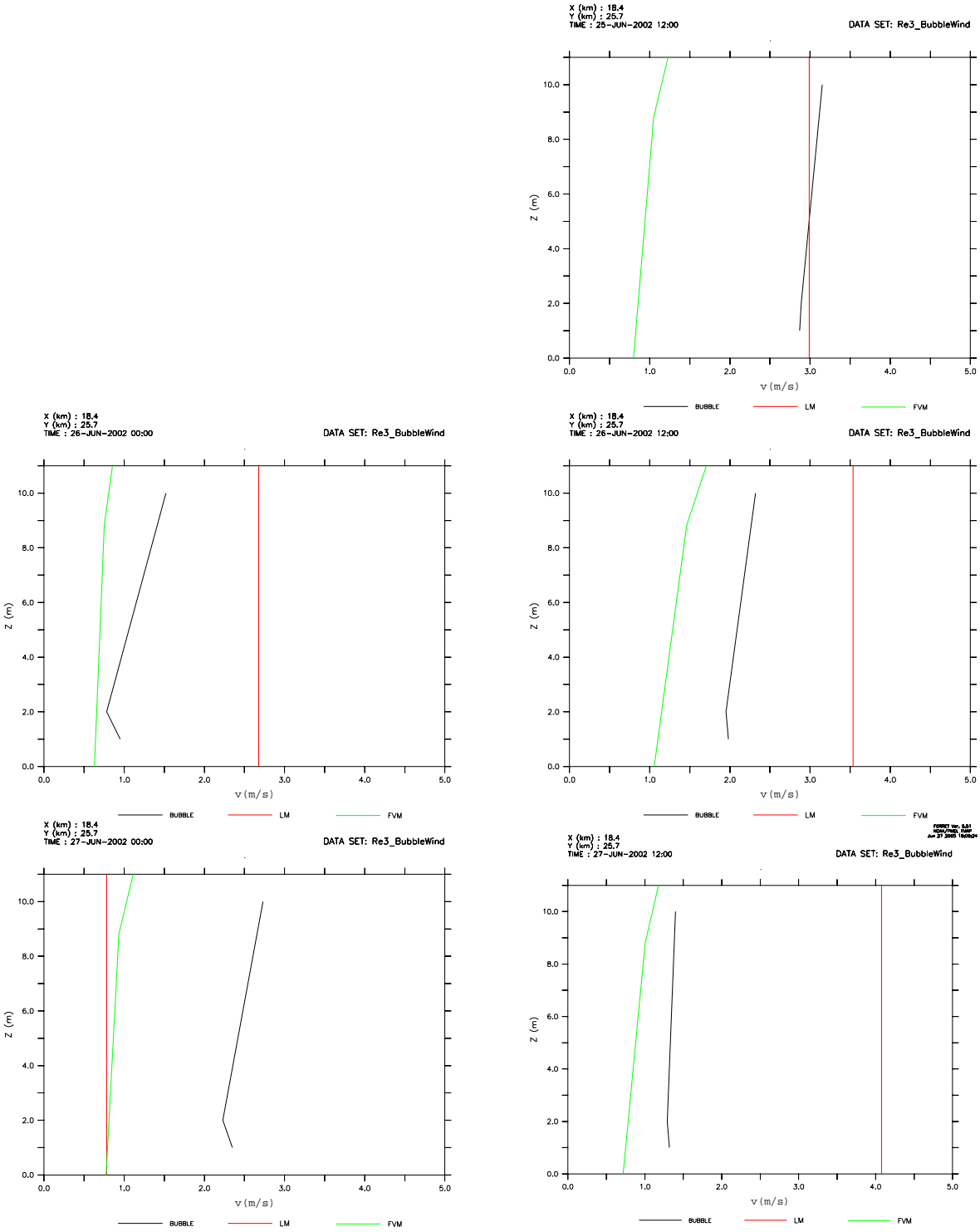

Figure 5.26: Vertical profiles of horizontal wind speeds in Lange Erlen (Re3) during the IOP. Comparison (in metres per second) between BUBBLE's measurements (black lines), LM's simulation results (red lines) and FVM's simulation results (green lines).

(a) 25th June 2002, 12:00 UTC time

(b) 26th June 2002, 00:00 UTC time

(c) 26th June 2002, 12:00 UTC time

(d) 27th June 2002, 00:00 UTC time

(e) 27th June 2002, 12:00 UTC time

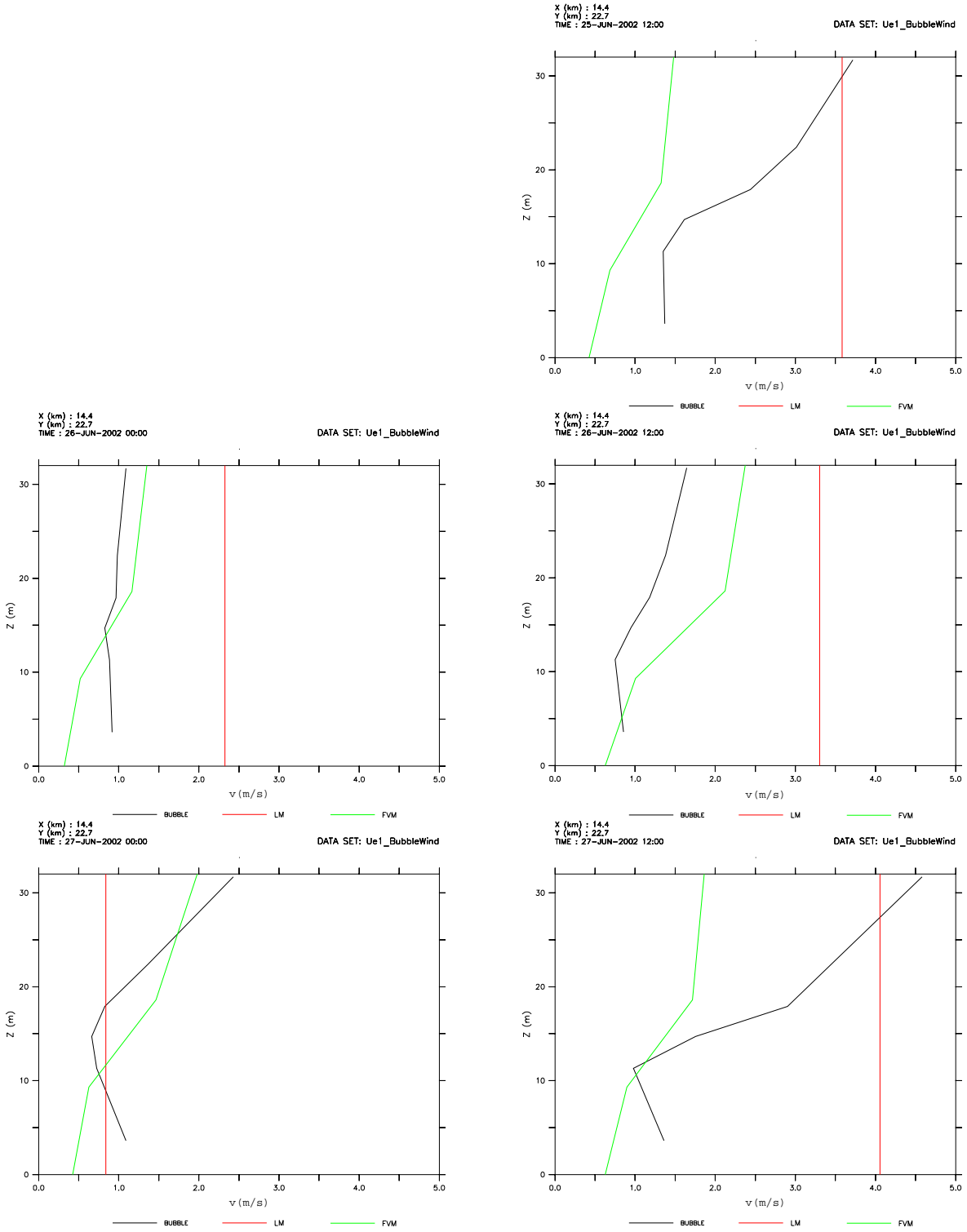

Figure 5.27: Vertical profiles of horizontal wind speeds in Sperrstrasse (Ue1) during the IOP. Comparison (in metres per second) between BUBBLE's measurements (black lines), LM's simulation results (red lines) and FVM's simulation results (green lines).

(a) 25th June 2002, 12:00 UTC time

(b) 26th June 2002, 00:00 UTC time

(c) 26th June 2002, 12:00 UTC time

(d) 27th June 2002, 00:00 UTC time

(e) 27th June 2002, 12:00 UTC time

5.5 FVM's Results Analysis

5.5.1 Temperatures—Inter-Model Comparisons

The observation of Figures 5.8 to 5.12 reveals that FVM brings out local refinements. LM basically gives only one degree Celsius of difference throughout the whole BUBBLE domain, whereas FVM gives up to five (see Figure 5.8 (b)). Not only are temperatures more shaded but also closer to the measurements, as confirmed later on.

Actually, as can be seen in Figure 5.28, the ground temperatures supplied by LM are largely reliant on topography. FVM adds an urban component.

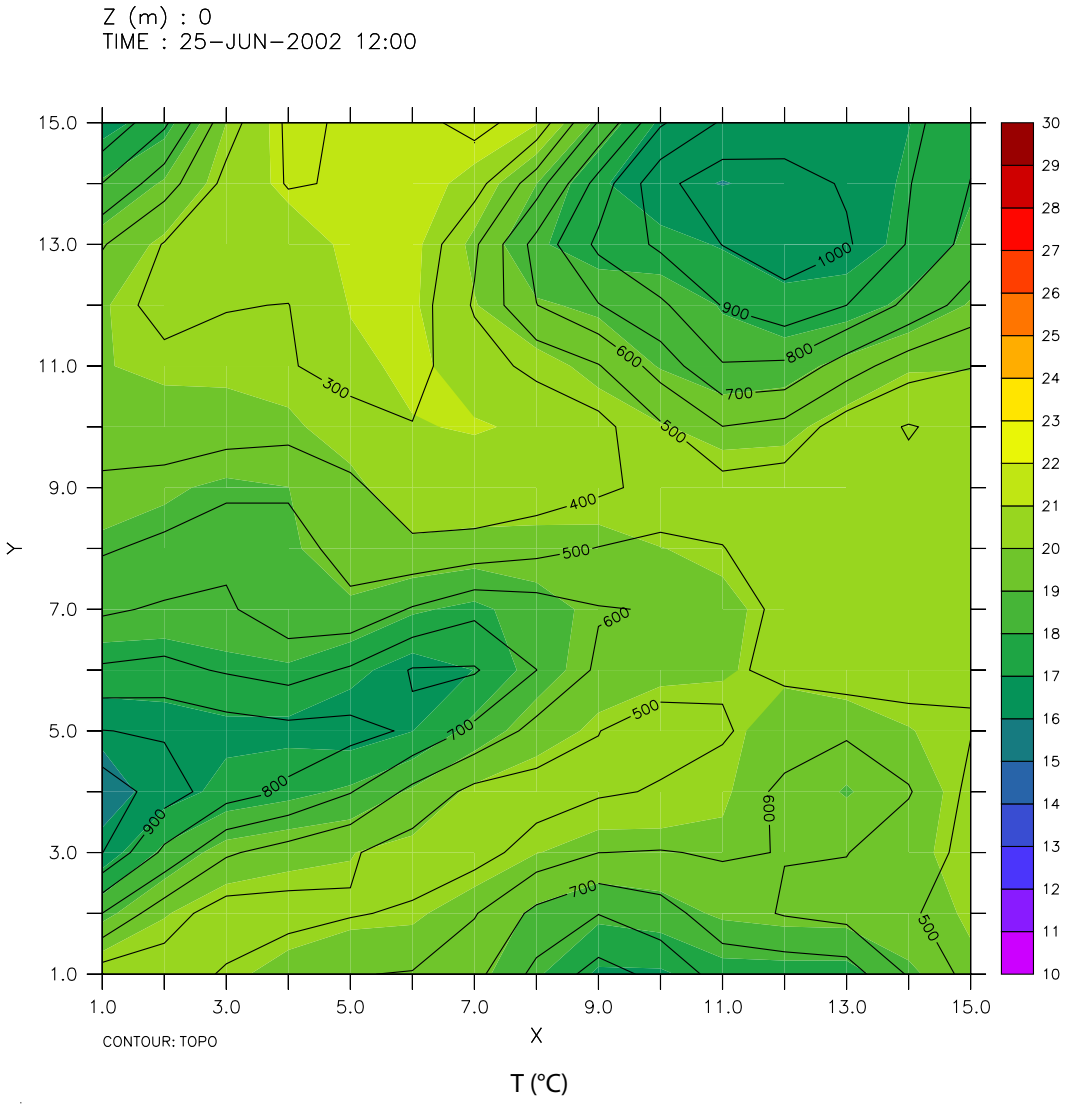

Figure 5.28: Comparison of ground temperatures given by LM with topography (on a larger domain).

The time plots (Figures 5.13 to 5.15) show a better agreement of FVM with measurements than LM. FVM's improvement comes mainly from better reproducing maximum peaks occurring in the afternoon. However, LM seems to overestimate less temperatures during the minima taking place around 6 o'clock UTC in the morning. Both model values are very close to one another at the very beginning of the simulation because the forcing is still very high then. For this reason FVM's values shouldn't be taken into account before the first half-day.

According to Table 5.2, FVM supplies results which yield a better fit to measurements than LM in eight cases out of eleven. Discrepancies in the three remaining stations (Rp11, Se1 and Sp3) seem to be due to an overestimation by LM of temperatures during minima and maxima peaks, perhaps because these three sites are either rural or suburban. Incidentally, FVM's predictions appear to be particularly good at urban sites (Ue1, Ue4 and Up11).

As regards vertical profiles, as presented in Figures 5.16 and 5.17, FVM produces an improvement in every case (except perhaps in the situation of Figure 5.17 (e)) quantitatively as well as qualitatively. LM's profiles are upright because the top of its first levels are 65 metres above the ground. Generally, the slope and the patters of the profiles are very well reproduced by FVM, even though its levels are not equally defined as those of the measurements.

5.5.2 Wind Speeds—Inter-Model Comparisons

The FVM-related parts of Figures 5.18 to 5.22 do not show more shade levels than the LM-related parts, but the wind speed reductions follow closer the shape of the built-up area.

As was the case for temperatures, the time plots (Figures 5.23 to 5.25) show a better agreement of FVM with measurements than LM. This is confirmed by Table 5.3 in which LM matches better measurements than FVM only once, namely in station Rp11. This station is the only one carrying out a high-altitude measurement (240 m). This indicates that FVM's results should perhaps not be used at such heights.

Apart from the situation encountered on 25th June at midday in station Re3, the vertical profiles obtained by FVM tally better with measurements (in Re3 and Ue1) than those obtained by LM (see Figures 5.26 and 5.27).

Vertical profiles of wind speed measurements often yield a minimum between 10 and 15 metres above the ground. This is does not appear in FVM's profiles. These minima are probably due to vortex or helicoid (helix-shaped) flows taking place within the canyon. Such flows result in minima in the represented absolute scalar horizontal speeds. Christen (2005), who undertook some of the measurements within the BUBBLE project, shows that vortex and helicoid flows mainly occur when the above-roof flow is perpendicular or oblique to the canyon (see Figure 5.29).

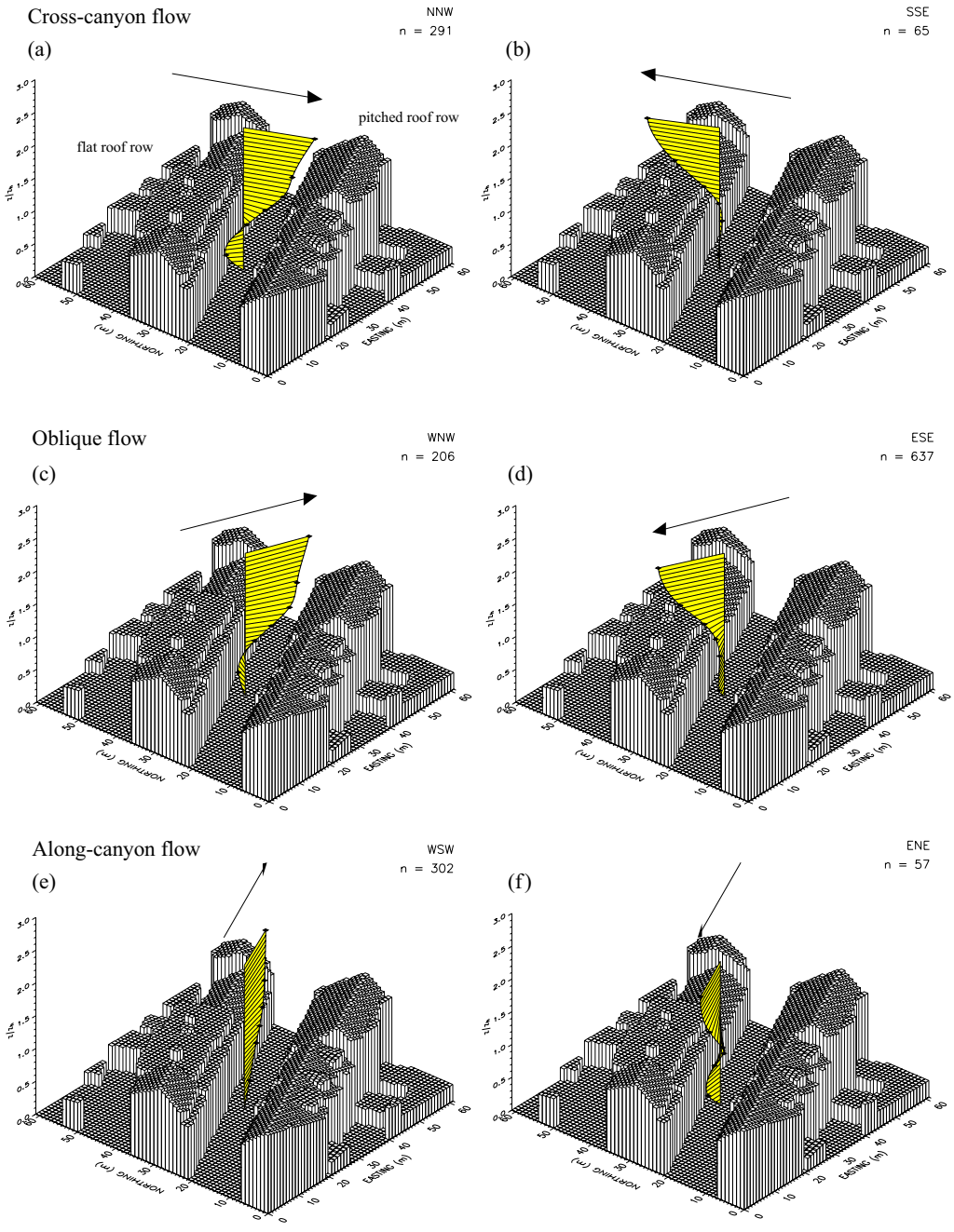

Figure 5.29: 3D visualization of the horizontal local wind velocity, and corresponding horizontal wind direction above the street canyon at Sperrstrasse (Ue1) for selected cases. Datasource: Sonics level A to F (see Figure 5.3), hourly averages, November1, 2001 to July 15, 2002, all stabilities. Each panel shows the average profile from the indicated wind direction and n refers to the number of observations (60-minute blocks). Black dots represent the exact values at measurement heights. In between a cubic spline interpolation was performed.(Christen, 2005)

FVM isn't likely to produce these minima because an average is performed on the whole levels. Anyway, it does not make sense to expect such local accuracies from a mesoscale model. This task rather falls to a microscale model.

On the other hand, the *inflection point* occurring between 15 and 20 metres is well reproduced by FVM. Inflection points (that is the point where the curve crosses its tangent) arise from the mixing of two streams of different velocities. Roughly, one can say one is the above-roof flow, one is the in-canyon flow. The height of the inflexion point with the strongest local wind gradient[4] $\partial\bar{u}/\partial z$ was measured by Christen (2005) between $0.5\,z_h$ and $2\,z_h$, z_h being the mean building height of the canyon. FVM always gives the inflection height within this range.

Incidentally, this inflection height can be defined as an *effective* building height. The dissimilarity between it and z_h may be an indication that many low building do not influence the flow. This dissimilarity tends to disappear with uniformly high elements.

All in all, the qualitative behaviour is better reproduced by FVM than by LM.

[4]Several inflexion points can be observed.

Chapter 6

Natural Ventilation Potential of the Basel Region

Even though the applicability of the results of the mesoscale model FVM in URBVENT is hardly conceivable on a general basis—*i.e.* over the whole European continent—, the current chapter presents the outcomes of URBVENT during the *Intensive Operation Period* (IOP) of the BUBBLE project and over the Basel area[1].

The method presented in Chapter 4 can be applied to this region by using the horizontal dicretization employed by FVM, namely a division of both the x-axis and the y-axis by 40. In so doing, the URBVENT method is able to assess 1600 sites. Yet the four criteria of the method have to be computed over this area.

6.1 Criteria Assessment

The wind and temperature fields computed by FVM are taken advantage of in the calculation of the first two criteria of the method—*wind hours* and *stack hours* (see Chapter 4). The last two criteria—*noise hours* and *pollution hours*—can be obtained more accurately than within the URBVENT piece of software.

Noise levels L_{noise} are not directly available from FVM's results but are deduced in the current work from the percentage of rural soil coverage (designated by α in equation (3.6.3)) by assuming that they are a decreasing function of this percentage. This assumption doesn't seem to be too thoughtless since noise levels are closely linked with road traffic, which is in turn linked with the urban feature of a given location (unless 'extra' noise sources, such as airports or building sites, are encountered).

[1] See section 5.2 ('The BUBBLE Project') for more information on this period.

Pollutants concentrations $L_{\text{pollution}}$ result from their emissions, from their dispersion and from their chemical transformations. Emissions are known from a land register released by Meteotest[2] exhibiting the temporal and spatial evolution of approximately twenty pollutants. Starting from this, FVM is able to calculate their dispersion and thus their local concentrations. Nitrogen dioxide (NO_2) has been taken as tracer gas to inform the overall pollution level. Considering a sole pollutant is quite reasonable because all the other pollutants tend to vary in the same way through time and also because the current analysis is purely ordinal.

The spatial distribution of these emissions has been supposed to follow the urban density distribution of the city. This assumption was necessary because the grid of the land register was too coarse. The pollutant dispersal is then computed by FVM according to the wind velocity and to the turbulence intensity. Chemical transformations are not computed though, but this is not crucial because pollution emissions are forced every hour and because NO_2 tend to be chemically destroyed anyway before reaching the countryside or vertically carried away by the turbulence.

Once the required data are computed, the criteria can be calculated by way of their definitions 4.5.8, 4.5.9, 4.5.13 and 4.5.14, which are recalled here:

$$WH = \frac{1}{N}\sum_{i=1}^{N} v_i^{\text{local}} \tag{6.1.1}$$

$$SH = \frac{1}{N}\sum_{i=1}^{N} \left|\frac{T_{\text{i}i} - T_{\text{e}i}}{T_{\text{e}i}}\right| \tag{6.1.2}$$

$$NH = 10 \cdot \log_{10}\left(\frac{1}{N}\sum_{i=1}^{N} 10^{\,L_{\text{noise}i}/10}\right) \tag{6.1.3}$$

$$PH = \frac{1}{N}\sum_{i=1}^{N} L_{\text{pollution}_i} \tag{6.1.4}$$

The summations are made over the N hours of the considered period, expanding from the 25th until the 27th June 2002. In order to compute the internal temperature T_{i}, the chosen building has been assumed to have the following characteristics[3]. It was:

- a brick façade building;
- south-oriented;
- full-time occupied.

[2]Meteotest is a Swiss engineering company specialized in weather, environment and geographical data. Homepage: `http://www.meteotest.ch/`

[3]Compare with section 4.7.1.3 ('Temperatures')

6.2 Multicriteria Aggregation

In what follows, two base sites[4] have been arbitrarily selected among the 1 600 mentioned above. The 1 598 remaining sites have been assessed by Qualiflex[5] and ranked in three classes according to whether they were ranked higher than the two base sites, lower than them or in between. This gives rise to shaded maps such as the one shown in Figure 6.1 (bottom), for each of which Qualiflex has been run 1 600 times (if the base sites themselves are counted). The topmost maps of Figure 6.1 represent the partial rankings of the 1 600 sites in each of the four criteria. These rankings are the starting point of Qualiflex's evaluation. The following weights have been assigned to the criteria:

- *wind hours*: 5
- *stack hours*: 5
- *noise hours*: 1
- *pollution hours*: 1

More importance has been attached here to driving forces than to constraints.

[4]See section 4.6.3 ('General Procedure for Evaluating a Site') for a definition of a *base site*.

[5]See section 4.6.6 ('Principles of the Multi-criteria Analysis Method *Qualiflex*') for a description of the procedure.

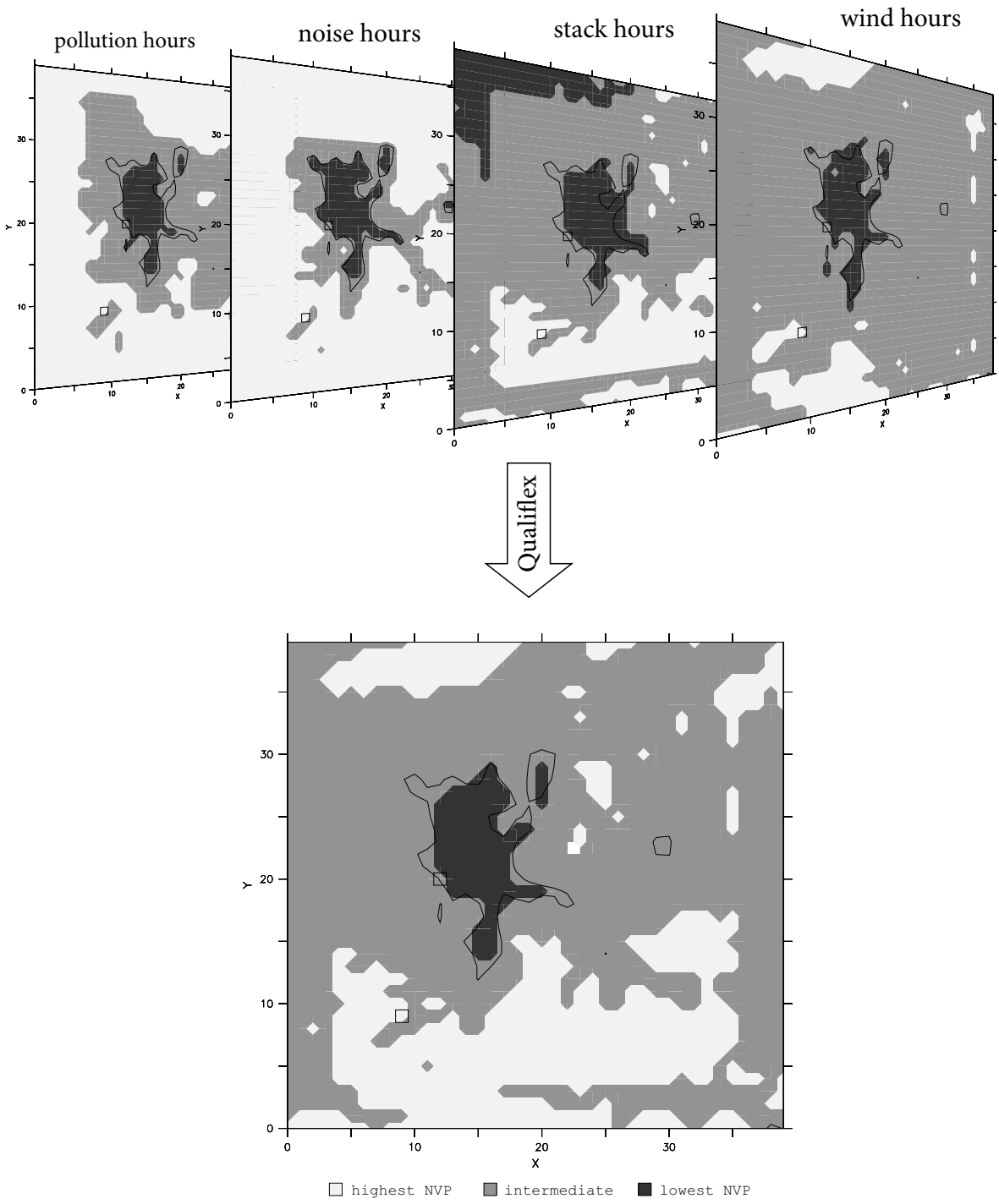

Figure 6.1: Natural ventilation potential of the region of Basel during the IOP.
Top: partial rankings of the 1 600 sites according to the four criteria: *wind hours* (foremost map), *stack hours*, *noise hours* and *pollution hours* (hindmost map).
Bottom: global rankings from the point of view of the natural ventilation potential carried out by Qualiflex. In each map, the two base sites are represented by two squares and the built-up area by a black line. The three classes are better NVP (light grey), intermediate (grey) and worse NVP (dark grey).

Note that the overall appearance of the map can be significantly different than the one of Figure 6.1, depending on the base sites selected, as shown in Figure 6.2.

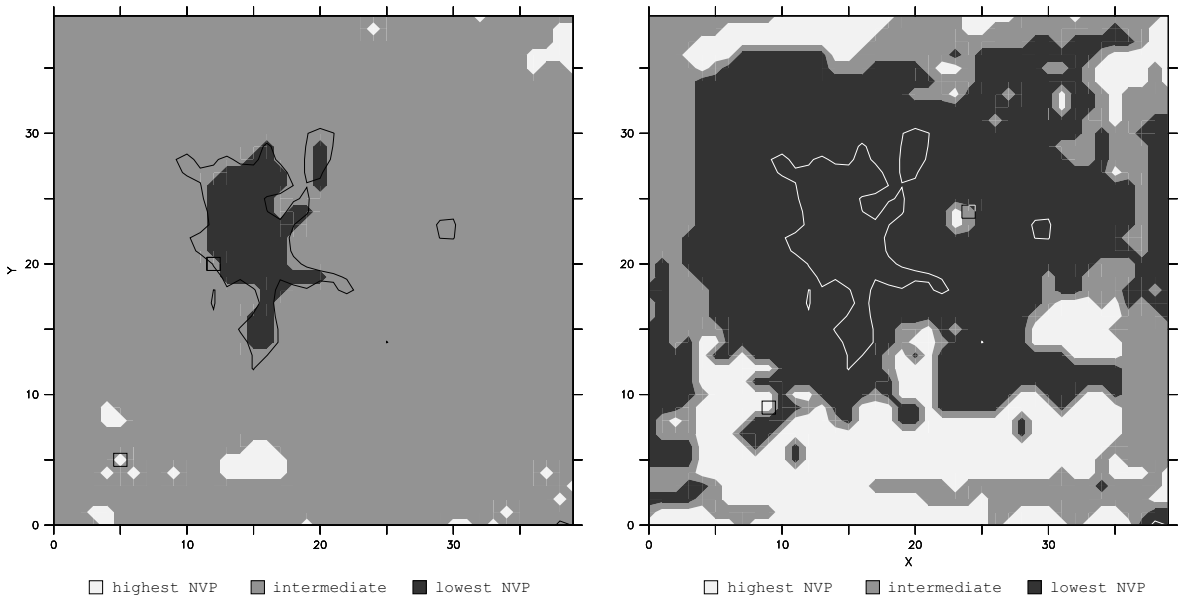

Figure 6.2: Natural ventilation potential of the region of Basel during the IOP. The two base sites are represented by two squares.

With a view to refining the rankings, the number of *base sites* can be arbitrarily increased. Figure 6.3 displays the same natural ventilation potential assessment as earlier, this time with eight base sites, creating thus nine classes.

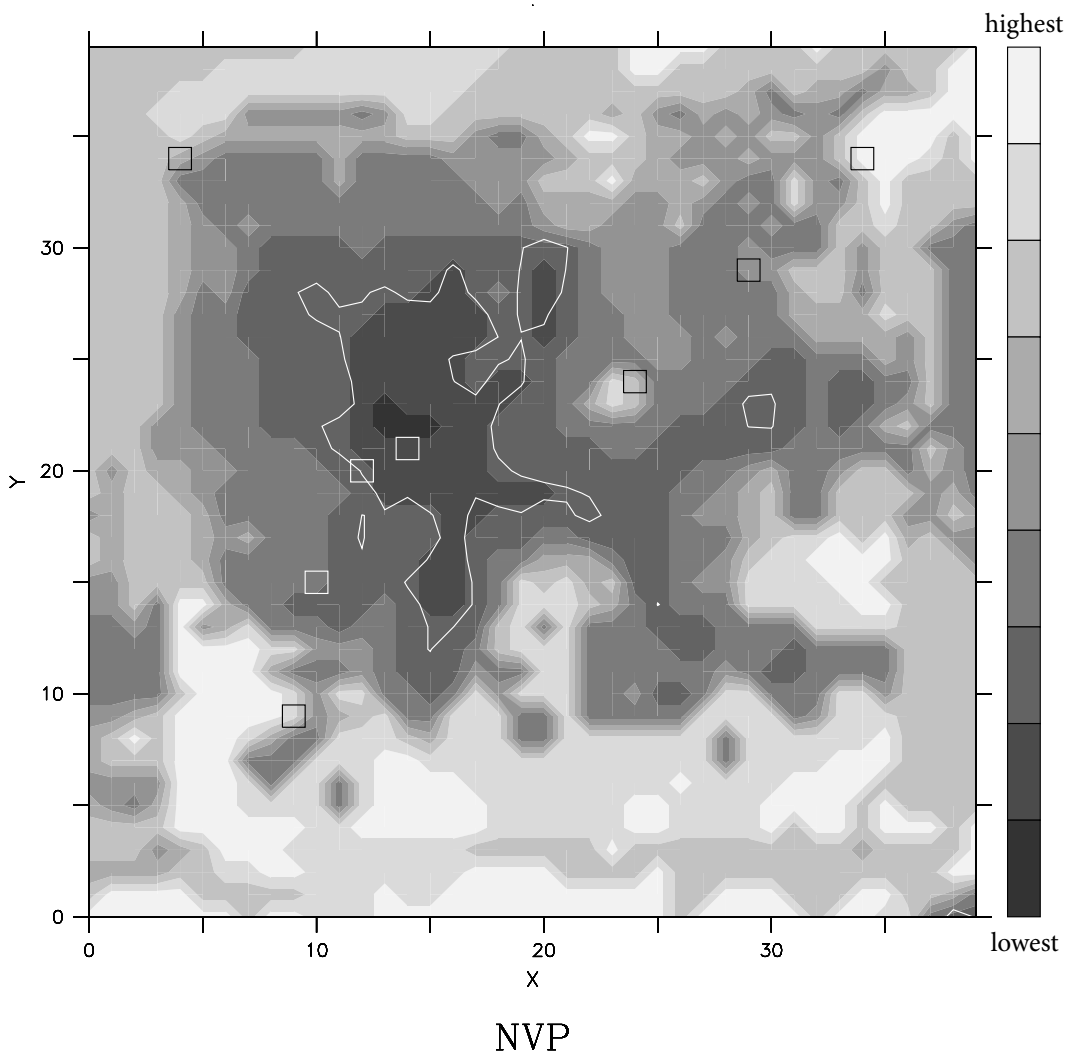

Figure 6.3: Natural ventilation potential of the region of Basel during the IOP. Eight base sites (squares) are used here.

The *fraction of time when free cooling is possible* is represented by Figure 6.4. This fraction is given by equation 4.7.1 and corresponds to the fulfilment of both the following conditions:

1. the air is too warm indoors[6] ($T_{\mathrm{fr}} > T_{\mathrm{cu}}$);
2. the outside air is cool enough to cool down the building ($T_{\mathrm{e}} \leq T_{\mathrm{cu}}$).

[6] in absence of heating, ventilation and cooling

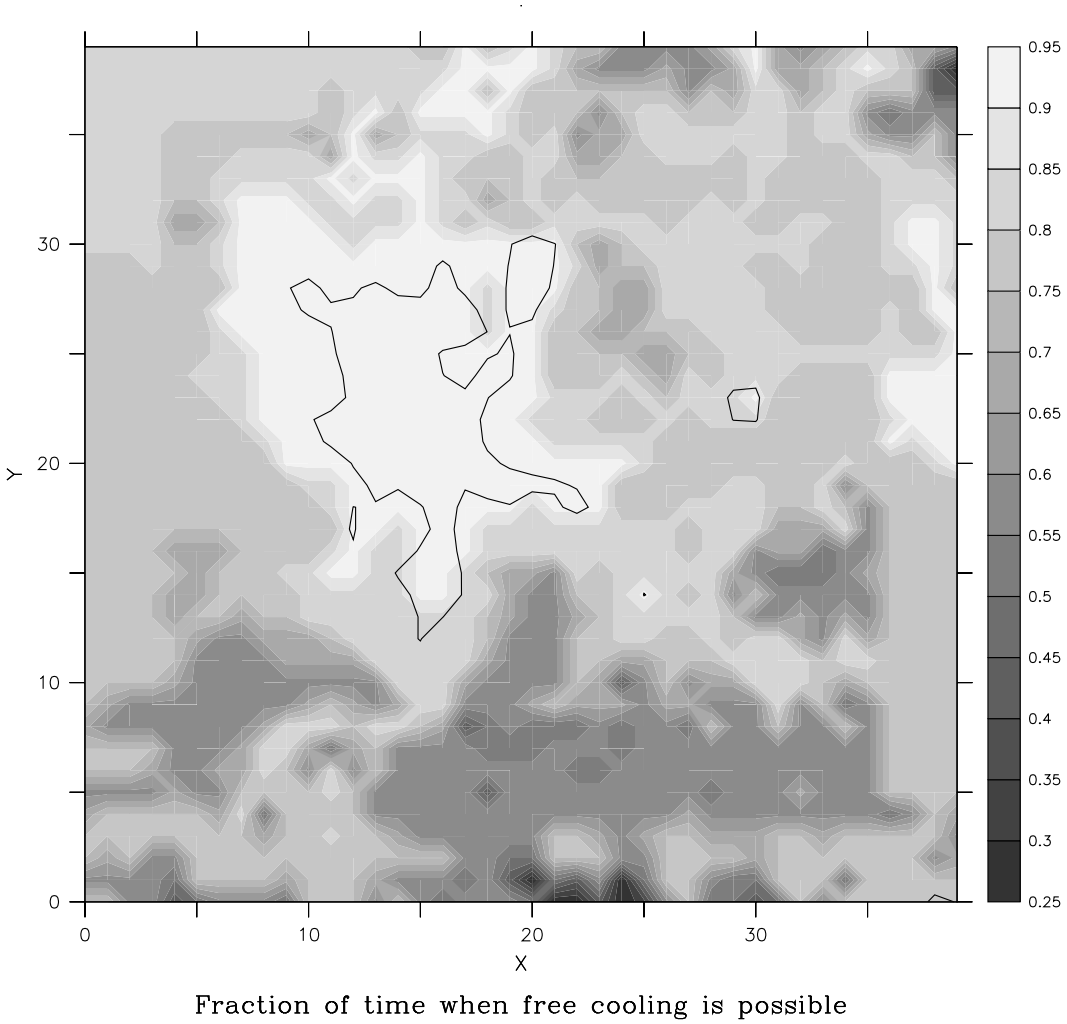

Figure 6.4: Fraction of time when free cooling is possible over the region of Basel during the IOP.

It can be interesting to sort of 'combine' the two previous results by assessing this time the *passive cooling potential* (PCP) of the region whose criteria are given by

equations 4.7.3 to 4.7.6 and which a reminded here:

$$WH_{\mathrm{PCP}} \overset{\mathrm{def.}}{=} \frac{1}{N} \sum_{i=1}^{N} v_i^{\mathrm{local}} \ \delta_{\mathrm{fc}i} \tag{6.2.1}$$

$$SH_{\mathrm{PCP}} \overset{\mathrm{def.}}{=} \frac{1}{N} \sum_{i=1}^{N} \left| \frac{T_{\mathrm{i}i} - T_{\mathrm{e}i}}{T_{\mathrm{e}i}} \right| \ \delta_{\mathrm{fc}i} \tag{6.2.2}$$

$$NH_{\mathrm{PCP}} \overset{\mathrm{def.}}{=} 10 \cdot \log_{10} \Big(\frac{1}{N} \sum_{i=1}^{N} 10^{\ L_{\mathrm{noise}i} \ \delta_{\mathrm{fc}\,i}/10} \Big) \tag{6.2.3}$$

$$PH_{\mathrm{PCP}} \overset{\mathrm{def.}}{=} \frac{1}{N} \sum_{i=1}^{N} L_{\mathrm{pollution}_i} \ \delta_{\mathrm{fc}i} \tag{6.2.4}$$

This passive cooling potential is given by Figure 6.5.

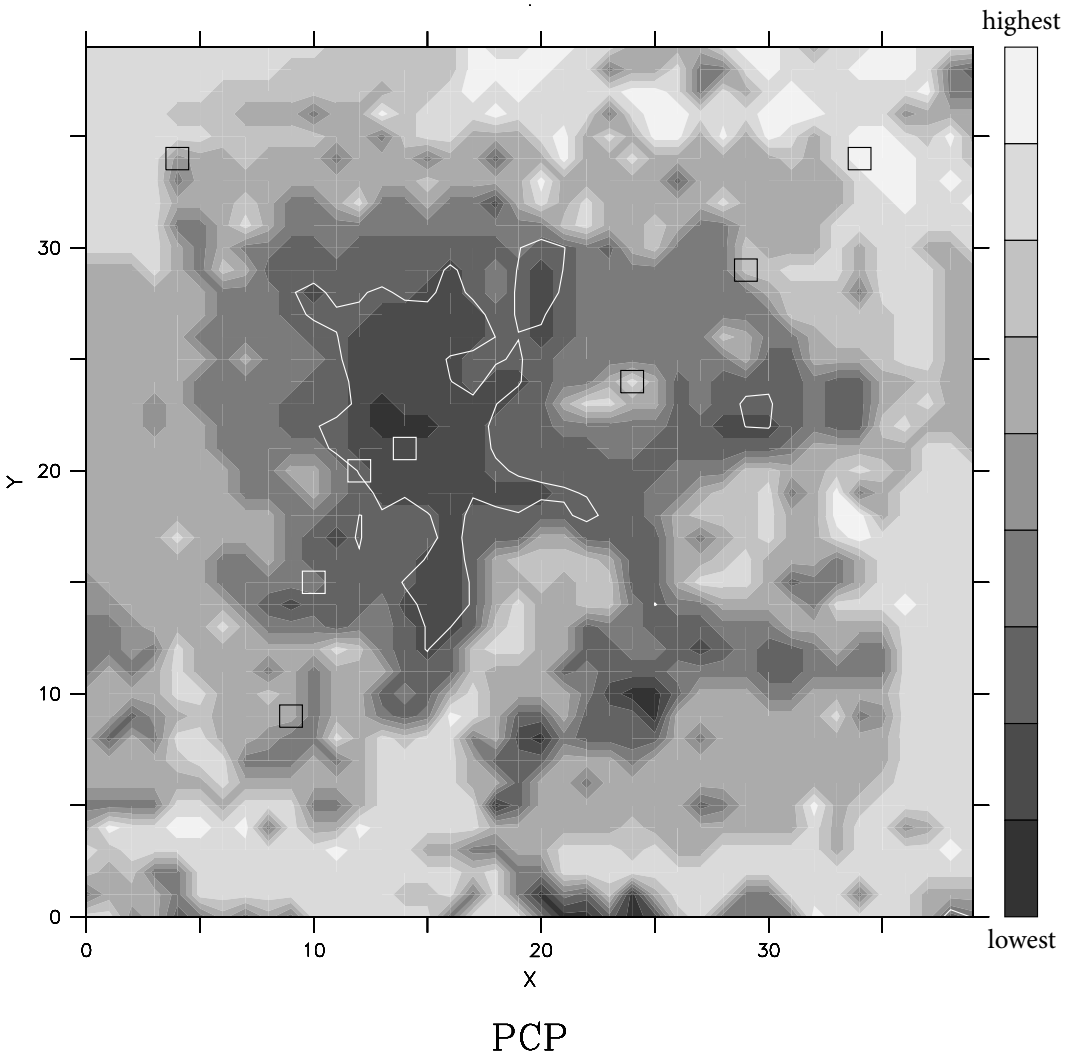

Figure 6.5: Passive cooling potential of the region of Basel during the IOP. Eight base sites (squares) are used here.

If the purely ordinal rankings used thus far are not deemed satisfactory, a more 'intrinsic' result can be provided via the *air change rate induced by stack effect* computed by way of equation 4.2.4 and represented by Figure 6.6. The example—consisting in a very simple two-opening room associated with Figure 4.13—is taken up again here. The following parameters values have been chosen:

- area of the apertures: $A = 2$ m^2 ;
- discharge coefficient: $C_d = 0.6$;
- difference in height between the apertures: $h = 9$ m ;
- number of occupants: 10.

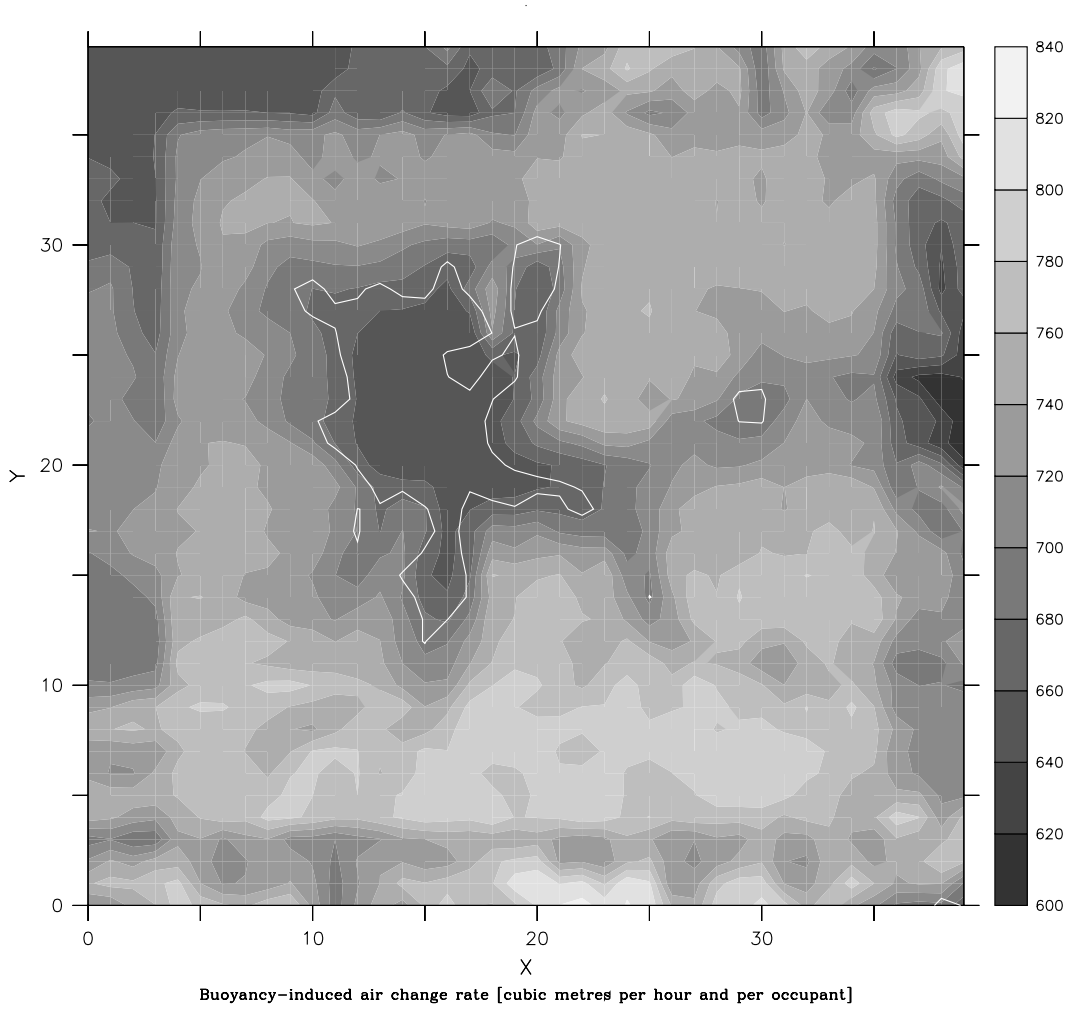

Figure 6.6: Buoyancy-induced air change rate.

The *degree hours of cooling saved by ventilation* is shown in Figure 6.7. This represents the energy required to bring the internal temperature down to the upper limit of comfort, but only when possible exclusively by ventilation (otherwise it would be a matter of *degree hours for cooling*, by means of air-conditioning).

The *degree hours for heating* and the *degree hours for cooling* are not represented because they are simply nil.

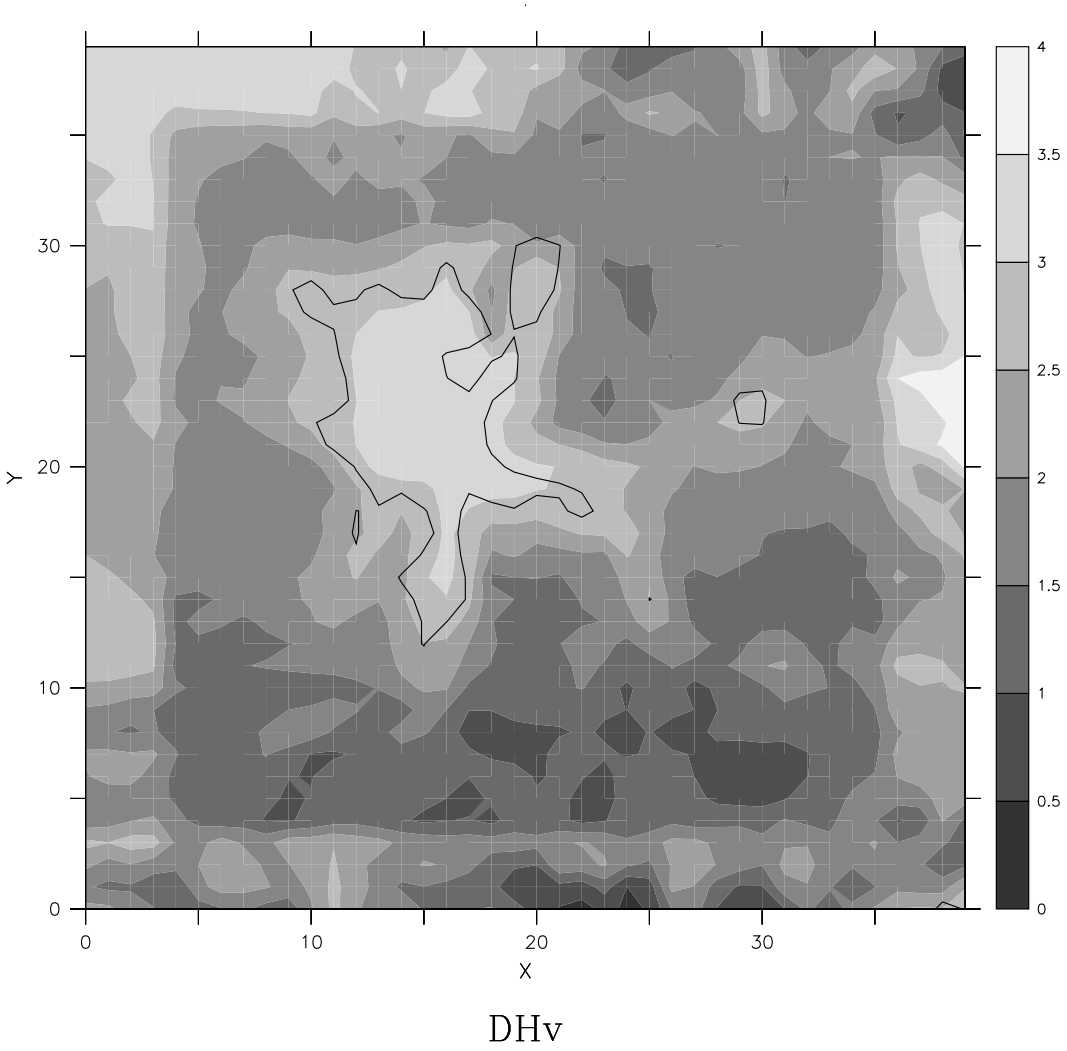

Figure 6.7: Degree hours of cooling saved by ventilation.

6.3 Results Analysis

The results showing the natural ventilation potential assessment of the Basel region are of no great surprise: the denser the city, the lower the potential for natural ventilation. *Wind hours*, *noise hours* and *pollution hours* are obviously lower in built-up areas due to the wind speed reduction in the city and to the (supposed) link of constraints with urbanization.

This is a little less evident when it comes to *stack hours*, since the city-increased external temperature doesn't directly come into play. In fact, stack effect is reduced

because the differences between the internal and the external temperatures are less marked in the urban context, as one can see in Figure 6.8.

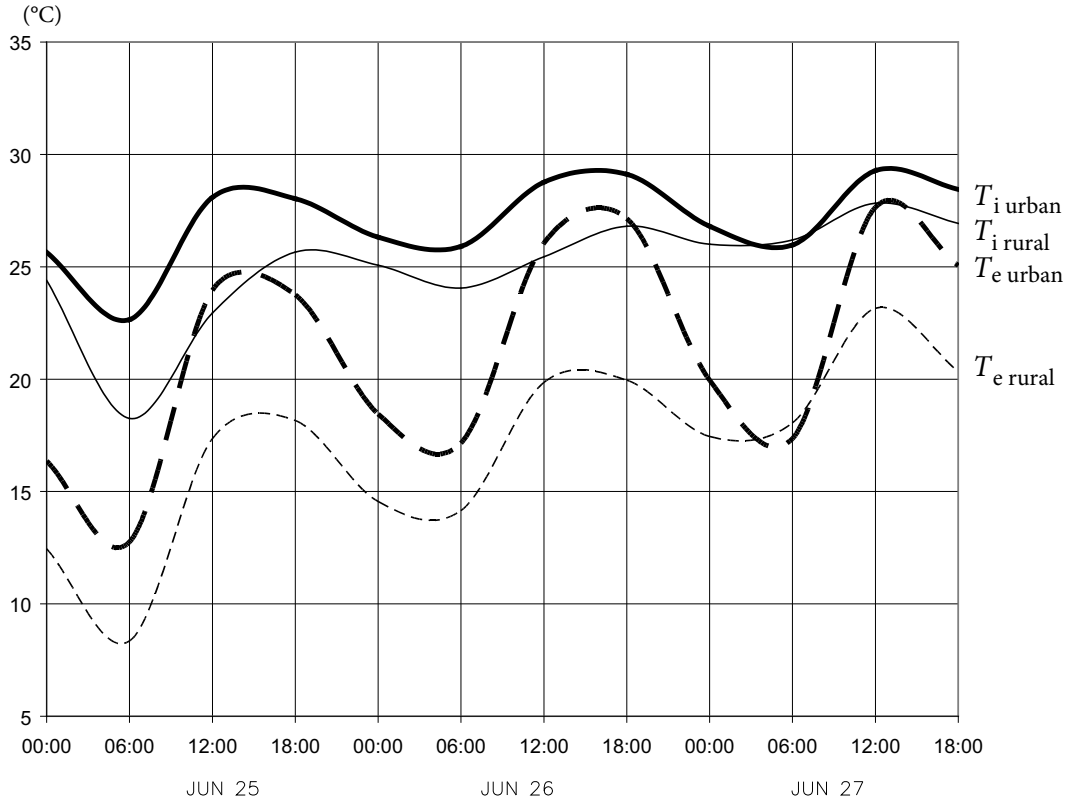

Figure 6.8: External (dashed) and internal (solid) temperatures at a rural site (thick) and at an urban site (bold) for a heavy construction.

These internal temperatures are the result of Ecotect's calculations and of the assumptions made in the URBVENT method, in particular in equation 4.5.10. Note that the internal gains are important, in particular because the building is supposed to be uninterruptedly occupied.

By way of comparison, inside the lightweight house, the internal temperature follows more closely the external one, as pointed out by Figure 6.9[7]. To make up for it, the buoyancy-induced draught is significantly lower and the indoor air remains quite cold—even sometimes too cold during that three-day summer period when rural temperatures do not exceed 23 °C.

[7]This evolution is comparable to the temperatures measured in our relatively light-structured laboratory, the Solar Energy and Building Physics Laboratory.

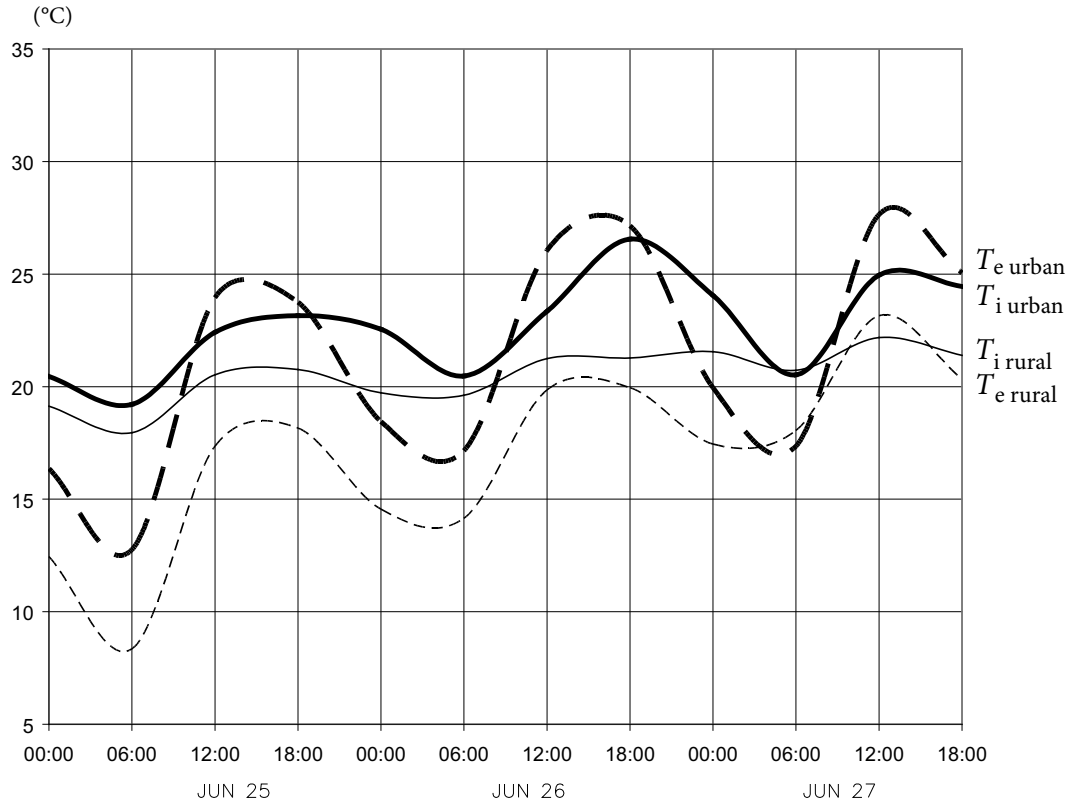

Figure 6.9: External (dashed) and internal (solid) temperatures at a rural site (thick) and at an urban site (bold) for a lightweight house.

Surely more surprising is the *fraction of time when free cooling is possible*, represented by Figure 6.4. This fraction is actually more important in the urban area because more cooling is required and because, even so, the outside air is cool enough there. In the countryside, the indoor air is simply already cool enough without ventilation.

The *passive cooling potential* (Figure 6.5) exhibits the same geographical appearance than the natural ventilation potential except for the horizontal strip comprised between $Y = 0$ and $Y = 10$. In this strip, passive cooling is indeed less applicable—or rather needs less to be applied.

The *buoyancy-induced airflow* of Figure 6.6 is closely linked with stack hours, so that it resembles Figure 6.1 (stack hours). This flow is less important in urban zones and, in the remainder, slightly higher in the southern parts of the domain. At all events, the air change rate largely exceeds the minimum 30 m^3 required for the welfare of occupants—as far as a high enough stack exists, such as the nine-meter one assumed

here.

With regard to *degree hours of cooling saved by ventilation* (Figure 6.7), the situation is comparable to the one encountered for the *fraction of time when passive cooling is possible*. More cooling is saved in the urban zones—up to 3.9 °C—than in rural ones. The explanation is that more cooling is needed to reach the comfort zone in the city and that all of this cooling can be provided by natural ventilation only.

In fact, *degree hours of cooling* (by air-conditioning) are equal to zero all over the domain, meaning that substantial energy savings can be made with the help of natural ventilation and that air-conditioning can be completely avoided in this region for the kind of building studied (brick façade building).

6.4 Verification of the Results

An attempt is made in the current section to validate these last results in the vein of the verification undertaken in Chapter 4 (section 4.8). As was the case for the previous verification, the current one should be taken with an open mind insofar as the ideal conditions, *i.e.* the suppositions made in section 4.4 ('Assumptions of the Methodology') are hardly ever fulfilled.

Besides, an ideal verification should resort to ventilation rates measured in houses of a same given type, all over the studied domain and during the period of interest.

6.4.1 The EXPOLIS Study

The EXPOLIS (Air Pollution Exposure Distributions within Adult Urban Populations in Europe) study (Jantunen *et al.*, 1998) about population exposures to air pollution was chosen to support the current verification. This study focuses on working age urban populations in Europe, exposed to air pollutants in their homes, workplaces and other common urban microenvironments. Measurements of ambient fine particulate matter ($PM_{2.5}$), volatile organic components (VOC) compounds, carbon monoxide (CO) and so forth were undertaken inside and outside buildings. Amongst the four cities selected for this study was Basel.

For this validation's purpose, these measurements are an indirect way to assess natural ventilation by comparing internal and external concentrations of pollutants.

Provided that the pollutant has no internal source and that it decays naturally, one can indeed reasonably suppose that, by high ventilation rates, its internal and external concentrations tend to level out.

In a publication analyzing the results of the Expolis study, Hänninen *et al.* (2004) use a so-called *infiltration factor* defined as

$$F_{\mathrm{INF}} = \frac{C_{\mathrm{ai}}}{C_{\mathrm{a}}} \tag{6.4.1}$$

where C_{ai} is the concentration of ambient pollutant that has infiltrated indoors, C_{a} is the ambient (outdoor air) concentration.

The indoor concentration C_{i} is the sum of C_{ai} and of the indoor-generated concentration C_{ig}:

$$C_{\mathrm{i}} = C_{\mathrm{ai}} + C_{\mathrm{ig}} \tag{6.4.2}$$

In the absence of indoor-generated particles ($C_{\mathrm{ig}} = 0$), the infiltration factor can be simply written as:

$$F_{\mathrm{INF}} = \frac{C_{\mathrm{i}}}{C_{\mathrm{a}}} \tag{6.4.3}$$

where C_{i} is the total indoor concentration. This formula holds for sulphur (emitted as gaseous sulphur dioxide and oxidized to sulphate in the atmosphere) (Hänninen *et al.*, 2004), which was chosen for this verification.

Dockery & Spengler (1981) elaborated on the mass-balance equation, assuming uniform mixing within the building and steady state conditions over the sampling period. This mass-balance equation gives the following expressions for C_{ai} and C_{ig}.

$$\begin{cases} C_{\mathrm{ai}} &= \frac{Pa}{a+k} C_{\mathrm{a}} \\ C_{\mathrm{ig}} &= \frac{Q}{V(a+k)} \end{cases} \tag{6.4.4}$$

where P is the penetration efficiency, a the air exchange rate, k the decay rate indoors, Q the source strength and V the interior volume of the building, which are all constant under the assumed steady state conditions.

The first equation of (6.4.4) and the definition of the infiltration factor give:

$$F_{\mathrm{INF}} = \frac{Pa}{a+k} \tag{6.4.5}$$

The air exchange rate thus reads:

$$\boxed{a = \frac{kF_{\mathrm{INF}}}{P - F_{\mathrm{INF}}}} \tag{6.4.6}$$

Hänninen *et al.* (2004) assumed a value of approximately 1.0 for P and a value of 0.39 h^{-1} for k.

In order to be able to compare air exchange rates with the NVP results of this chapter, EXPOLIS sites were selected only if:

- the site was located in Basel;
- the measurement were made during the same period of the year as the period studied in the current chapter (that is three weeks before and three weeks after it);
- a window at least was open during the 48-hour measurements.

These conditions restricted the original set of fifty Basel sites to the five sites shown in Table 6.1, ordered decreasingly by air exchange rates.

Table 6.1: Air exchange rates of the EXPOLIS sites. Longitudes and latitudes are expressed in the Swiss National System.

site	$a\,[\mathrm{h}^{-1}]$	$F_{\mathrm{INF}}\,[\ ]$	longitude [m]	latitude [m]	measurements period
site 1	19.62	0.98	609 944	266 357	15–17.06.1997
site 2	5.57	0.93	612 813	268 937	16–18.07.1997
site 3	3.51	0.90	611 871	265 614	07–09.07.1997
site 4	2.88	0.88	612 238	265 566	04–06.06.1997
site 5	-2.03	1.24	611 852	267 742	11–13.06.1997

6.4.2 Natural Ventilation Potential of the EXPOLIS Sites

There are two ways of comparing the ranking of these sites by air exchange rates and their ranking by the URBVENT method. First, if the purpose is to validate the above NVP maps, a map as the one of Figure 6.3 can be used. Figure 6.10 shows a close-up of the NVP map together with the five EXPOLIS sites. As noise and pollution levels do not come into play in the EXPOLIS experiments, the weights of the noise and pollution criteria are set to zero in the multicriteria analysis. The same weights have been assigned to the wind and buoyancy criteria. The eight base sites used in section 6.2 are used again here.

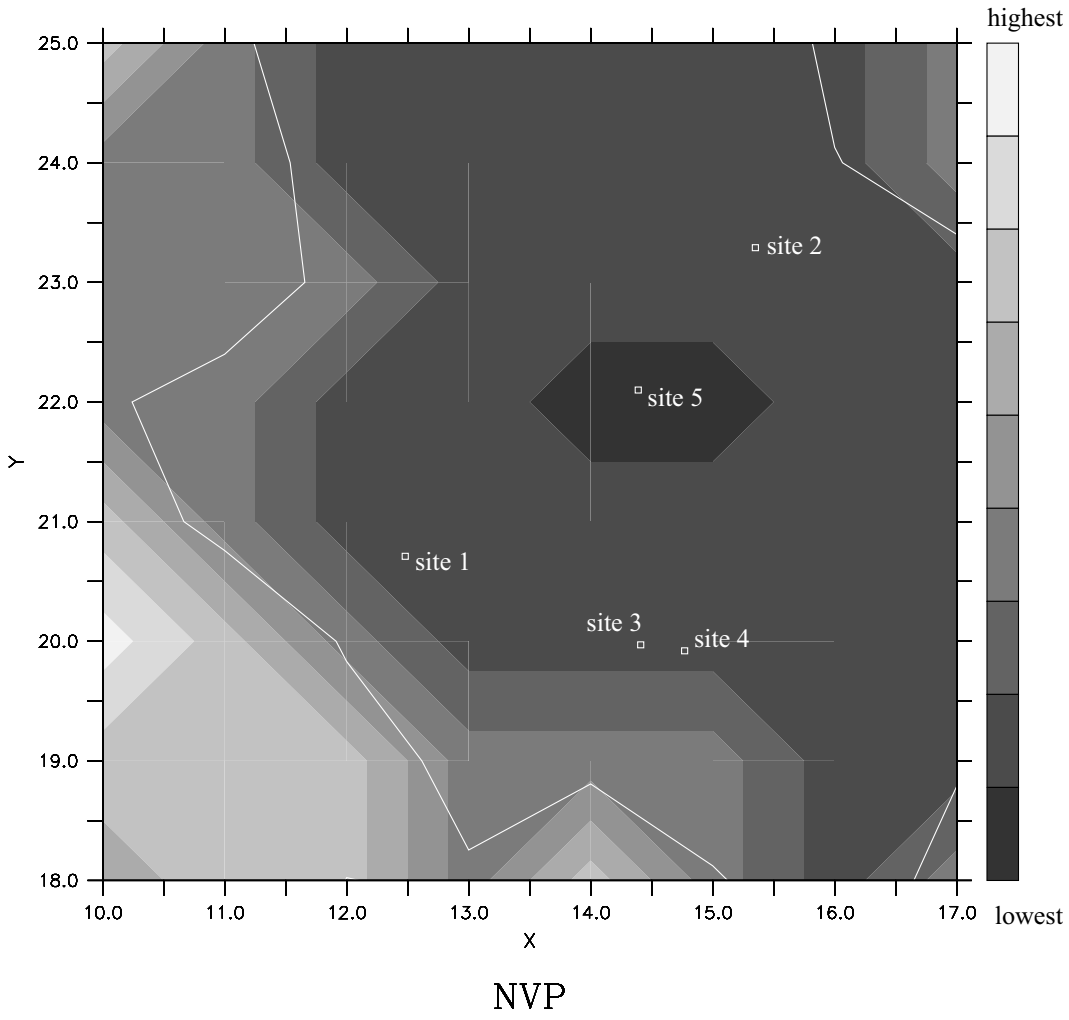

Figure 6.10: Natural ventilation potential of the region of Basel during the IOP and location of the Expolis sites. (Eight base sites are used here.)

The results are not as meaningful as could be since four sites fall in the same NVP zone. The reason for this is that the Expolis study focus in locations downtown.

A perhaps better and more straightforward way to make the comparison simply consists in ranking the Expolis sites with the Urbvent method. The result is shown in the second column of Table 6.2.

6.4.3 Verification Results

The number of Expolis sites fulfilling the conditions to be accepted and their distribution throughout the FVM domain are clearly not sufficient to conduct a proper verification. Nonetheless, the map of Figure 6.10 is in agreement with the ranking of

Table 6.2: Rankings of the EXPOLIS sites by way of air exchange rates (first column) and by way of the URBVENT method (second column).

ranking by air exchange rates a (highest a in the upmost row)	ranking by URBVENT (highest NVP in the upmost row)
site 1	site 1
site 2	site 3
site 3	site 4
site 4	site 2
site 5	site 5

the sites according to air exchange rates, since site 5, which has the lowest exchange rate is located in a zone of lower NVP than the other sites.

Moreover, Table 6.2 shows that, except site 2, the sites are ranked in the same order according to exchange rates and according to URBVENT .

6.4.3.1 Causes of Error

In spite of the bad position of site 2, the results are satisfactory because the causes of error are multiple:

- The year of the EXPOLIS experiments (1997) is different from the year simulated by FVM (2002). Meteorological conditions may have changed from one year to the other.
- The buildings may not be identical to one another and may not be similar to the one assumed in section 6.1.
- Some indoor-generated sulphur may have been emitted as the infiltration factor of site 5, which is greater that one, suggests it.[8]
- The penetration efficiency P and the decay rate k are just estimates (Hänninen *et al.*, 2004) and may be different for each building.
- Natural ventilation may not have been exploited at best during the EXPOLIS experiments.

Actually, the current verification is an indirect way of assessing the natural ventilation potential . In an ideal case, air changes measurements should have been undertaken in similar buildings during the BUBBLE experiment.

[8]Because $F_{\mathrm{INF}} > 1$, site 5 has in fact a negative air exchange rate. This value is obviously unphysical and should be disregarded. Despite this, one can still confidently state that site 5 has the lowest air exchange rate.

Chapter 7

Conclusion

7.1 Achievements

A semi-qualitative multicriteria analysis method was developed with the objective of assessing the *natural ventilation potential* of an urban site. The method takes into account driving forces—*wind pressure* and *stack (buoyancy) pressure*—and constraints—*noise pollution* and *atmospheric pollution*—related to natural ventilation, in order to state whether or not a given site is appropriate for natural ventilation (and passive cooling).

The method has been implemented in a user-friendly software tool as part of the European project URBVENT and has been well received by both academics and practitioners. This tool covers the whole European territory and uses meteorological data extracted from an archive of results obtained from a weather forecast simulation model used by the Swiss national weather service (MeteoSwiss). The influence of the urban fabric, which was not accounted for in the above-mentioned model, was estimated by way of a terrain correction factor and a canyon module developed by the University of Athens. The tool relies on user-entered data related to noise pollution and atmospheric pollution. The verification carried out in section 4.8 ('Software Verification') is in excellent agreement with real cases of naturally ventilated buildings across Europe.

With a view to refining this tool, a mesoscale atmospheric simulation model, in conjunction with an urban module, both developed at the *Air and Soil Pollution Laboratory* of the Swiss Federal Institute of Technology in Lausanne was employed. Its interpolation preprocessor has been reprogrammed within the present work. In addition to this more accurate calculation of urban wind and temperature fields, noise

and pollution levels were delivered by the model, in particular as the result of pollutants transport calculations—which was the initial purpose of the mesocale model. The model went through a validation process that showed substantial improvement compared to MeteoSwiss' LM model. The drawback of this refined approach is its very improbable general applicability over a more extended region such as the whole Europe, as was the case in the URBVENT tool. The number of parameters and of boundary conditions required is by far too large, at least for the time being. In fact, the method was implemented over a much less extended area, namely the Basel (Switzerland) region.

The results over Basel show that the natural ventilation potential, which is strictly related to airflow rate and therefore to indoor air quality, is as expected higher in rural areas than in urban ones. On the other hand, the *fraction of time when passive cooling is possible*, defined as the fraction of time when the internal building temperature can be brought down to thermal comfort by the sole means of natural ventilation, turns out to be higher in urban areas (up to 92 %) than in rural ones (up to 25 %) in the summertime. This arises from the fact that the building of interest (in this case an uninterruptedly occupied brick façade building) needs less cooling in rural zones. Additionally, a further calculation of the degree hours of cooling saved by ventilation demonstrates that substantial energy savings can be made with the help of natural ventilation and that air-conditioning can be completely avoided in this region for the kind of building studied.

One of the goals of the present work was to show the feasibility and the applicability of *qualitative modelling* (sometimes referred to as *soft computing*) in the field of urban planning. The outcome is satisfactory in this respect, and is in good agreement with the verification undertaken with the help of the air pollution exposure study EXPOLIS.

7.2 Prospects

In the exchange process between buildings and their urban environments, a rather complex feedback mechanism takes place. The present work primarily addresses the exchange from the environment to the building. It would be valuable to study the influence on the environment of given types of buildings erected on a whole area.

As a matter of fact, the buildings included in the urban module used thus far in this work do influence the environment but their modelling does not include natural

ventilation or any air exchanges with the exterior whatsoever. Besides, in this module, the temperature inside the buildings is constant for the whole simulation period.

In this regard, a forthcoming *Swiss National Research Programme*—'Multiscale Modelling of Building–Urban Interactions'—will aim to extend the capabilities of the currently used mesoscale atmospheric model to "facilitate accurate urban climate predictions. This new modelling capability will then be deployed to quantify the effectiveness of heat island mitigation strategies." In this, the main contributions to fluxes between the building and the atmosphere—as well as the best and simplest ways to model them—will be identified. Computational fluid dynamics is planned to be applied so as to identify the modifications to be made to the current turbulence parametrization.

The Research Programme allows a scenario-testing phase to appraise the effectiveness of different measures to mitigate the heat island effect, for example by modifying the colours of building surfaces or increasing the areas of landscaping.

One of the workpackages of the Research Programme plans to attain a *servicing strategy map*, that is a geographically sensitive tool providing, for each specific location in the city, the most sustainable servicing strategy in that accounts for occupants' comfort. Guidance will thus be supplied to designers in accordance with the most environmentally benign strategy. The mainstream of the present work will hence be prolonged this time by envisaging more passive and active techniques than just natural ventilation and passive cooling, and by turning to a more sophisticated dynamic thermal simulation program than the one used in this work, namely *ESP–r* (Clarke, 2001).

This Research Programme, the present work and many other projects belong to the emerging field of the so-called *urban physics* and convey the concern that cities ought to be regarded as a whole in order to be compatible with the objectives of sustainable development.

References

Adnot, Jérôme. 2005. Développement de la climatisation en Europe et impacts sur le réseau électrique. *In: Cycle de formation "énergie et environnement", CUEPE, Université de Genève.*

Akbari, H., Pomerantz, M., & Taha, H. 2001. Cool surfaces and shade trees to reduce energy use and improve air quality in urban areas. *Solar Energy*, **70**(3), 295–310.

Bahadori, Mehdi N. 1978. Passive Cooling Systems in Iranian Architecture. *Scientific American*, **238**(2), 144–154. ISSN 0036-8733.

Beausoleil-Morrison, I. 2000. *The adaptive coupling of heat and airflow modelling within dynamic whole-building simulation.* Ph.D. thesis, University of Strathclyde.

Bland, B.H. 1992. Conduction in dynamic model: analytical tests for validation. *Building Services Engineering Research and Technology*, **3**(4), 197–208.

Bluyssen, P. M., Cox, C., Maroni, M., Boschi, N., Raw, G., Roulet, C. A., & Foradini, F. 2003. European Project HOPE (Health Optimization Protocol for Energy-Efficient Buildings). *In: Healthy Buildings 2003, Singapore.*

Bougeault, P., & Lacarrère, P. 1989. Parameterisation of orography-induced turbulence in a mesobeta-scale model. *Mon. Wea. Rev.*, **117**, 1872–1890.

Brager, G. S., & de Dear, R. J. 1998. Thermal adaptation in the built environment: A literature review. *Energy and Buildings*, **27**, 83–96.

Buizza, R., Tribbia, J., Molteni, F., & Palmer, T. N. 1993. Computation of optimal unstable structures for a numerical weather prediction model. *Tellus*, **45A**, 388–407.

CEN. 1999. *EN 832 - Thermal performance of buildings - Calculation of energy use for heating - Residential buildings.* Brussels, CEN.

CEN. 2004. *EN ISO 13790 - Thermal performance of buildings - Calculation of energy use for heating.* Brussels, Genève, CEN, ISO.

Chandra, S., Fairey, P., & Houston, M. 1983. *A Handbook for Designing Ventilated Buildings.* Tech. rept. FSEC-CR-93-83. Florida Solar Energy Center, Florida.

Charney, J. G. 1954. Numerical prediction of cyclogenesis. *Proc. Nat. Acad. Sci. U. S.*, **40**, 99–110.

Charney, J. G., Fjørtoft, R., & von Neumann, J. 1950. Numerical integration of the barotropic vorticity equation. *Tellus*, **2**, 237–254.

Chen, Q. Y. 2004. Using computational tools to factor wind into architectural environment design. *Energy and Buildings*, **36**, 1197–1209. ISSN 0378-7788.

Christen, Andreas. 2005. *Atmospheric Turbulence and Surface Energy Exchange in Urban Environments—Results from the Basel Urban Boundary Layer Experiment (BUBBLE).* Ph.D. thesis, University of Basel, Switzerland. PhD Thesis no. B 7159.

CIBSE. 1999. *Guide A: Environmental Design.* Chartered Institution of Building Services Engineers, London. ISBN/ISSN 0900953969.

Clappier, A., Perrochet, P., Martilli, A., Muller, F., & Krueger, B. C. 1996. A new nonhydrostatic mesoscale model using a CVFE (Control Volume Finite Element) discretisation technique. *Pages 527–531 of:* Borrell, P. M., Borel, P., Cvitas, T., Kelly, K., & Seiler, W. (eds), *EUROTRAC Symposium 1996, Southampton.* Computational Mechanics Publications.

Clappier, A., Martilli, A., Grossi, P., Thunis, P., Pasi, F., Krueger, B. C., Calpini, B., Graziani, G., & van den Bergh, H. 2000. Effect of sea breeze on air pollution in the Greater Athens Area. Part I: Numerical simulations and field observations. *Journal of Applied Meteorology*, **39**, 546–562.

Clappier, Alain. 1998. A correction method for use in multidimensional time-splitting advection algorithms: Application to two- and three-dimensional transport. *Month. Weath. Rev.*, **126**, 232–242.

Clarke, J.A. 1977. *Environmental systems performance*. Ph.D. thesis, University of Strathclyde.

Clarke, J.A. 2001. *Energy simulation in building design*. 2nd edn. Butterworth Heinemann, London.

Coiffier, Jean. 2000. Un demi-siècle de prévision numérique du temps. *La Météorologie*, **8**(30), 11–31.

Collella, P., & Woodward, P. 1984. The Piecewise Parabolic Method (PPM) for gas dynamical simulations. *J. Comp. Phys.*, **54**, 174–201.

De Dear, R. J., & Brager, G. S. 1999. *Annex 35, Energy conservation in buildings and community systems*. Tech. rept. International Energy Agency, Sydney, Australia.

Dockery, D.W., & Spengler, J.D. 1981. Indoor–outdoor relationships of respirable sulfates and particles. *Atmospheric Environment*, **15**, 335–343.

EECCAC. 2002. *Energy Efficiency and Certification of Central Air Conditioners*. Tech. rept. Study for the D.G. Transportation-Energy (DGTREN) of the Commission of the E.U., Co-ordinator: J. Adnot, September 2002.

European Commission. 2002 (August). *Directive 2002/EC of the European Parliament and of the Council on the energy performance of buildings*.

Feustel, H. E., & Dieris, J. 1992. A survey on air flow models for multizone structures. *Energy and Buildings*, **18**, 72–100.

Feustel, Helmut E., Allard, Francis, Dorer, Viktor B., Herrlin, Magnus K., Mingsheng, Liu, Phaff, Hans C., Utsumi, Yasuo, Yoshino, Hiroshi, & Grosso, Mario. 1990. *Fundamentals of the Multizone Air Flow Model – CoMIS.* Air Infiltration and Ventilation Centre, Coventry. AIVC Technical Note 29, 115 pages, Code TN 29, ISBN 0-946075-44-1.

Flourentzou, F., Greuter, G., & Roulet, C. A. 2003. Hermione, une nouvelle méthode d'agrégation qualitative basée sur des règles. *In: 58èmes journées du groupe de Travail Européen d'Aide Multicritère à la Décision, Moscou, 9–11 octobre 2003.*

Fountain, M., Brager, G., & de Dear, R. 1996. Expectations of indoor climate control. *Energy and Buildings*, **24**, 179–182.

Fürbringer, Jean-Marie. 1994. *Sensibilité de modèles et de mesures en aéraulique du bâtiment à l'aide de plans d'expériences.* Ph.D. thesis, École polytechnique fédérale de Lausanne, Lausanne, Suisse. Thèse No 1217.

Fürbringer, Jean-Marie, Roulet, Claude-Alain, & Borchiellini, Romano. 1996. *Evaluation of CoMIS – Appendices.* Tech. rept. École polytechnique fédérale de Lausanne, Lausanne, Suisse.

Georgakis, Chrissa, & Santamouris, Matheos. 2005. *Natural Ventilation in the Urban Environment.* BEST (Buildings, Energy & Solar Technology) Series. London, Sterling, VA: Earthscan Publications Ltd. ISBN 1-84407-129-4. Chap. 4: Wind and Temperature in the Urban Environment, pages 81–102.

Ghiaus, C. 2003. Free-running building temperature and HVAC climatic suitability. *Energy and Buildings*, **35**(4), 405–411.

Gough, M.C.B. 1982. *Modelling heat flow in buildings: An eigenfunction approach.* Ph.D. thesis, University of Cambridge.

Grimmond, C.S.B., & Oke, T.R. 1999. Aerodynamic Properties of Urban Areas Derived from Analysis of Surface Form. *Journal of Applied Meteoroogy*, **38**, 1262–1292. ISSN 0894-8763.

Hänninen, O.O., Lebret, E., Ilacqua, V., Katsouyanni, K., Künzli, N., Srám, R.J., & Jantunen, M. 2004. Infiltration of ambient $PM_{2.5}$ and levels of indoor generated non-ETS $PM_{2.5}$ in residences of four European cities. *Atmospheric Environment*, **38**, 6411–6423. ISSN 1352-2310.

Hémon, D., & Jougla, E. 2003. *Surmortalité liée à la canicule d'août 2003. Rapport d'étape (1/3). Estimation de la surmortalité et principales caractéristiques épidémiologiques.* Tech. rept. Inserm, Paris.

Hensen, J.L.M. 1991. *On the thermal interaction with building structure and heating and ventilating systems.* Ph.D. thesis, University of Eindhoven.

Hinkelmann, K. 1959. *The Atmosphere and Sea in Motion.* Rossby Memorial Volume, Rockefeller Institute Press, USA. Chap. Ein numerisches Experiment mit den primitiven Gleichungen, pages 486–500.

I., Orlanski. 1975. A rational subdivision of scales for atmospheric processes. *Bull. Amer. Meteor. Soc.*, **56**, 527–530.

Janak, M. 1997. Coupling building and lighting simulation. *In: Building Simulation '97, 5th Int IBPSA Conference, Prague.*

Jantunen, M.J., Hänninen, O., Katsouyanni, K., Knoppel, H., Künzli, N., Lebret, E., Maroni, M., Saarela, K., Srám, R., & Zmirou, D. 1998. Air pollution exposure in European cities: the "EXPOLIS" study. *Journal of Exposure Analysis and Environmental Epidemiology*, **8**(4), 495–518.

Johner, N., Roulet, C.-A., Oostra, A., & Foradini, F. 2005. Correlations between SBS, perceived comfort, energy use and other building characteristics in European office and residential buildings. *Pages 740–745 of: Indoor Air 2005, Beijing*, vol. 1. Tsinghua University Press. ISBN 7-89494-830-6.

Judkoff, R., & Neymark, J.A. 1995. A testing and diagnostic procedure for building energy simulation programs. *In: 2nd Building Environmental Performance Analysis Club Conference 94, York.*

Junier, Martin. 2004. *Gas phase chemistry mechanisms for air quality modelling: generation and application to case studies.* Ph.D. thesis, École polytechnique fédérale de Lausanne, Lausanne, Suisse. Thèse No 2936.

Kelly, N. 1998. *Towards a Design Environment for Building Integrated Energy Systems: The Integration of Electrical Power Flow Modelling with Building Simulation. (Unpublished).* Ph.D. thesis, University of Strathclyde.

Khansari, Mehdi, & Yavari, Minouch. 1986. *Espace persan, architecture traditionnelle en Iran.* Pierre Mardaga, éditeur. ISBN 2-87009-249-0.

Kuo, H. L. 1965. A theory of parameterization of cumulus convection. *J. Atmos. Sci.*, **22**, 40–43.

Li, Y., & Delsante, A. 2001. Natural ventilation induced by combined wind and thermal forces. *Building and Environment*, **36**, 59–71. ISSN 0360-1323.

Lomas, K.J., Eppel, H., Martin, C.J., & Bloomfield, D.P. 1997. Empirical validation of building energy simulation programs. *Energy and Buildings*, **26**(3), 253–267.

Louis, J.-F. 1979. A parametric model of vertical eddy fluxes in the atmosphere. *Boundary-Layer Meteorol.*, **17**, 187–202.

Martilli, A., Clappier, A., & Rotach, M. W. 2002. An urban surface exchange parameterisation for mesoscale models. *Boundary-Layer Meteorol.*, **104**(2), 261–304. ISSN: 0006-8314 (paper), 1573-1472 (online).

Martilli, Alberto. 2001. *Development of an urban turbulence parameterisation for mesoscale atmospheric models.* Ph.D. thesis, École polytechnique fédérale de Lausanne, Lausanne, Suisse. Thèse No 2445.

MeteoSwiss. 1982-2000. *Klimaatlas der Schweiz.* Gesamtleitung: Walter Kirchhofer, Swiss Meteorological Institute (MeteoSwiss) (ed.). ISBN 3-302-09606-2.

Nakhi, A. 1995. *Adaptive construction modelling within whole building dynamic simulation.* Ph.D. thesis, University of Strathclyde.

Naut, H. 2005. *Dans l'œil du cyclone.* TSR television programme *Territoires21.* Production: Hélène Naut. Broadcast March 30, 2005.

Nicholson, Sharon E. 1975. A Pollution Model for Street-Level Air. *Atmospheric Environment*, **9**, 19–31. ISSN 1352-2310.

Nicol, J.F. 2001. Characterising occupant behaviour in buildings: towards a stochastic model of occupant use of windows, lights, blinds heaters and fans. *Pages 1073–1078 of: Proc BS'01, 7th Int IBPSA Conference, Rio.*

OPB. 1986. *Ordonnance sur la protection contre le bruit du 15 décembre 1986.* État 3 juillet 2001.

Palmer, T. N., Shutts, G. J., & Swinbank, R. 1986. Alleviation of systematic westerly bias in general circulation and numerical weather prediction models through an orographic gravity wave drag parameterization. *Quart. J. Roy. Meteor. Soc.*, **112**, 2056–2066.

Plackett, R. L., & Burman, J. P. 1943. Design of optimum multifactoral experiments. *Biometrika*, **33**, 305–325.

Robinson, D., Stankovic, S., Morel, N., Deque, F., Rylatt, M., Kabele, K., Manolakaki, E., & Nieminen, J. 2003. Integrated resource flow modelling of urban neighbourhoods: Project SUNtool. *In: Building Simulation 2003, Eindhoven.*

Roulet, C.-A., Cretton, P., Fritsch, R., & Scartezzini, J.-L. 1991. *Stochastic model of inhabitant behavior in regard to ventilation.* Technical Report. Annex 20, Air Flow Patterns within Buildings. International Energy Agency.

Roulet, C.-A., Van der Maas, J., & Flourentzos, F. 1996. A Planning Tool for Passive Cooling of Buildings. *In: INDOOR AIR '96 Nagoya - Japan.*

Roulet, Yves-Alain F. 2004. *Validation and application of an urban turbulence parameterisation scheme for mesoscale atmospheric models.* Ph.D. thesis, École polytechnique fédérale de Lausanne, Lausanne, Suisse. Thèse No 3032.

Santamouris, M. 2005. Passive and low energy cooling – The state of the art and future priorities. *In: Passive and Low Energy Cooling for the Built Environment (PALENC 2005, 1st international conference).* Heliotopos.

Santamouris, M., & Asimakopoulos, D. 1996. *Passive Cooling of Buildings.* London: James & James. ISBN 1-873936-47-8.

Sayigh, A., & Marafia, A. H. 1998. Thermal comfort and the development of bioclimatic concept in building design. *Renewable and Sustainable Energy Reviews*, **2**(1/2).

Schärlig, A. 1990a. *Décider sur plusieurs critères.* Collection Diriger l'entreprise. Presses Polytechniques et Universitaires Romandes, Lausanne, Switzerland.

Schärlig, A. 1990b. *Pratiquer Électre et Prométhée.* Collection Diriger l'entreprise. Presses Polytechniques et Universitaires Romandes, Lausanne, Switzerland.

Smagorinsky, J. 1962. A primitive equation model including condensation processes. *In: Proceedings of the International Symposium on Numerical Weather Prediction.* Special volume of the Journal of the Met. Soc. of Japan, Tokyo.

Tang, D. 1984. *Modelling of heating and air-conditioning systems.* Ph.D. thesis, University of Strathclyde.

Temam, Roger. 2005. Équations de Navier-Stokes – Le cœur intime des tourbillons. *Les dossiers de La Recherche – Mathématiques: nouveaux défis et vieux casse-tête*, **20**(August-October), 42–47. ISSN 1775-3809.

Tremback, C. J., & Kessler, R. 1985. A surface temperature and moisture parameterisation for use in mesoscale numerical models. *In: 7th Conference on Numerical Weather Prediction, June 17-20, Montreal, Quebec, Canada.* Am. Meteorol. Soc., Boston, Mass.

Van der Maas, J., & Maldonaldo, E. 1997. A new thermal inertia model based on effusivity. *Solar Energy*, **19**, 131–160.

Wouters, P. 2004. Energy Performance Regulations: Which impact can be expected from the European Energy Performance Directive ? *Air Information Review (AIVC newsletter)*, **26**(1), 1–8.

MARIO GERMANO
physics engineer

born on 27th January 1975
Italian citizenship
married

education

2006 — **PhD at the Swiss Federal Institute of Technology, Lausanne**
research fellow and lecturer at the Solar Energy and Building Physics Laboratory

2001 — **certificate in applied computer science, University of Montreal, Canada**
one-year training in programming, operations research, multimedia
Citation of Excellence

1999 — **degree in physics, Swiss Federal Institute of Technology, Lausanne, Switzerland**
research at the Institute of Experimental Physics: theoretical model, simulation and study of the magneto-optical properties of a spin chain in interaction with an electromagnetic field

professional experience

2001-2006 — **research fellow and lecturer at the Solar Energy and Building Physics Laboratory (LESO-PB), Swiss Federal Institute of Technology, Lausanne**
- researcher within the European project URBVENT
- development of a numerical atmospheric model
- assistant lecturer for the first-term building physics course (person in charge)
- researcher within the Swiss National Research Programme 54 'Multiscale Modelling of Building-Urban Interactions'

2000 — **part-time employment, University of Montreal, Canada**
assistant for an introductory IT course :
Word, Excel, Internet, Access

2000 — **internship at ALSTOM Power**
three-month full-time training period within the Gas Turbine Department, head office
- installation and optimisation of a neural network-based piece of software: anomalies and fault detection in gas turbines
- handling and processing of a remote turbine monitoring system and connection of a new turbine to this system

professional experience (continued)

1998-99	**part-time employment, University of Lausanne** lab work assistant
1997	**internship at NESTLÉ** one-month full-time training period within the Food Strategic Business Unit, head office : power calculation of a food mixer

languages

French
English
Italian
German

computer knowledge

programming languages
C, C++, Java, Visual Basic, Delphi, MapBasic, HTML, JavaScript, Pascal, Fortran, Bash

operating systems
Windows, Unix, MacOS, DOS

software
MatLab, Excel, LaTeX, PowerPoint, Photoshop, Director, Access, MapInfo, ESP–r

publications

3 international journal papers
3 peer-reviewed conference papers
1 chapter in an edited book